ABSTRACT

ALHAMMADI, KHALID. Applying Wide Field of View Retroreflector Technology to Free Space Optical Robotic Communications. (Under the direction of Professors Edward Grant and John Muth.)

This dissertation deals with research into the design and implementation of a new wide field of view retroreflector device for autonomous mobile robot communication. In order to demonstrate effective and efficient optical communication for robots, the research had first to address the problem of expanding the field of view of retroreflectors. Experimentation shows that the device is beneficial for robotics navigation and localization, and for underwater optical communication. The retroreflector is similar to other conventional cat's-eye retroreflector designs, but the use of a fisheye lens and compensating lens to collimates the light before it enters a spherical retroreflector was found facilitate a wider field of view. Using this approach the retroreflector FOV was increased to 180 degrees although at the expense of divergence angle due to spherical aberration. The combination of both a laser transceiver unit and the retroreflector formed a very useful device for several short-range wireless optical communication scenarios including robot to robot communication in situations whereby navigation and localization was executed for collaborating robots and potentially underwater optical communication in turbid water. For ease in testing and implementation visible and near infrared wavelengths were used with a relatively low speed, polarization independent, liquid crystal modulator. While the data rate and range of the tested system are limited, the results of the project indicate that with high speed optical modulators and a suitable pointing and tracking system that collaborative robot activities and robot to robot communications can be substantially advance by using free space optical communications with wide field of view retroreflectors.

APPLYING WIDE FIELD OF VIEW RETROREFLECTOR TECHNOLOGY TO FREE SPACE OPTICAL ROBOTIC COMMUNICATIONS

By

KHALID ALHAMMADI

A dissertation submitted to the Graduate Faculty of

North Carolina State University

in partial fulfillment of the degree of

DOCTOR OF PHILOSOPHY

in

ELECTRICAL ENGINEERING

Raleigh, North Carolina

September 2006

Dr. Edward Grant, Committee Chair

Dr. John F. Muth, Co-Chair

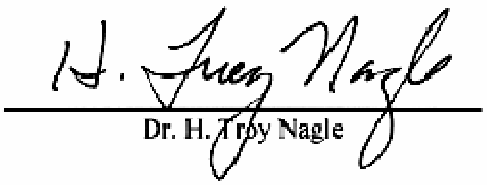

Dr. H. Troy Nagle

Dr. C Frank Abrams

BIOGRAPHY

KHALID ABDULLA ALHAMMADI received his Bachelor of Science degree in Electrical Engineering from United Arab Emirates University (Alain, UAE) in 1992. In 1998, he received his Master of Science degree with honors in Electrical and Computer Engineering from Vanderbilt University (Tennessee, USA). Upon earning his Master degree, Khalid joined Ph.D. program at North Carolina State University (Raleigh, USA) from a scholarship provided by Abu Dhabi National Oil Company (ADNOC). His Ph.D. research is focused on free space optical robotic communications. This thesis completes the requirements for his Ph.D. degree.

Upon submission of this dissertation, which was successfully defended in September 2006, Khalid will return to his home country, UAE, to join the faculty in the electrical and computer engineering department of Petroleum Institute (PI) as an assistant professor.

ACKNOWLEDGEMENTS

Allah is the Light of the heavens and the earth. The Parable of His Light is as if there were a Niche and within it a Lamp: the Lamp enclosed in Glass: the glass as it were a brilliant star: Lit from a blessed Tree, an Olive, neither of the east nor of the west, whose oil is well-nigh luminous, though fire scarce touched it: Light upon Light! Allah doth guide whom He will to His Light: Allah doth set forth Parables for men: and Allah doth know all things. (Qur'an, 24:35)

I would like to express my deepest gratitude to all of those people, without their help, this manuscript would not have been completed. First, I am dearly grateful to my advisors, Dr. Edward Grant for his guidance and mentorship during the course of the study and Dr. John Muth for his assistance and helpful discussions with my project. I extend my thanks to Dr. Michael Escuti for his assistance and valuable discussion with the optical modulator part of the project.

I also thank all those who assist me during the course of the study. In particular, thanks are due to my colleagues in the CRIM-TEAM for their valuable insights. Conversations with Leonardo Mattos, Carey Merritt and Kyle Luthy were instrumental in the research presented in this thesis. Conversations with other graduate students, including Frederick Livingston, Matthew Craver, Brooks Adcock and Yash Gawdi were also helpful. I cannot forgo the help of Rudy Salas in electronics and circuit design.

I am grateful to the government of my country, the UAE University and ADNOC for the full funding of my graduate studies. I hope that their continuous faith in my ability can be repaid through good teaching and research.

I am especially indebted to my family for their love, never-ending support and encouragement during the course of my educational endeavors and pursuit of life. I ask Allah to help me earn their satisfaction.

I am extremely grateful to my Lord Most Merciful Most Wise by whose mercy I was able to achieve my goal. I ask Allah to help me stay on his straight path throughout my life and be a thankful slave.

TABLE OF CONTENTS

LIST OF TABLES

LIST OF FIGURES

Chapter 1

Introduction

1.1 Research Motivation and Objective

Recently there has been an increase in interest for autonomous distributed robotic systems whose tasks are executed not by a single robot, but by teams of collaborating robots, references [1.1-1.4]. Team members cooperate to: (1) explore unknown spaces; (2) exchange sensor information, (3) provide surveillance data, and (4) manipulate heavy objects. The teamwork required to accomplish these tasks cannot be done without effective and efficient communication between robot team members. Today, free-space laser communication systems have become an extremely accurate and reliable form of high-speed, wireless data transfer for many different applications [1.5-1.7]. The research reported on in this dissertation deals with the design and implementation of a laser-based communication system for cooperating autonomous mobile robots.

A free-space optical communication system includes both an optical transmitter and an optical receiver system. The transfer of information here is intended to be between two systems, with transmission being performed with optical rather than microwave radiation (RF). The advantages of an optical communication system compared to a microwave communication system in free space includes: (1) being capable of transmitting data at high speed, (2) low power consumption, (3) small size and weight, and (4) immunity to RF interference. However, optical communication systems become complex when they are required to carry out optical tracking and pointing [1.8-1.10].

Various scanning techniques have been implemented for acquiring and tracking signals transmitted and received optically, these include: (1) gimballing, (2) MEMS mirrors, (3) corner-cubes, and (4) Cat's-eye retroreflectors [1.11-1.14]. In the literature related to the design and application of Cat's-eye retroreflectors, Beer and Marjaniemi [1.15] present an excellent design of a Cat's-eye retroreflector system; one consisting of two mirrors. Their system performance was excellent at 10 degree full field and it attracted researcher's attention to the design of Cat's-eye retroreflectors. Later Cat's-eye designs were based on a solid sphere of glass [1.16, 1.17]. Although these solid sphere retroreflectors have unlimited fields of view (FOV), they do not allow for the inclusion of an optical modulator. Recently, Biermann *et al* [1.18] returned to and expanded the work of Beer and Marjaniemi by designing their Cat's-eye retroreflector from multiple lenses as opposed to glass spheres. Their design produced a diffraction-limited Cat's-eye retroreflector with a FOV of 30 degrees. It became apparent, from the literature, that if a retroreflector system was to be used with mobile robots, a new retroreflector design, one with a very large FOV, was required. The design must allow components to be placed near the focal region.

The research here proposes a wide-angle retroreflector design that simplifies the overall system and resolves some of the issues highlighted above. Retroreflector systems were designed from two separate lenses: (1) a Cat's-eye lens, and (2) a fisheye lens. The Cat's-eye lens retroreflects incident light whereas the fisheye lens expands the FOV of the retroreflector to nearly 180 degrees. The retroreflector device in this research was assembled using commercial "off-the-shelf" components and demonstrated a FOV of 120 degrees. This FOV was limited by the availability of the "off-the-shelf" fisheye lens apertures. The device allows enough space for a modulator of approximately 2mm thick to be placed into the system. A thorough examination of the literature indicates that no other researchers have used this approach for a retroreflector systems design.

In this research, the design and implementation of a wide-angle FOV retroreflector modulator device for robotic applications is presented. The device is simple and compact so

that it can be carried by a small robot. Currently, it can modulate and retroreflect a beam of incident light source at 1000 bit per second (1kbps). Other optical modulators with high speed modulation rates, such as MQW modulator [1.19-1.21], can be integrated into this retroreflector device. The effectiveness of this device for solving real life problem is demonstrated in two real applications: robot to robot optical communication and underwater communication.

The design of this wide-angle FOV retroreflector was executed using the Optalix and TracePro optical design programs. In addition a MATLAB routine was written to observe the behavior of the Cat's-eye lens retroreflection. Optics Software for Layout and Optimization (OSLO) lens design software was also utilized for analyzing and optimizing the design parameters. However, the description of the design is general so that an in-depth knowledge of these programs is not required in order to understand the results obtained.

1.2 Literature Review

Currently, in optical communication applications, retroreflectors are coupled with elector-absorptive "shutters" to modulate incident light in free-space optical communication. The reflected light is returned directly to the source along line-of-sight as an ON-OFF modulated signal, see Figure 1.1.

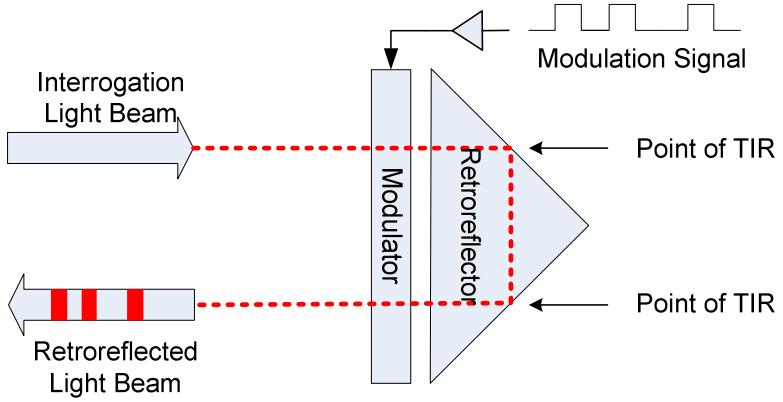

Figure 1.1 Generic modulating retroreflector example

One specific reason for implementing such a device is that only one of the platforms has an onboard laser, telescope, and tracker. Thus, the device is well suited to problems in which only one platform needs carry a large payload and can also serve as the interrogator. This interrogator illuminates the platform carrying the modulating retroreflector with a laser beam. The retroreflector modulator imposes a modulation on the interrogating beam and passively retroreflects it back to the interrogator. This system design is attractive for asymmetric communication links, applications where one end of the link cannot carry the weight, power and expense of a conventional free-space optical communication terminal.

There are two basic types of retroreflectors: (1) corner-cube reflectors (CCR's), see Figure 1.2, and (2) lens-and-mirror combinations, which are commonly termed Cat's-eye. Both systems share interesting and useful properties: (1) they are both completely passive, and (2) they retroreflect simultaneously the light from all sources within their FOV, but with a displacement separating the incoming and reflected rays.

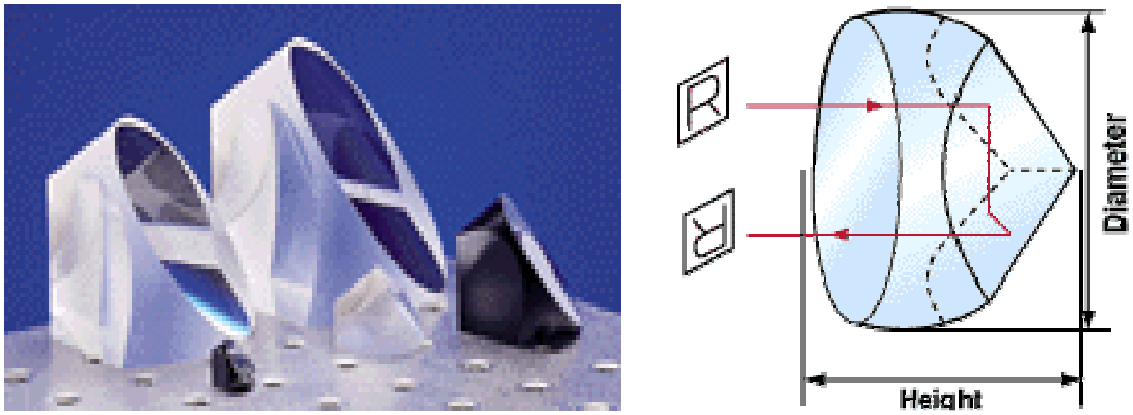

Figure 1.2 Corner-Cube-reflector (CCR) actual picture and technical image

CCR devices have good performance at data rates of 10 Mbits/s or less, but for higher data transmission rates Cat's-eye devices are preferable [1.21]. In addition, Cat's-eye reflectors have a wider acceptance angle than CCR's. This is one of the reasons that Cat's-eye was chosen for the research in this dissertation. In the next subsections: (1) a mathematical proof

of the retroreflection behavior of Cat's-eye is derived, and (2) a brief discussion of currently available wide-angle retroreflector devices and their performance is given. The chapter ends with a short description of a "fisheye-lens" and its behavior.

1.2.1 Retroreflector behavior of half-coated spherical lens (Cat's-eye)

A lens is a device that causes light to either converge or to diverge. Focusing and other effects are based on the angle of incidence of the light wave, related to the contour of the lens surface, and lens refractive index (lens dielectric constant). The light wave changes it path abruptly at two mediums interface.

At the interface between an optical medium '1' with refractive index n_1 and a medium '2' with index n_2 (Figure 1.3), Snell's law of refraction (Willebrord Snell, 1580–1626 [1.20]) is valid:

$$n_1 \sin(\theta_1) = n_2 \sin(\theta_2) \qquad \textbf{(1-1)}$$

where θ_1 *and* θ_2 are called the angle of incidence and angle of emergence at the interface.

To trace a ray of light in an optical system, matrices are used as a powerful tool to study geometrical optics. Based on two major assumptions: (1) the wavelength, λ, is negligibly small in comparison to lens aperture, and (2) incident rays are paraxial rays, i.e., close to and almost parallel to optical axis, such matrices are linearized, thereby simplifying the mathematical analysis. This becomes obvious for a linearized form of the law of refraction, equation 1-2.

$$n_1 \theta_1 \cong n_2 \theta_2 \qquad \textbf{(1-2)}$$

A free light ray is treated like a straight line. In optics, systems with axial symmetry are especially important, and an individual light ray is described by the distance from the optical axis and the angle to the surface normal. Therefore, to study the retroreflector behavior of a Cat's-eye, a half-coated spherical lens of radius r and refractive index n is considered. Assuming a light ray has a measured distance (y_1) from the axis and an angle of incident θ_1, the reflected ray will be displaced from the optical axis by distance (y_2) and have an angel θ_2, see Figure 1.3.

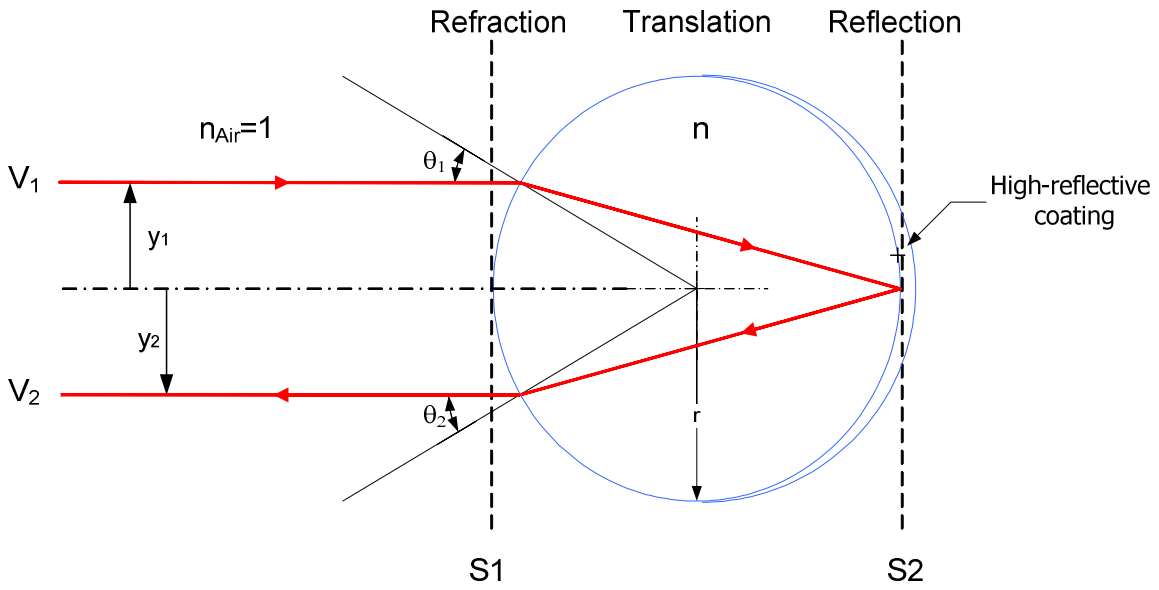

Figure 1.3 Retroreflectivity behavior of Cat's-eye lens

Using the matrix method, an optical system can be described by the system matrix M or ABCD matrix, which is a function of the optical elements only:

$$\begin{bmatrix} y_2 \\ V_2 \end{bmatrix} = \begin{bmatrix} A & B \\ C & D \end{bmatrix} \begin{bmatrix} y_1 \\ V_1 \end{bmatrix} \qquad \textbf{(1-3)}$$

The system matrix M for the spherical lens is written as a set of translation, refraction and reflection matrices, and these matrices apply as the ray passes through the system. This system of matrices is described by equation 1-4.

$$M = \underbrace{\begin{bmatrix} 1 & 0 \\ \dfrac{-(-n_{air}+n)}{+r} & 1 \end{bmatrix}}_{refraction\,S2} \underbrace{\begin{bmatrix} 1 & \dfrac{-2r}{-n} \\ 0 & 1 \end{bmatrix}}_{translation\,S2} \underbrace{\begin{bmatrix} 1 & 0 \\ \dfrac{-(-2n)}{-r} & 1 \end{bmatrix}}_{reflection\,S2} \underbrace{\begin{bmatrix} 1 & \dfrac{2r}{n} \\ 0 & 1 \end{bmatrix}}_{translation\,S1} \underbrace{\begin{bmatrix} 1 & 0 \\ \dfrac{-(n-n_{air})}{+r} & 1 \end{bmatrix}}_{refraction\,S1}$$
$$= \begin{bmatrix} \dfrac{n-4n_{air}}{n} & \dfrac{-4r}{n} \\ \dfrac{2n_{air}(-2n_{air}+n)}{nr} & \dfrac{n-4n_{air}}{n} \end{bmatrix} \quad \textbf{(1-4)}$$

Under normal atmospheric conditions the refractive index in air varies between 1.00002 and 1.00005. Therefore, when using $n_{\text{air}} = 1$ for air medium and $n = 2$ for the lens material, the matrix M becomes:

$$M = \begin{bmatrix} -1 & -2r \\ 0 & -1 \end{bmatrix} \quad \textbf{(1-5)}$$

This leads to V_2=-V_1. In addition, since paraxial rays are considered, an approximation can be applied to small angles, i.e., $V_i = n_i \sin\theta_i = n_i \theta_i$. Knowing that, $n_2 = n_1 = n_{air}$, then $\theta_2 = -\theta_1$. Therefore, this spherical lens acts as a retroreflector.

Yongbing *et al* [1.22] studied the Cat's-eye parameters that result in a minimum divergence angle of the reflected beam. These parameters are shown in Figure 1.4. In order to realize the function of retroreflection, i.e., to make the reflected light parallel to the incident light, the following equation must be satisfied:

$$\theta_1 = \theta_2 + \theta_3 \quad \textbf{(1-6)}$$

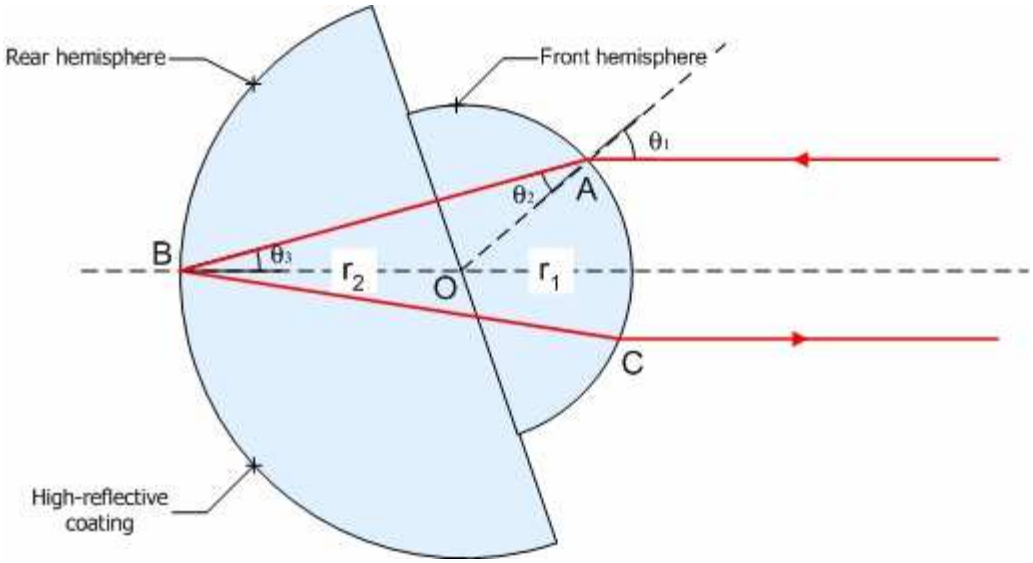

Figure 1.4 Analyses of Cat's-eye parameters for least divergence of the reflected beam

According to the law of refraction, the incident and refracted rays are governed by

$$\frac{1}{n} = \frac{\sin(\theta_2)}{\sin(\theta_1)} \approx \frac{\theta_2}{\theta_1} \qquad \textbf{(1-7)}$$

Applying the Sine Rule to the triangle ΔABO gives:

$$\frac{OA}{OB} = \frac{r_1}{r_2} = \frac{\sin(\theta_3)}{\sin(\theta_2)} \approx \frac{\theta_3}{\theta_2} \qquad \textbf{(1-8)}$$

From the above three equations, 1-6, 1-7 and 1-8, the following expression can be derived:

$$r_2 \approx \frac{r_1}{n-1} \qquad \textbf{(1-9)}$$

Equation 1-9 shows that r_1 and r_2 depend only upon the refractive index n. Therefore, when n=2, r_1 equals r_2, which means that the Cat's-eye becomes a sphere. The spherical Cat's-eye

retroreflector is therefore free of the problems associated with the misalignment of the centers of two hemispheres, and it is also free from any undesirable effects of the adhesives used to join two hemispheres.

1.2.2 Wide-angle retroreflector devices

Currently in use are open-air corner cubes with an acceptance angle of $\pm 20^{o}$, corner cube prisms with an acceptance angle of $\pm 50^{o}$, and a Cat's-eye with an acceptance angle of $\pm 60^{o}$ [1.23], see Figure 1.5.

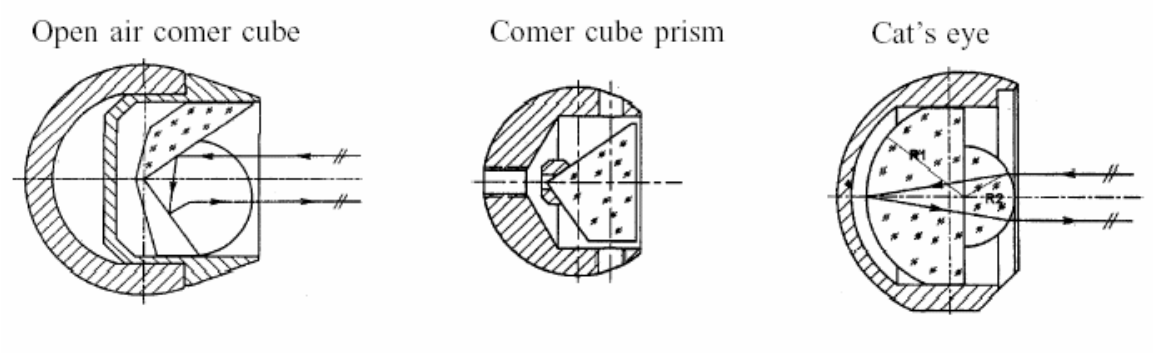

Figure 1.5 Different types of retroreflector [1.23]

Unless a large aperture modulator is used with these retroreflectors, the FOV of such reflectors will be reduced dramatically. Unfortunately, the modulation speed is limited by the RC time response of the modulator device and is inversely proportional to the aperture size of the modulator [1.19]. Hence, the dilemma is how to design a wide-angle retroreflector that uses a small optical modulator with an acceptable efficiency.

Arrays of smaller retroreflectors are often used to obtain a large reflecting area or an increase in FOV. Figure 1.6 shows two examples of such an arrangement. A multiple corner-cube reflectors arranged with common vertices as building blocks [1.24] and array of 5

retroreflectors arranged on an umbrella-type that provides a maximum FOV of about ±60 degree [1.21].

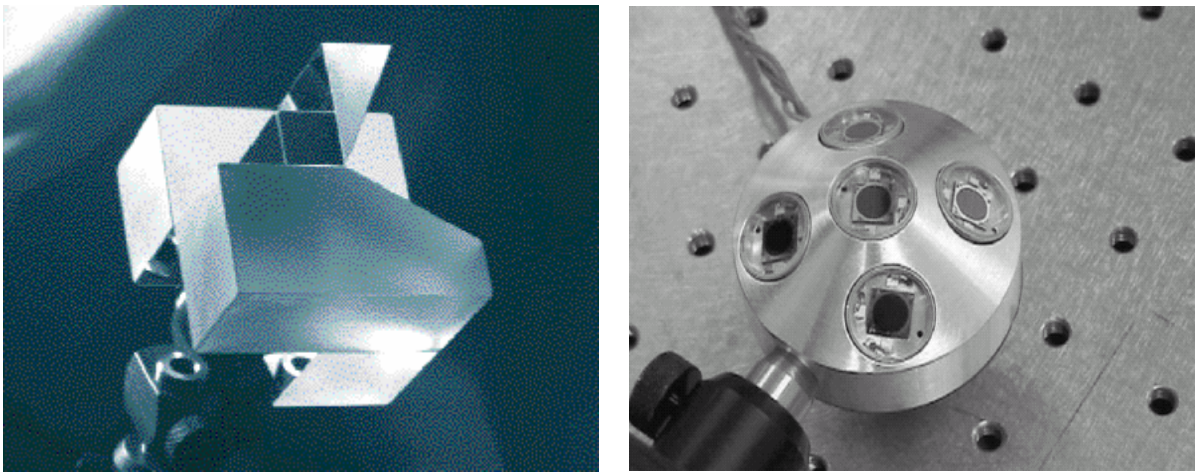

Figure 1.6 Arrays of smaller retroreflectors with a special arrangement to increase device FOV

Although, these complicated retroreflectors partially resolved the problem of expanding FOV, when they reflect coherent radiation, each element in the array acts as a separate source. As a consequence, an interference pattern is produced in the return beam. In addition, the rising complexity of the device when integrated with a modulator: (1) increases weight, and (2) power consumption, become challenging issues. This engineering trade-off must be addressed.

1.2.3 Fisheye lenses

Maxwell's fisheye lenses [1.25] are spherical inhomogeneous spheres that belong to the class of complete, perfectly focusing optical systems. The standard Maxwell form of the spherical symmetric index of refraction is given in [1.26]. The governing equation is:

$$n(r) = \frac{2}{1+(r/R)^2} \qquad \textbf{(1-10)}$$

decreasing from a value of $n(0)=2$ at the center to $n(R)=1$ at the outer surface. Here, r is distance from the center of the sphere to a point in the sphere and R is the radius of the sphere.

Because these lenses are free of geometric aberration, people are trying to reproduce fisheye lenses by GRIN (graded index) technology [1.27-1.30]. A fisheye lens generally has a front lens group with a larger negative refractive power than that of an ordinary inverted telephoto type wide-angle lens. An example of a commercial fisheye lens made by Nikkor manufacture [1.31] is shown in Figure 1.7. Notice how several lenses were compound together to mimic the behavior of a true fisheye.

Figure 1.7 Fisheye-Nikkor 6mm f/2.8

The power of a fisheye lens for wide-angle use is that it allows light flux to be distributed in small areas at the edges of the FOV. This is very obvious from the fisheye simulation demonstration obtained from OSLO optics software, see Figure 1.8. From Figure 1.9, a comparison of the two pictures of the same scene with and without a fisheye lens. Notice the

scene around the edge of the picture how the fisheye lens captured more FOV than a normal lens.

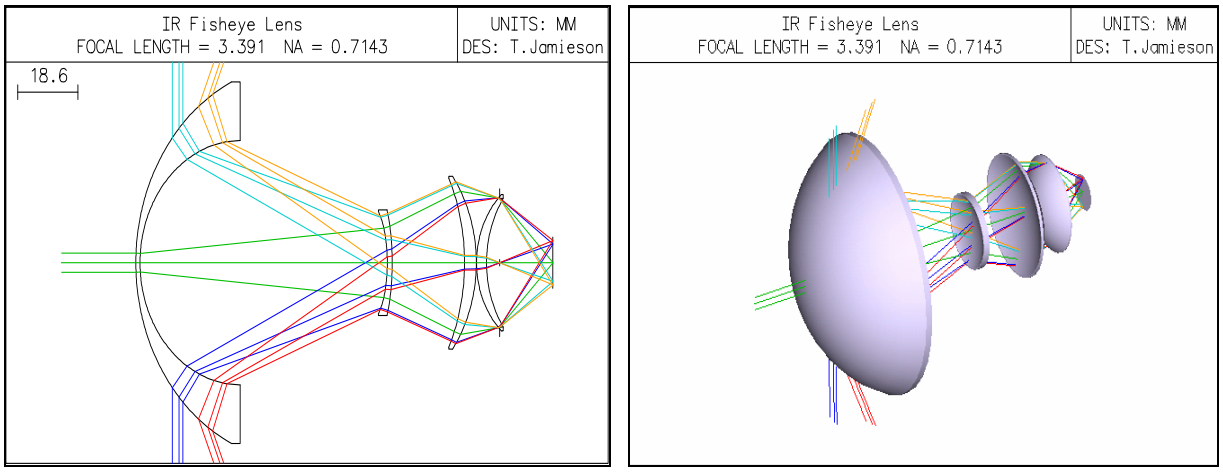

Figure 1.8 OSLO demo of Fisheye lens in photographic system

In conclusion, a retroreflector design using a Cat's-eye lens is shown in this chapter to have a small FOV, especially when a modulator is placed at the front aperture. A Fisheye lens offers a perfect solution to the small FOV limitation of the Cat's-eye retroreflector, and expands its FOV significantly. Obviously, the fact that these two lenses interact with incident light differently is a major contributing factor to their FOV performance. So, before integrating these two separate lenses into one system, to form a wide FOV retroreflector device, an in-depth study was required to explore the performance and the limitations of the lenses.

Figure 1.9 Pictures of a garden taken with normal camera lens (top) and with fisheye lens (bottom)

The dissertation is structured as follows: Chapter 1 presented a literature review on retroreflector technology and fisheye lens. Chapter 2 presents a proposed design and

performance analysis of a wide-angle retroreflector. Chapter 3, briefly, elaborates on two modulator devices and their performances. Chapter 4 concentrates on the design and implementation of a practical optical communication system that uses the retroreflector designed in Chapter 3. Lastly, in Chapter 5 an experimental setup and preliminary results are obtained from autonomous mobile robots communication experiments. Robot localization trials with the system show that the optical communication system shows that it is effective within a limited range. The results also indicate that the performance obtained was limited by the robot sensors and control algorithms, and with a need to expand the optical communication system hardware and software to extend the range of application. That is, a controlled gimballing system and light detection search algorithm must be developed in the next phase of the research.

1.3 *References*

[1.1] Galeotti, J. "The EvBot: a Small Autonomous Mobile Robot for the Study of Evolutionary Algorithms in Distributed Robotics." Master Thesis in Electrical and Computer Engineering. North Carolina State University, 2002.

[1.2] Evans, W., J. Jennings, and G. Whelan. "Cooperative Search and Rescue with a Team of Mobile Robots." *IEEE International Conference on Advanced Robotics* (1997).

[1.3] Kumar, V. *Introduction to Robotics*. Course Material at University of Pennsylvania.1998 <http://www.seas.upenn.edu/~exen695/>.

[1.4] Kelly, A. *Introduction to Mobile Robot*. Course Material, 1996 <www.frc.ri.cmu.edu/~alonzo/cource>.

[1.5] McGillen, C. and T. Rappaport. "Infrared Location System for Navigation of Autonomous Vehicles." *IEEE International Conference on Robotics and Automation*

(1988).

[1.6] Tsumura, T. “Improving Positioning, Guidance, System and Communication Technology of AVCS by Optics.” *IEEE Conference on Intelligent Transportation System* (1997). 765-768.

[1.7] Hollar, S. “COTS Dust.” Master Thesis in Mechanical Engineering, University of California, Berkeley, 2000.

[1.8] Shinhak Lee, James W. Alexander, and Muthu Jeganathan, "Pointing and tracking subsystem design for optical communications link between the International Space Station and ground", *Free-Space Laser Communication Technologies XII, Proc. SPIE*, January, 2000.

[1.9] M. Last, B. S. Leibowitz, B. Cagdaser, A. Jog, L. Zhou, B. Boser, and K. S. J. Pister, “Toward a wireless optical communication link between two small unmanned aerial vehicles,” in *Proc. IEEE International Symposium on Circuits and Systems*, Bangkok, Thailand, 2003.

[1.10] Bernhard Epple “Development and Implementation of a Pointing, Acquisition and Tracking System for Optical Free-Space Communication Systems on High Altitude Platforms”, diploma thesis, Institute of Computer Science, LMU, Munich, 2005.

[1.11] Komatsu, N., H. Okubo, and T. Tsumura. “A 3-D positioning and Attitude Measurement System Using Laser Scanners and Corner Cubes.” *IEEE/RSJ International Conference on Intelligent Robots and Systems, Yokohama, Japan* 1 (1993): 604-611.

[1.12] Minato, A., Y. Sasano, and N. Sugimoto. “Optical Design of Cube-corner Retroreflectors having Curved Mirror Surfaces.” *Applied Optics* 31 (1992): 6015-6020.

[1.13] Khan, J., K. Pister, and L. Zhou. Corner-Cube Retroreflectors Based on Structure-Assisted Assembly for Free-Space Optical Communication. Berkeley: University of California, 2002.

[1.14] Aoki, N., N. Komatsu, and T. Tsumura. “Vehicle to Vehicle Optical Two Way Communication by Use of Laser and Corner Cube.” *IEEE InternationalConference on Intelligent Transportation System* (1997). 787-790.

[1.15] R. Beer and D. Marjaniemi, “Wavefront and construction tolerances for a cat’s-eye retroreflector,” *Applied Optics*, 5(7), 1191-1197 (1966).

[1.16] O. Nakamura, M. Goto, K. Toyoda, N. Takai, T. Kurosawa, and T. Nakamata, ‘‘A laser tracking robot-performance calibration system using ball-seated bearing mechanisms and a spherically shaped cat’s eye-retroreflector,’’ *Rev. Sci. Instrum.* **65(**4), 1006–1011 (1994).

[1.17] T. Takatsuji, M. Goto, S. Osawa, R. Yin, and T. Kurosawa, ‘‘Wholeviewing-angle cat’s-eye retroreflector as a target of laser trackers,’’ *Measurement Science and Technology*, **10**, N87–N90 (1999).

[1.18] M. L. Biermann, W. S. Rabinovich, R. Mahon, and G. C. Gilbreath, "Design and analysis of a diffraction-limited cat's-eye retroreflector," *Opt. Eng.* **41**(7), 1655–1660 (2002).

[1.19] US Naval Research Laboratory, “Large-Aperture Multiple Quantum Well Modulating Retroreflector for Free-Space Optical Data Transfer on Unmanned Aerial Vehicles”, *Society of Photo-Optical Instrumentation Engineers* (2001).

[1.20] Wikimedia Foundation, Inc. http://en.wikipedia.org/wiki/Snell's_law

[1.21] W. S. Rabinovich, R. Mahon, H. R. Burris, G. C. Gilbreath, P. G. Goetz, C. I. Moore, M. F. Stell, M. J. Vilcheck, J. L. Witkowsky, L. Swingen, M. R. Suite, E. Oh, and J. Koplow, “Free-space optical communications link at 1550 nm using multiple-quantum-well modulating retroreflectors in a marine environment”, *Optical Engineering* - Volume 44, Issue 5, 056001 (12 pages) May 2005.

[1.22] Lin Yongbing, Zhang Guoxiong and Li Zhen, “An improved Cat’s-eye retroreflector used in a laser tracking interferometer system”, *Measurement Science and Technology* 14 (2003) N36-N40.

[1.23] Yang, B., Friedsam, H., “Ray-tracing studies for a whole-viewing-angle retroreflector”, *International Workshop on Accelerator Alignment* 1999, Grenoble (FR), 10/18/1999--10/22/1999 ; PBD: 2 Feb 2000

[1.24] Edouard Schmidtlin of *NASA's Jet Propulsion Laboratory*, Pasadena, California**,** Refer to NPO-20174, NASA Tech Briefs (1997).

[1.25] J.C. Maxwell, “Solution of problems,” *Cambridge and Dublin Mathematics Journal* **8**, 188 (1854).

[1.26] Uslenghi, P., “Electromagnetic and optical behavior of two classes of dielectric lenses**”,** *IEEE Transactions on Antennas and Propagation*, Volume: 17 Issue: 2, Page(s): 235- 236, Mar (1969)

[1.27] J. M. Gordon, "Spherical Gradient-Index Lenses as Perfect Imaging and Maximum Power Transfer Devices ," *Appl. Opt.* **39**, 3825-3832 (2000)

[1.28] J. Kumler and M. Bauer, “Fisheye lens designs and their relative performance,” *Proceedings of the SPIE*, 4093, 360-369 (2000).

[1.29] G. Remus and V. D. P. Sastri, "Fisheye field spectrograph (ET)," *Appl. Opt.* **17**, 3076 (1978).

[1.30] D. T. Moor, “Gradient-index Optics: A Review”, *Applied Optics* **19**, No. 7, Page(s): 1035-1038, (1980).

[1.31] Malaysian Internet Resources, http://www.mir.com.my/rb/photography/companies/nikon/nikkoresources/fisheyes/6mmf28.htm

[1.32] BermanGraphics, http://bermangraphics.com/digicam/fisheye.htm

Chapter 2

Wide-Angle Retroreflector Design

2.1 Simulation of Cat's-Eye Retroreflector

To simulate and study Cat's-eye retroreflectivity behavior, commercial software packages for optical design were investigated. These included Roadrunner, Synapsis and Optalix. However, OSLO proved to be the best suited to this research, mainly because of its user-friendly interface and its large lens library. So, the first test with retroreflector design was by using OSLO-EDU software, even although it has restrictions on its number of surfaces and features.

Figure 2.1, shows simulation results for a spherical lens retroreflector. The simulation results indicate that the optimal refractive index of the spherical lens is less than two ($n \approx 1.93$). It shows that only incident light passing through the center of the retroreflector is returned along the original incident path. The off-axis light is reflected with a small divergence angle included. Consequently it causes the returned laser beam to be either convergent or divergent.

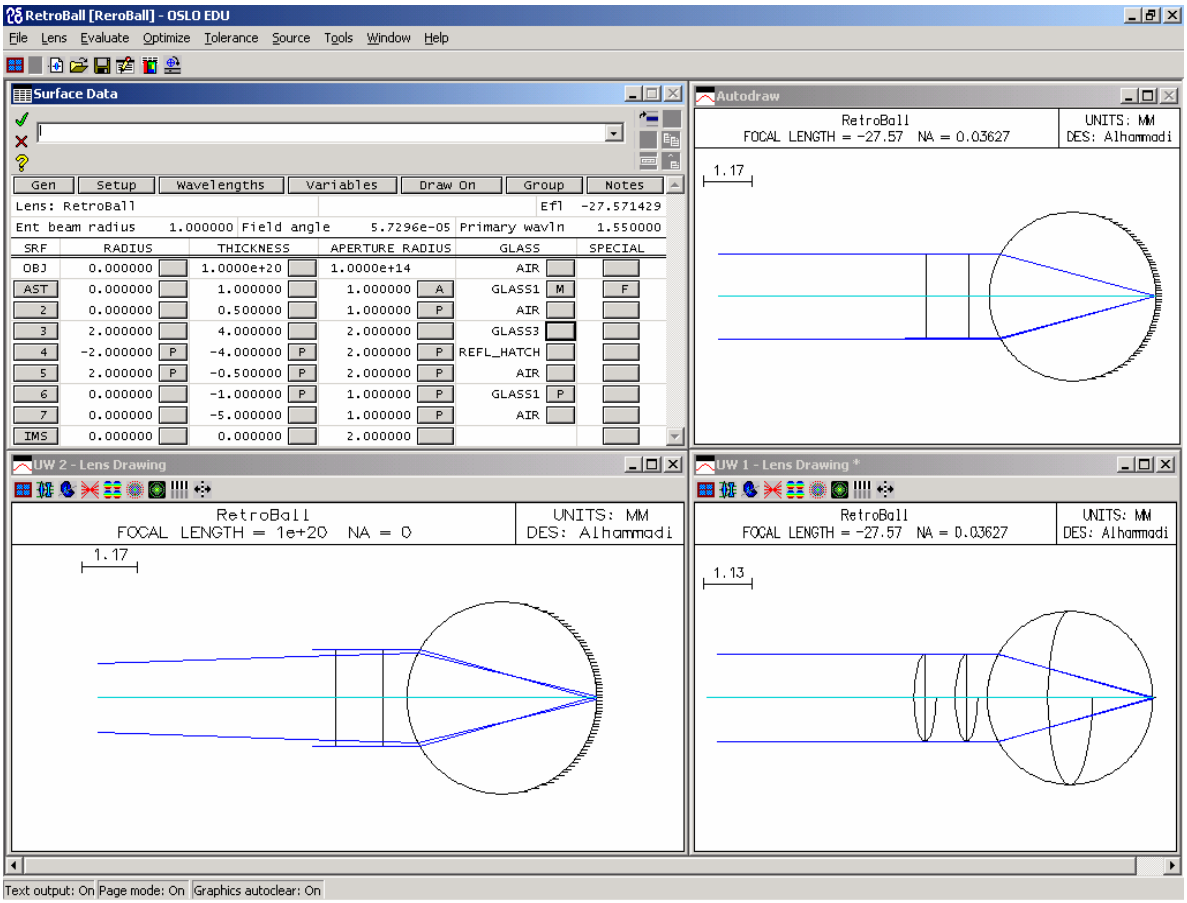

Figure 2.1 Retroreflector simulation of Cat's-eye spherical lens

2.2 In Depth Look on Cat's-Eye Performance

2.2.1 Cat's-eye efficiency

To study the efficiency of the reflectivity of a Cat's-eye retroreflector, Takatsuji *et al* reference [2.1] described a whole-viewing-angle Cat's-eye retroreflector, one that was uniformly covered with a coating of reflectivity *R*. The retroreflector reflectivity R_{Total} becomes equation 2-1:

$$R_{Total} = R(1-R)^2 \quad \textbf{(2-1)}$$

R_{Total} takes its maximum value of 0.148 when R = 0.333; in other words, it functions as a retroreflector with a reflectivity of 14.8%.

However, when the spherical surface is not coated; the reflectivity R of the boundary is expressed according to Fresnel's formula, equation 2-2:

$$R_{fresnel} = \left(\frac{n_1 - n_2}{n_1 + n_2}\right)^2 = \left(\frac{1-2}{1+2}\right)^2 = 0.111 \quad \textbf{(2-2)}$$

Using equation 2-2, the retroreflector reflectivity becomes R_{Total} = 0.0877. This means that less than 9% of the incident light will be reflected. Adding reflective coating to lens surface increases Cat's-eye reflectivity more than 50%. Hence, to maximize Cat's-eye reflectivity, one should coat part of the Cat's-eye with high reflective coating and other part with anti-reflection coating.

Here, a Cat's-eye with high reflective coating at the rear hemisphere was used. Assuming the 100% surface reflectivity from the coating, the retroreflector reflectivity of the half-coated Cat's-eye will be

$$R_{Total} = (1 - R_{fresnel})^2 = 0.79 \quad \textbf{(2-3)}$$

Where, R has the same value that was obtained above from Fresnel's formula above. This means that about 80% of the light beam will be reflected.

The above discussion shows that to achieve high retroreflective efficiency with these lenses, the back of the lens must be coated with a high reflective material. Under perfect conditions, the reflected beam could reach 80% of the incident beam. Therefore, in this work, the

spherical lens was half-coated with high reflective material. In addition, the retroreflective efficiency depends on the spherical lens refractive index. In section 2.2.2, a discussion on selecting the optimal refractive index to minimize the divergence in a reflected beam is presented. This selection maximizes the detected optical signal at the receiver.

2.2.2 Suggestions to improve Cat's-eye performance

Every conventional lens has an optical axis normal to the plane of symmetry, i.e., normal to the surface. When the direction of the optical beam is not parallel to the optical axis of the lens, a variety of optical aberrations arise. Such aberrations, spherical, coma or astigmatism could degrade the ultimate performance of the lens. A Cat's-eye lens is a type of biconvex (spherical) lens that suffers from these aberrations. A brief discussion of theses aberrations is given in Appendix A1.

In ray-tracing studies for a whole-viewing-angle reroreflector, Yang and Friedsam [2.2] show that Cat's-eye retroreflector has an annular light cone with a sharp boundary. Also, they proved that the retroreflector opening angle depends only on the refractive index of the sphere. This refractive index reaches its optimal value when:

$$n = 2 - 1.19\,\delta^{2/3} \tag{2-4}$$

for a given beam divergence δ. With this optimal refractive index, the minimum radius of Cat's-eye sphere is given as:

$$R_{\min} \approx \frac{\rho}{4\sqrt{\frac{2-n}{3}}} \tag{2-5}$$

where ρ is the radius of the acceptance aperture, i.e. incident laser beam radius. Yang and Friedsam's study proves that Cat's-eye lenses suffers from spherical aberrations for beams that do not satisfy the above relation.

Another interesting nonlinear relation for Cat's-eye retroreflectors exists between the ratio of beam height-lens radius (*h/R*) and beam divergence angle, as found in the Yongbing [2.3] study;

$$\theta_{div} = 2\sin^{-1}\left(\frac{h}{R}\right) - 4\sin^{-1}\left(\frac{h}{nR}\right) \qquad \textbf{(2-6)}$$

This nonlinear relationship imposes a restriction on the Cat's-eye radius, as shown in Figure 2.2. For example, in order to have a divergence angle less than 2mrad in the reflected beam, Cat's-eye radius must be at least 5 times the radius of the incident beam. In this research, an 8mm spherical lens and a 3mm laser beam diameter was used. According to Figure 2.2, the expected divergence of the reflected beam is no less than 13mrad. The overall reflected beam divergence will be more if the incident beam divergence and the modulator aperture diffraction were included. Decreasing the aperture dimension improves the retroreflected beam divergence, but reduces the optical system efficiency. Therefore, this optical system is not practical for long-range applications that require a beam divergence less than 0.1mrad.

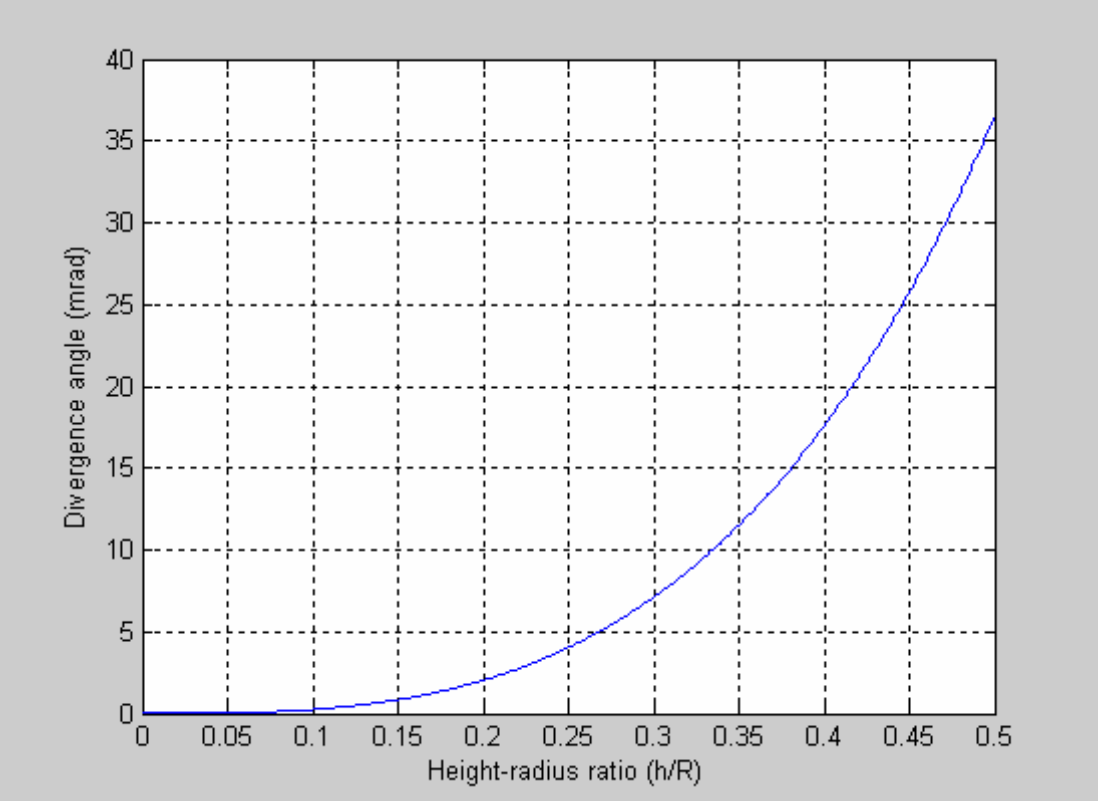

Figure 2.2 Nonlinear relation between h/R and beam divergence angle in Cat's-eye retroreflectors

To tackle the beam divergence problem and improve retroreflective efficiency, the spherical aberration of the Cat's-eye lens should be eliminated prior to it being integrated into the retroreflector modulator device. Therefore, a skew raytrace program was written in MATLAB, based on a technique developed by Lin [2.4, 2.5], to study Cat's-eye lens behavior on incident and reflected rays, see Appendix C1. Figure 2.3 illustrates the effect of Cat's-eye on the reflected beam. Rays further away from the optical axis retroreflected with a divergence angle larger than those closer to the optical axis. This aberration is called spherical aberration it is common in optical systems that use spherical lenses. In other words, a Cat's-eye lens works best with paraxial rays. That is why most authors in the literature [2.2, 2.3] recommended increasing the Cat's-eye radius in order to reduce its spherical aberrations.

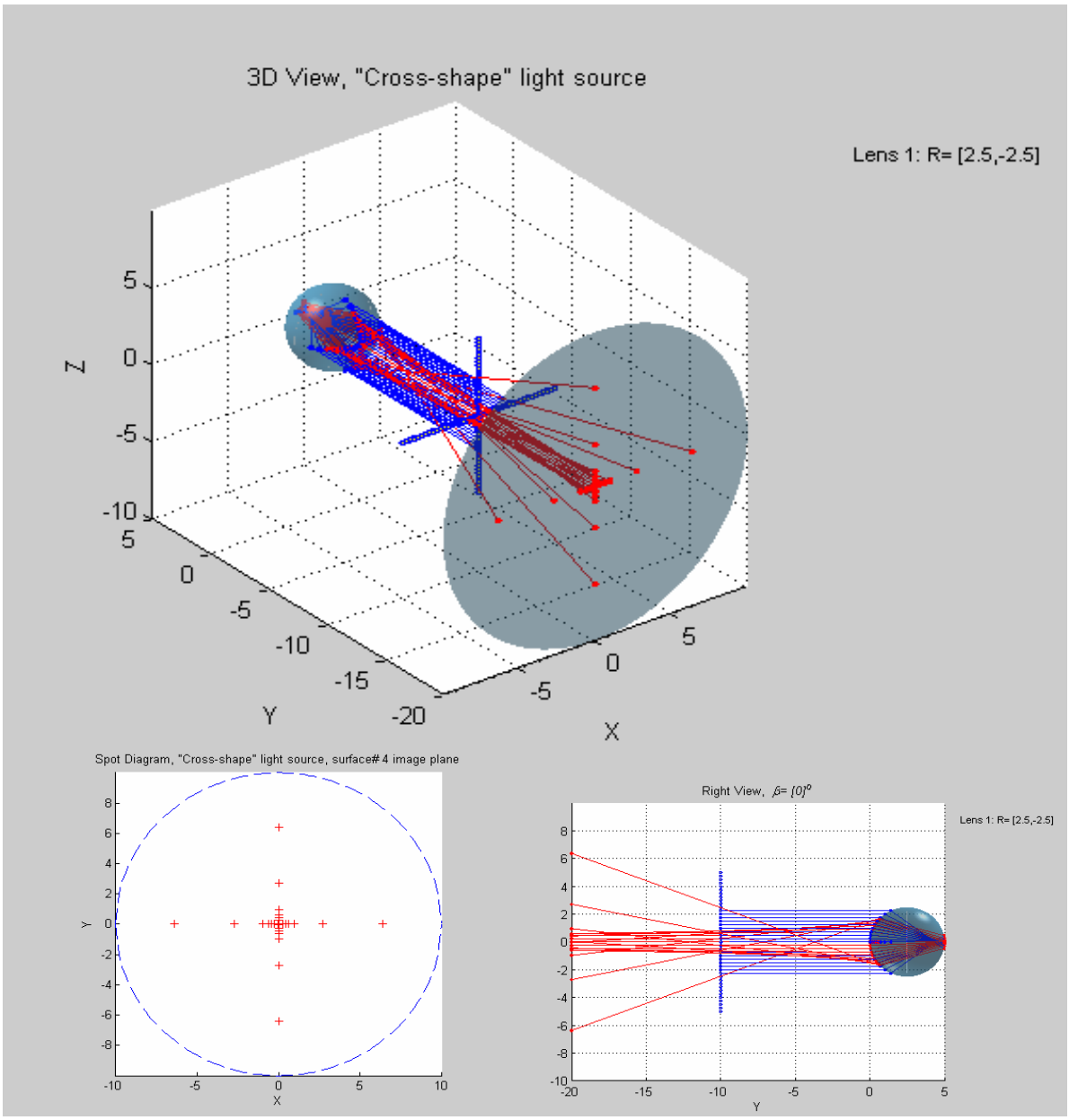

Figure 2.3 Aberration effect of Cat's-eye lens on a reflected beam

In this research, two solutions were considered to correct the described aberrations by using: (1) GRIN spherical lenses, and (2) achromatic lenses. The first proposed solution utilizes the unique feature of "GRadient-INdex" (GRIN) spherical lenses. In these lenses, there is no abrupt physical interface between two materials with different indices of refraction; rather, there is a gradient in the index of refraction. Therefore, to solve Cat's-eye problems and

increase its efficiency using this technology, the GRIN profile for aberration-free Cat's-eye needs to be obtained.

The general expression of the divergence angle θ_{div} of the returned light for two hemisphere Cat's-eye lens is given in [2.3] as:

$$\theta_{div} = 2\sin^{-1}\left(\frac{h}{r_1}\right) - 2\sin^{-1}\left(\frac{h}{nr_1}\right) - 2\sin^{-1}\left(\frac{h}{nr_2}\right) \quad \textbf{(2-7)}$$

where h is the height of the incident light and r_1 and r_2 are the radii of the Cat's-eye's two-hemispheres. It is clear that the divergence angle is dependent on the parameters r_1, r_2, h and n. By equating the equation 2-7 to zero and having $r_1 = r_2$, the GRIN profile equation for a free-aberration spherical Cat's-eye is obtained from:

$$n = 2\cos\left(\frac{\sin^{-1}(h/r)}{2}\right) \quad \textbf{(2-8)}$$

Figure 2.4 shows a curve of the proposed GRIN profile and shows the expected reflected rays from spherical GRIN Cat's-eye. The refractive index starts at 2 at the center of the sphere and ends with $\sqrt{2}$ at the outer surface when the trajectory of the GRIN profile is followed. Theoretically, a GRIN Cat's-eye will retroreflect the entire incident beam, within its aperture, free of divergence. Unfortunately, there is very little success in fabricating spherical GRIN lenses with current technology [2.6, 2.8].

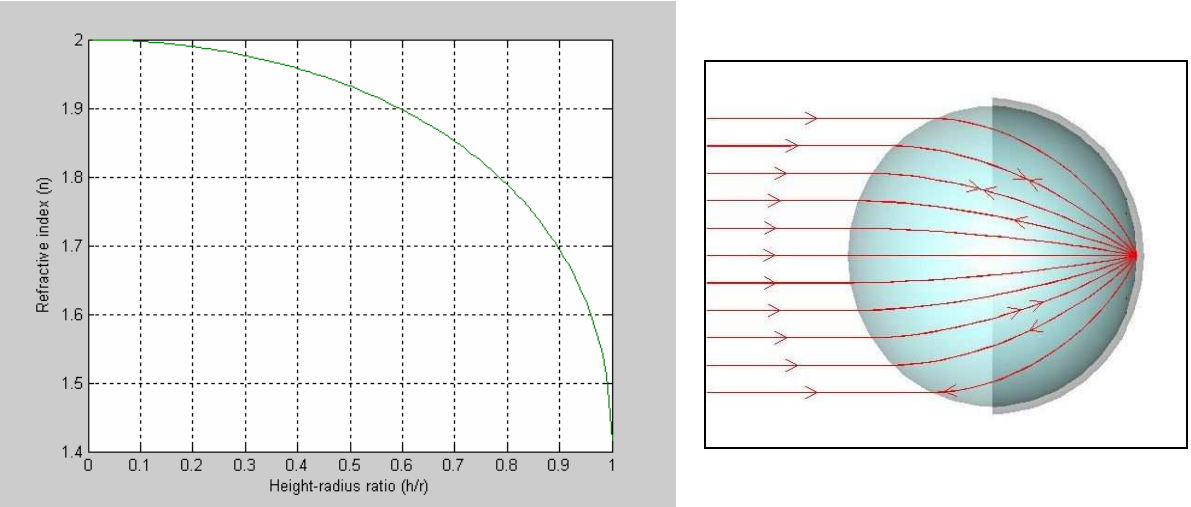

Figure 2.4 Proposed GRIN profile of Cat's-eye lens and the expected reflected rays

The second proposed solution uses of an achromatic lens placed in front of a Cat's-eye lens. Any focusing lens suffers from spherical aberration such that the beam is not focused at a single point at the focal point; rather it is focused on a spot. Unlike achromatic lenses, they are designed to eliminate this focusing drawback. Utilizing this achromatic characteristic, a perfect retroreflector device can be designed by placing the center of Cat's-eye at the focal point of an achromatic lens. Ideally, the reflected beam will have a zero divergence angle and no ray displacement. This design approach was simulated with a MATLAB ray-trace program and is shown in Figure 2.5. The advantages of this approach are the increase in power efficiency and a small optical modulator can be placed on front of Cat's-eye. Unfortunately, this design had one major drawback; it was very sensitive to beam incident angles. Any departure from the zero incident angle steered the focal point away from the Cat's-eye center and resulted in total loss of the reflected beam. Since the design objective is to increase retroreflector FOV, this approach was rolled out.

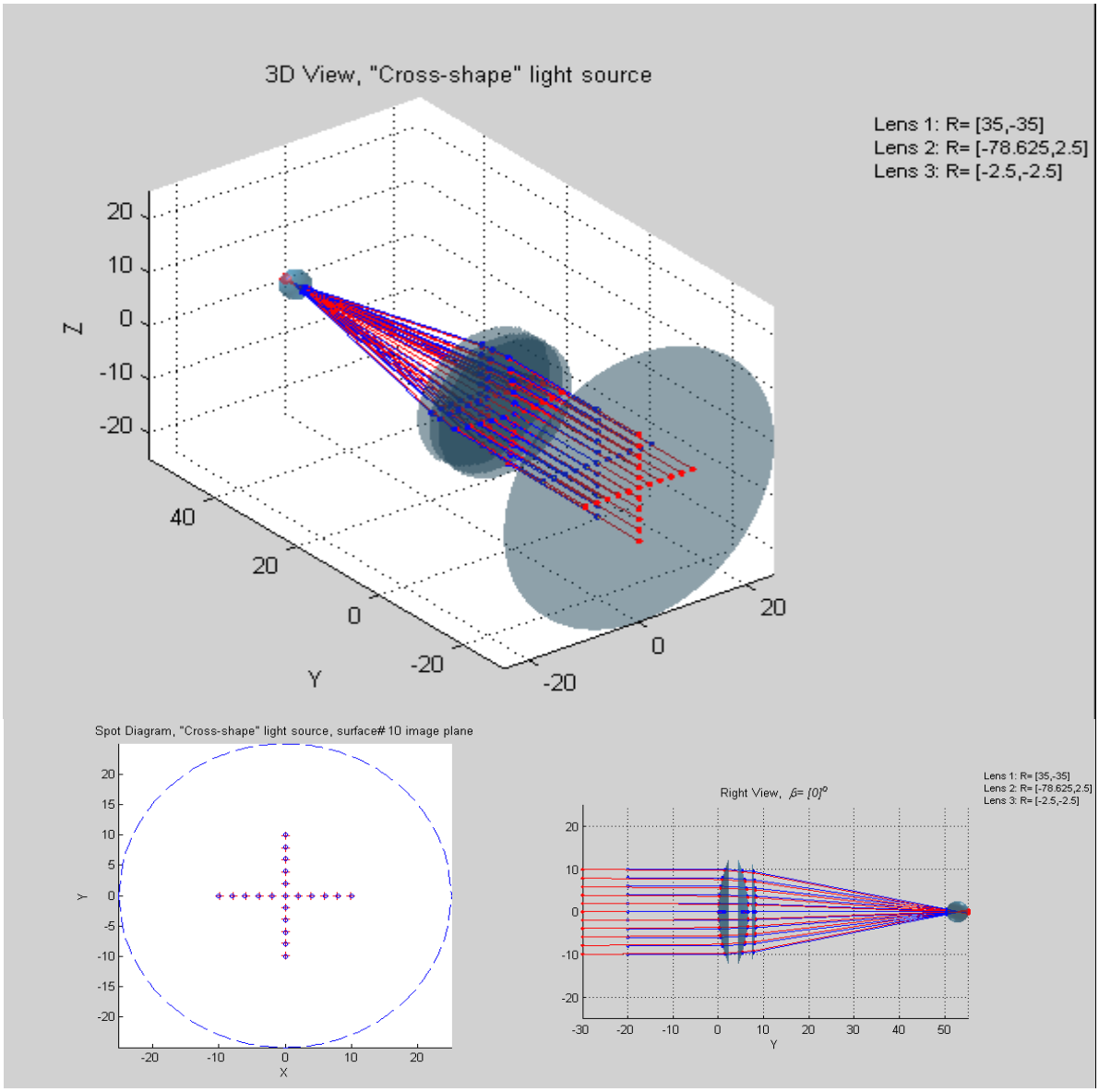

Figure 2.5 Improved retroreflectivity of Cat's-eye lens with the use of achromatic lens

2.3 Cat's-Eye and Fisheye Lenses for Wide-Angle Retroreflector Design

Prior to writing the MATLAB skew raytrace program, a commercial software package for optical design, called OptaLix, was used. The software helped greatly in designing and analyzing the transmission and the beam divergence of the new retroreflector. OptaLix was also used in testing MATLAB skew raytrace results.

Several design schemes were attempted in order to obtain the optimum performance for the proposed retroreflector device. Figure 2.6 shows an optical system consisting of meniscus, planoconcave, biconvex and cat's-eye lenses. All lenses were designed from LASF35 glass, which has a refractive index of 2. Although, the resulting beam divergence angle was high (~ 60mrad), the field-of-view of the retroreflector was nearly 180 degree. The spot diagram is taken at distance 2m from the front lens.

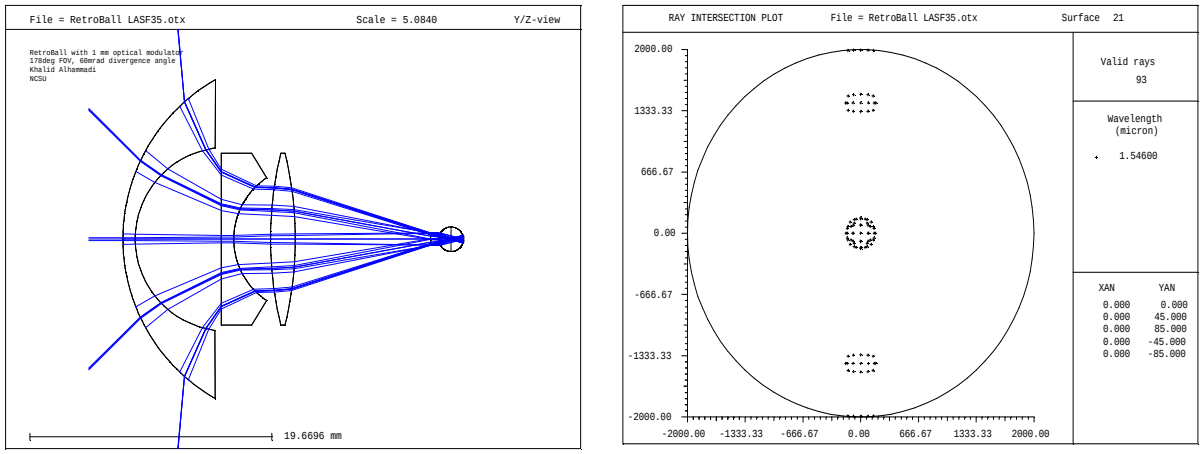

Figure 2.6 Retroreflector made of LASF35 glass with refractive index=2

Another simple design, as illustrated in Figure 2.7, was made of SF11 glass (n=1.77). The resulted FOV and beam divergence changed little from the previous design.

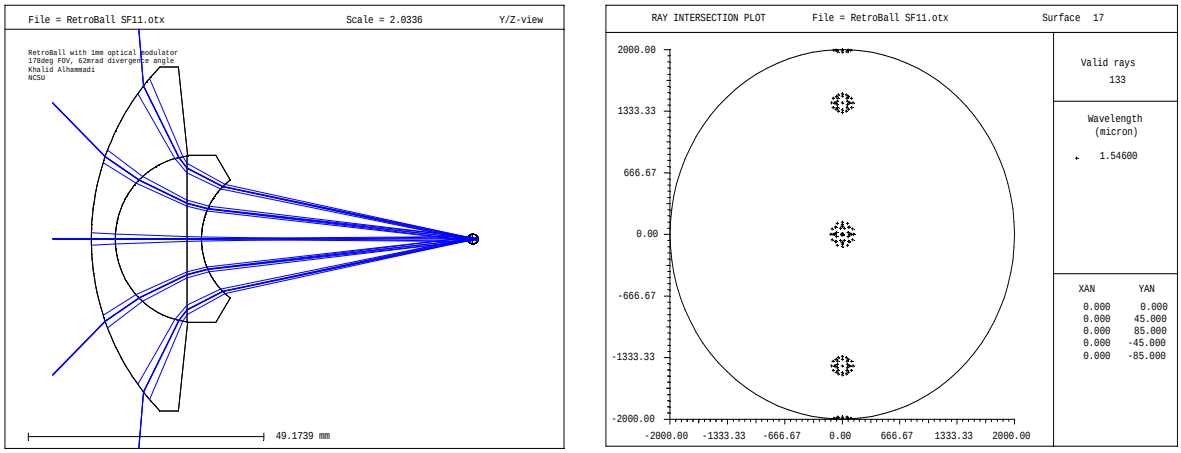

Figure 2.7 Retroreflector made of SF11 glass (refractive index= 1.784714)

From these two design schemes, and other schemes tested, two main points were observed. First, the meniscus lens plays a major role in increasing the FOV of the retroreflector. However, the optical modulator aperture and its thickness limited this FOV. Second, the divergence of the retroreflected beam is initiated by the Cat's-eye lens and increased through the meniscus lens.

Based on the above observations, the design was further simplified to consist only on the three main components, the modulator, and meniscus and Cat's-eye lenses. Figure 2.8 shows the proposed retroreflector device and its wavefront analysis. The overall system performance was excellent and a 150 degrees FOV was achieved. The design also provides ample space in front of Cat's-eye lens to insert different types of optical modulator.

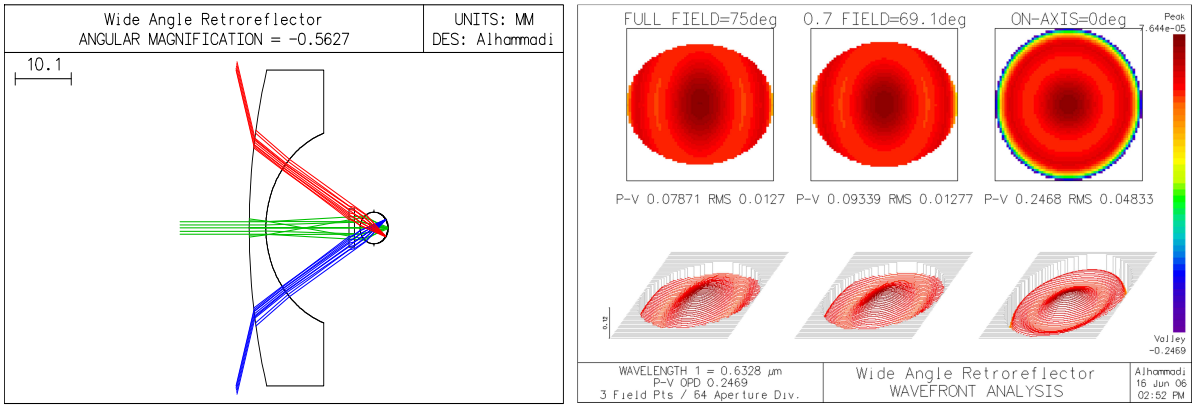

Figure 2.8 Proposed retroreflector design made of LASF35 glass (left) and its wavefront map (right)

In geometrical-optics theory a definition of aberration-free performance is that the system gives the same image performance by real-ray calculations as it does by paraxial calculations. Often the aberrations of a conventional optical system, consisting of lenses and mirrors, is evaluated by tracing paraxial marginal and chief rays through the system and calculating the sum of wavefront aberrations based on the paraxial parameters at each surface.

Ideally all aberrations should be minimized, but often there are trade-offs to be made. What determines the trade-offs among the design parameters is the eventual application. Unlike photographic systems, retroreflectors are used in optical communication with a monochromatic light source, i.e., no need for color correction. The main objective of the retroreflector is to give a uniformly strong return across the entire field of view of the device. Therefore, during the designing of a retroreflector with maximum FOV, minimizing wavefront error and astigmatism aberration to reduce beam divergence was the designer's main focus.

Wavefront error for an afocal system is a special case, owing to the fact that rays cannot be traced to the image surface. Therefore, the wavefront error is calculated at the exiting surface of the system. Figure 2.8 also shows a wavefront analysis for the designed retroreflector device, obtained using OSLO. In Figure 2.8, P-V is peak to valley error and RMS is root-mean-squared error. RMS error is the merit for testing system performance, since every ray

in the reflected beam has its unique divergence angle. The on-axis error is near 0.25mm P-V, which is about 0.05mm RMS wavefront error. However, the off-axis aberration is around 0.012mm RMS. Low wavefront error provides excellent light return. It is obvious that the aberration of on-axis wavefront is relatively larger than the off-axis wavefront due to the increase in beam height at the Cat's-eye aperture. The on-axis beam height is larger than the off-axis height; hence the divergence introduced by the Cat's-eye lens on the reflected beam is higher. This result is also confirmed by the plotted curves in the left part of Figure 2.9.

Astigmatism is related to the field curvature at the image surface (the last surface in this design). It occurs in the reflecting rays when the incident rays make an appreciable angle with the optical axis of the system. Figure 2.9 shows ray-trace analysis of the system. The astigmatism of the retroreflector was within 40mm for the tangential and sagittal planes at the edge of the field.

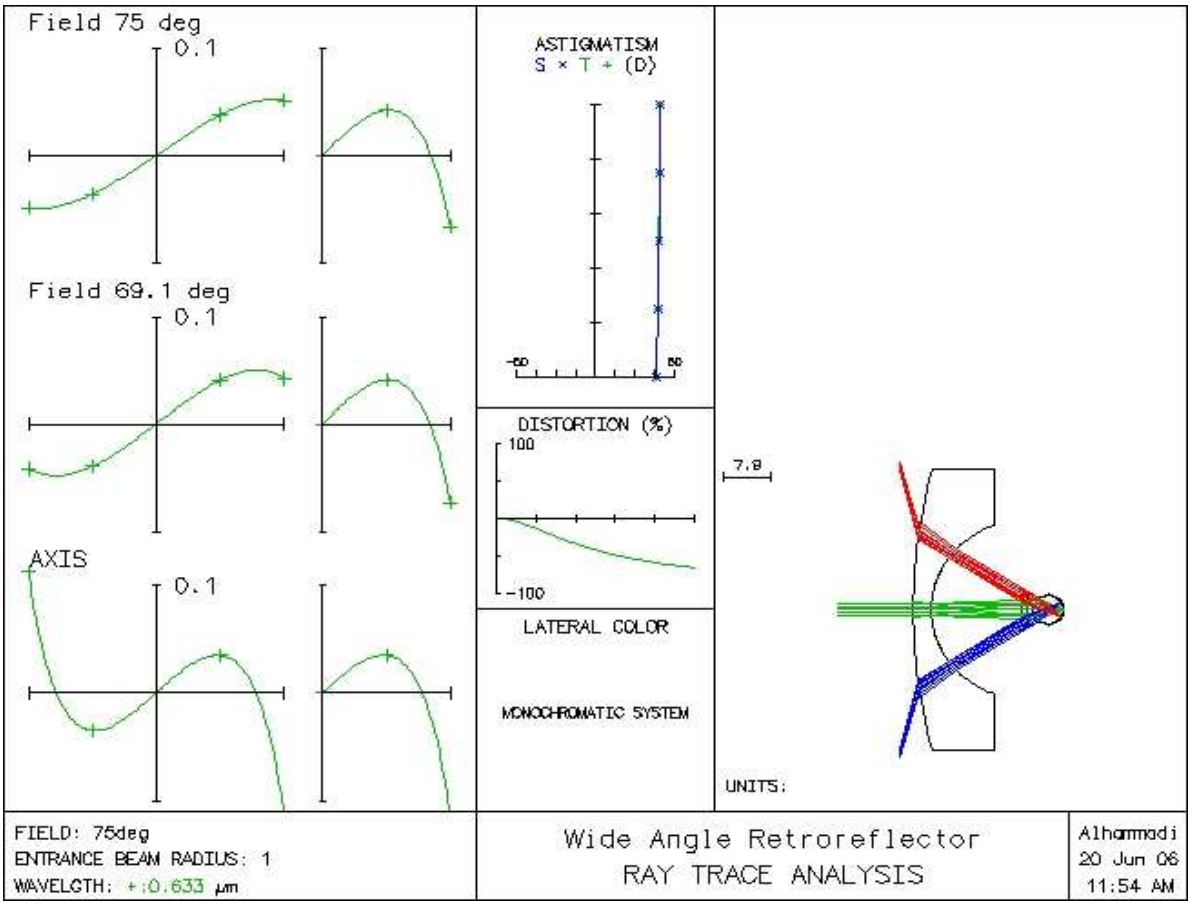

Figure 2.9 Performance of the retroreflector design with respect to various aberrations. Wavefront error as a function of aperture at different field angles (left). Ray-trace analysis (right)

It is worth noting that the above wavefront analysis is based on perfectly spherical lens surfaces. If the lens surfaces are not perfectly spherical then the wavefront errors will be different. In most cases the errors will be worse.

Using a MATLAB skew ray-trace program gave more control for optimizing the design parameter and clear graphical behavior for every ray. A 3D view of the retroreflector system is shown in Figure 2.10. A cross-shape of incident light (blue) is illuminating the retroreflector and retroreflected back (red) onto the image surface. Notice how the reflected light is diverged but most of its energy is contained close to the center of the incident beam.

The top view of the system and the spot diagram plot show the behavior of the system in greater detail.

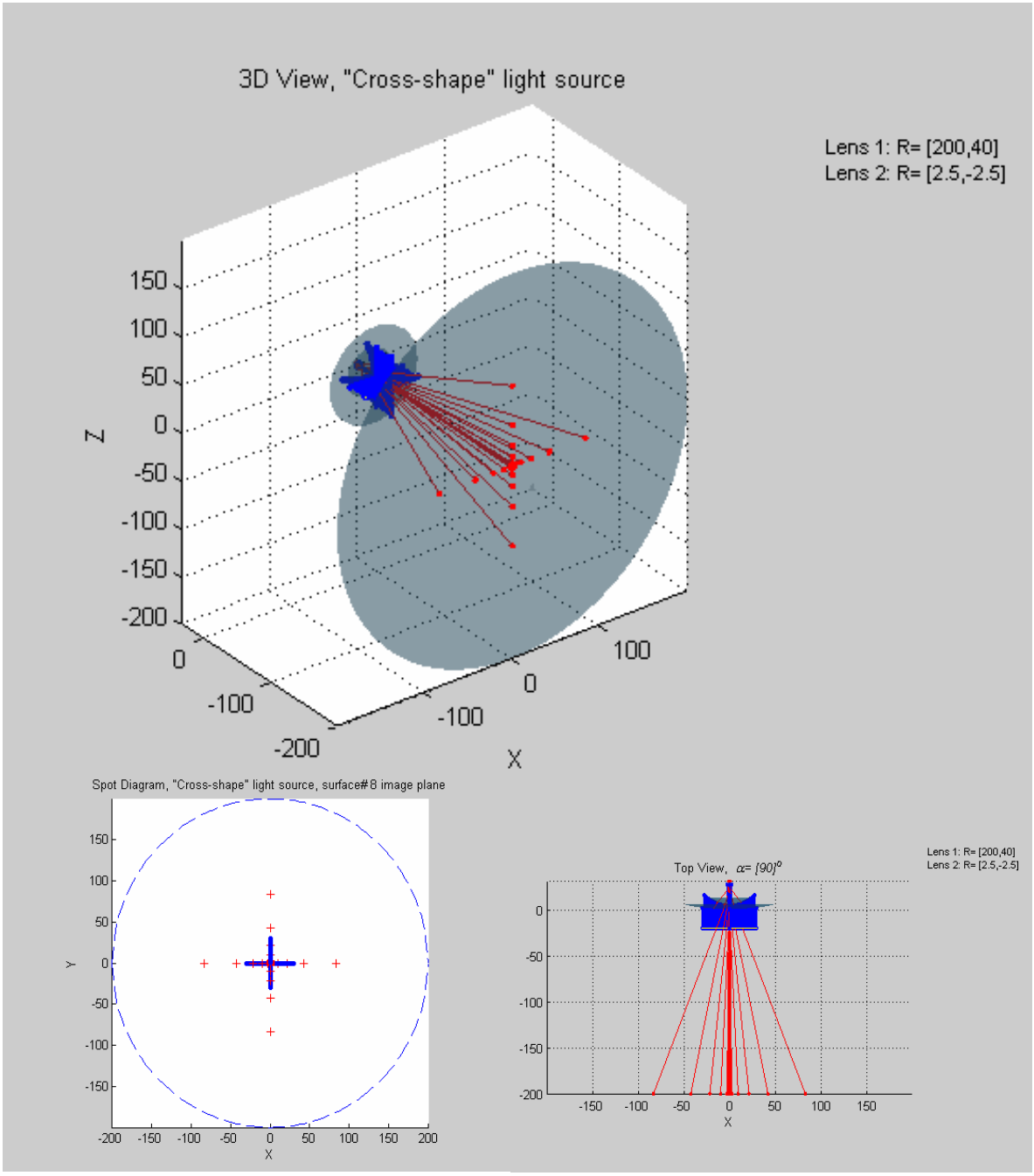

Figure 2.10 The proposed system when tested with cross-shape light source

Since every ray in the reflected beam has its unique divergence angle, the Root-Mean-Square (RMS) spot radius was chosen as the merit for testing the system performance. The RMS radius is a statistical measure that tests how well the energy is concentrated on the image surface. An ideal retroreflector will return a beam of light identical to the incident beam along the angle of incidence. In an afocal system, such as this, the RMS spot radius is a better indicator of performance than Geometric spot radius (spot size), which is simply the radius within which all of the energy falls. Appendix A2 elaborates more on RMS calculation and the minimum number of data needed to obtain valid results.

Using RMS spot radius of the reflected beam, one can study the relationship between beam's incident angle and its divergence angle. The simulation results on Figure 2.11 shows how an increase in a beam's incident angle increases the divergence in the reflected beam.

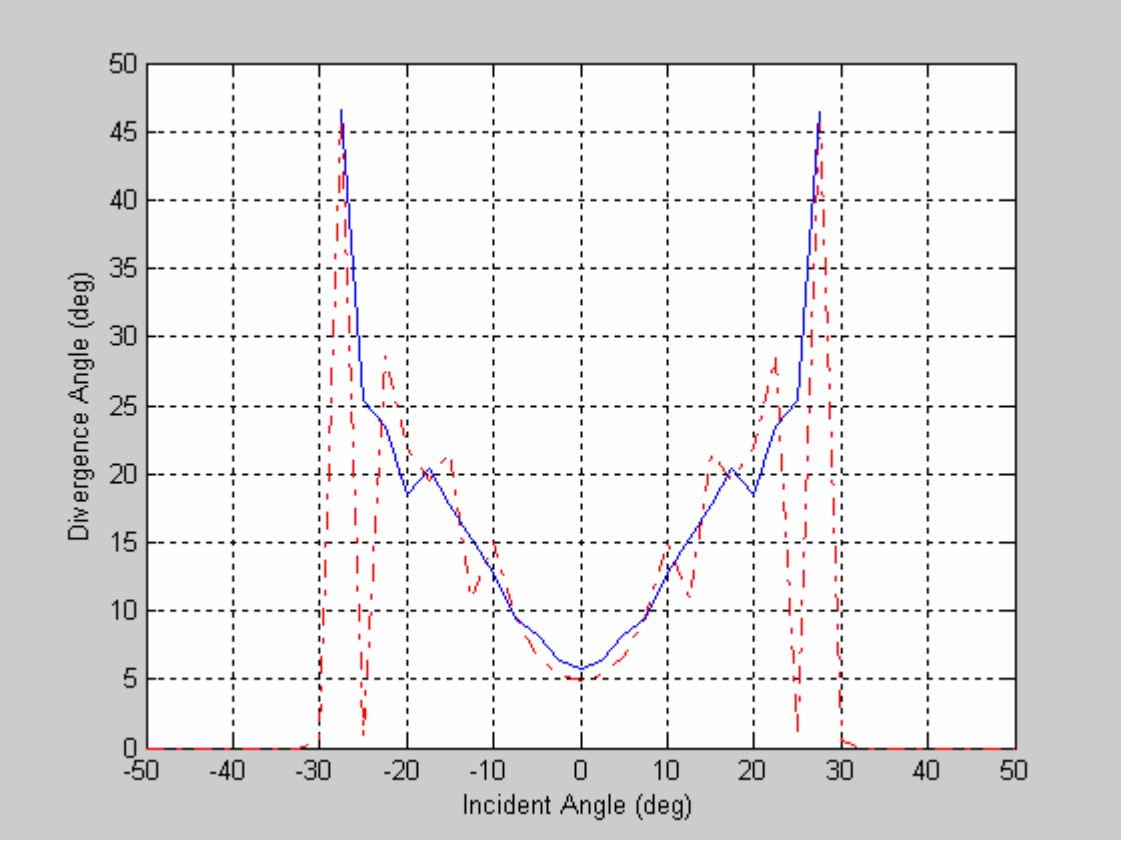

Figure 2.11 Exponential relationship between incident and divergence angles

The intensity of the reflected beam is also greatly affected by changes in beam incident angles. Figure 2.12 shows the reflected power being degraded exponentially as a result of an incident beam being deviated from the normal incidence. The value of the transmission is very dependent on the lens coating, beam splitter, beam divergence, reflector and detector size, etc. However, in simulation, it depends strongly, in addition to the above, on the number of rays traced through the system.

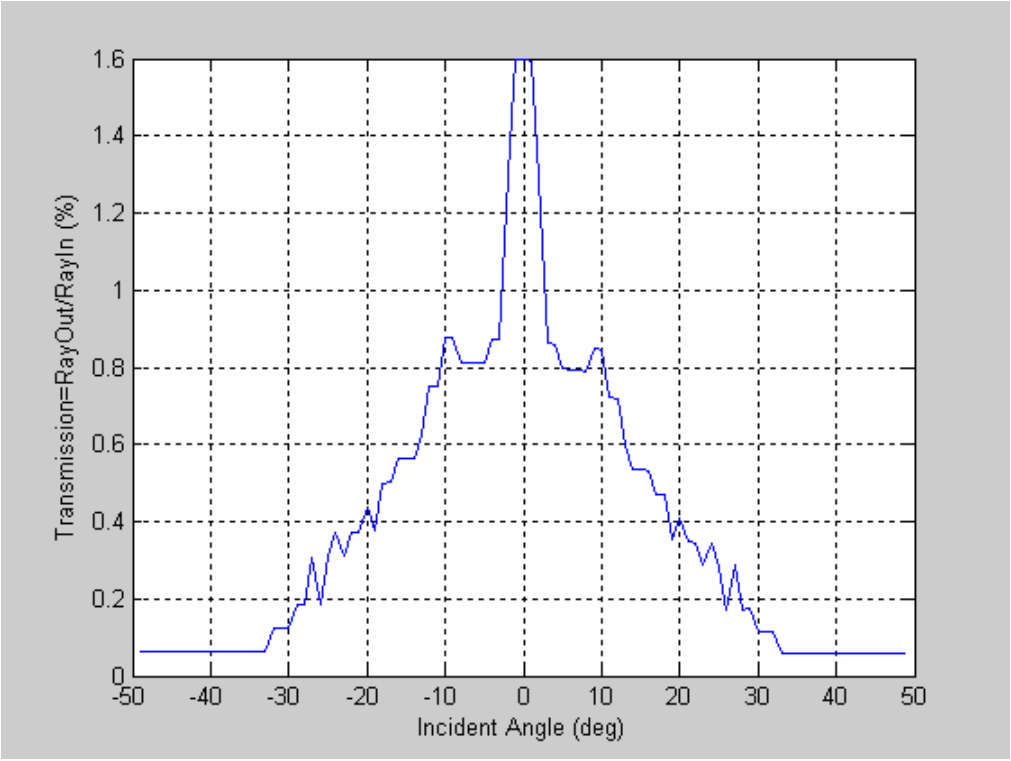

Figure 2.12 Effect of the beam incident angle on the reflected beam power

2.4 Experimental Setup

Searching for an off-the-shelf negative meniscus lens that fitted the design parameters was not an easy task. On the other hand, customized lenses are very expensive especially when ordered in small quantity. Therefore, the closest available meniscus lens to the designed parameters was purchased. Figure 2.13 shows TracePro simulation of the retroreflector

design with the purchased lens specifications. In the plot, the red lines are the incident rays at 60 degrees incident angle and the green lines represent the retroreflected rays. With this design, ray-trace simulation of the design shows that the full FOV of the device was limited to 120 degrees. The main reason was due to the aperture constrained of the purchased meniscus lens. We believe that increasing the aperture-radius ratio of the meniscus lens will increase the devices FOV. Radius, thickness, and glass information of the design parameters are listed in Table 2.1.

Table 2.1 Prescription data for the system design. All surfaces are spherical

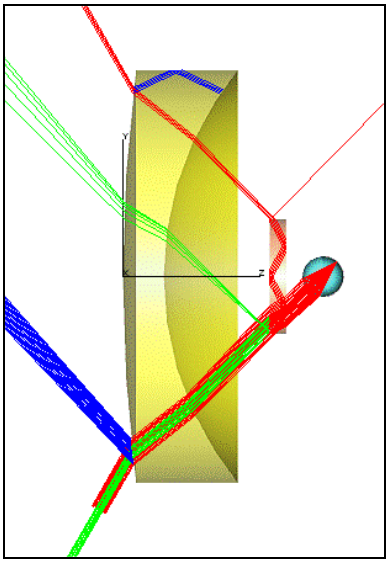

Surface number	Radius of Curvature, (mm)	Thickness (mm)	Aperture Radius (mm)	Glass type
1	200	5	25	Bk7
2	40	13	25	Air
3	∞	2	5	Bk7
4	∞	2	5	Air
5	2.5	5	2.5	LASF35
6	-2.5	__	2.5	Mirror

Figure 2.13 TracePro simulation of the retroreflector design with off-the-shelf lenses (rays at 60 degree incident angle)

A Cat's-eye lens and an optical modulator were simply packed together by a mounting adapter. Then, the fisheye lens was integrated to the package using a lens holder of 2 inches in diameter. Figure 2.14 illustrates the parts and the assembly order of the device packaging with a picture of the device including an LCD-type modulator. The overall package of the retroreflector is relatively small in size and weight.

The retroreflector device has a clear aperture of 25mm in diameter. The numerical aperture for the system is about 0.11, giving an infinity f-number to be f/4.5. It is better to have large a numerical aperture to collect as much incident light as possible. The overall diameter of the modulator aperture is 14mm.

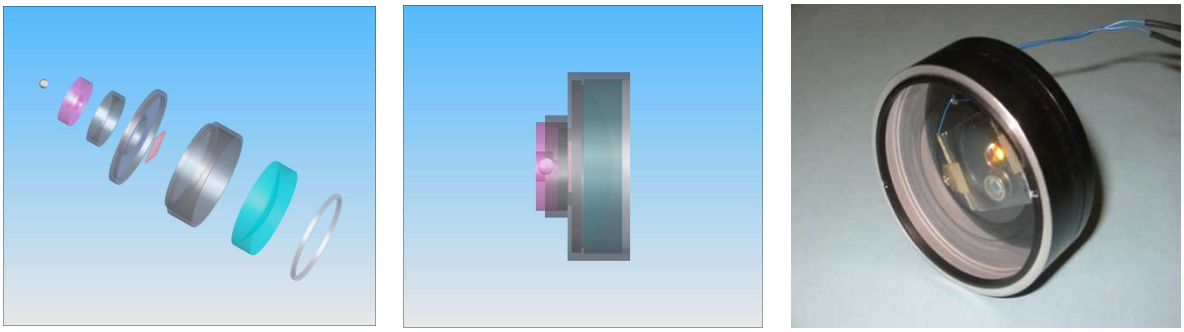

Figure 2.14 Assembly of the retroreflector device and an actual image of the device

Optical components are responsible for transmitting, modulating, deflecting, and detecting light beam. A schematic drawing of the optical system setup that was used in testing the performance of the assembled retroreflector device is shown in Figure 2.15. The retroreflector system was mounted on a rotation stage, so that by rotating the stage, the incident angle of a light beam can be altered. The optical modulator was replaced by a beam chopper to modulate the incident light. Figure 2.16 shows pictures of the experimental setup.

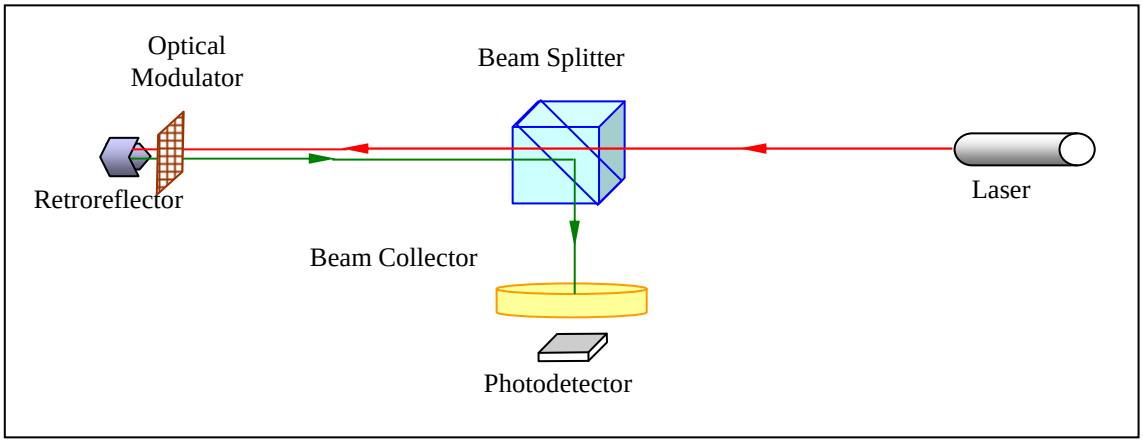

Figure 2.15 Optical components in retroreflector experimental setup

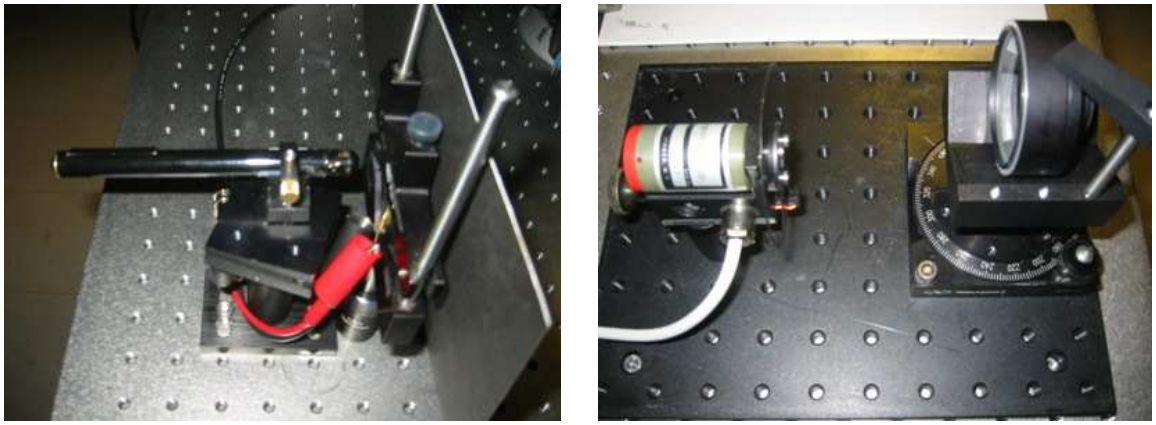

Figure 2.16 Experimental setup of laser pointer (left) and retroreflector with beam shutter (right)

In these experiments, a 50% beam splitter and focusing lens were added to record the reflected beam intensity by a photodetector. The light source used was a commercial laser pointer of a power less than 5 mwatts. The exact measure of the laser power was 3.5 mwatts. The utilization of the laser pointer in the current experiment has multiple advantages, from eye safety to being a small-size and low power consumption device. Table 2.2 outlines some characteristics of this laser pointer [2.9].

Table 2.2 Laser Pointer Characteristics

Class (CDRH standards)	IIIA Diode Laser
Full Divergence Angle	15 mrad (measured)
Max Output Power	Max < 5 mWatts (3.5 mW measured)
Wavelength	650 nm ± 10
Input Power	30 mA @ 12V with R_{limit}=284Ω

Two sets of experiment were conducted. First set was to obtain the full field-of-view of the retroreflector device. The second set was to determine the maximum working range of the device.

2.5 Retroreflector Preliminary Results

To test for the width of the FOV of a retroreflector device, and for effect that a changing laser beam incident angle has on the performance of the optical system, an extensive series of experiments was carried out. The main objective was to obtain the relationship between the beam incident angle and the retroreflected light intensity, to determine the range of the device at which it is suitable for real applications that require a large FOV.

2.5.1 Retroreflector FOV experiment

To carry out with the first set of experiments, the retroreflector device (as a target) was placed 7 feet away from a laser source. The laser source illuminated the retroreflector with a light beam passing through a small hole in a white board. Using a commercial-based digital camera, several pictures were taken for the reflected beam spot on the white board. It is clear from Figure 2.17 that the beam spot at zero incident angle is bright and circular. Since spherical aberration is common in optical systems that use lenses, fringe (concentric light circles) thickness was not equal in each beam spot. As the incident angle increased, the intensity of the retroreflected light spot was reduced and astigmatism was introduced in the direction of the rotation. Astigmatism is the limiting aberration with respect to field FOV. Above 60-degree incident angle, the reflected light was clipped by the edge of the lens holder and the light spot diminished.

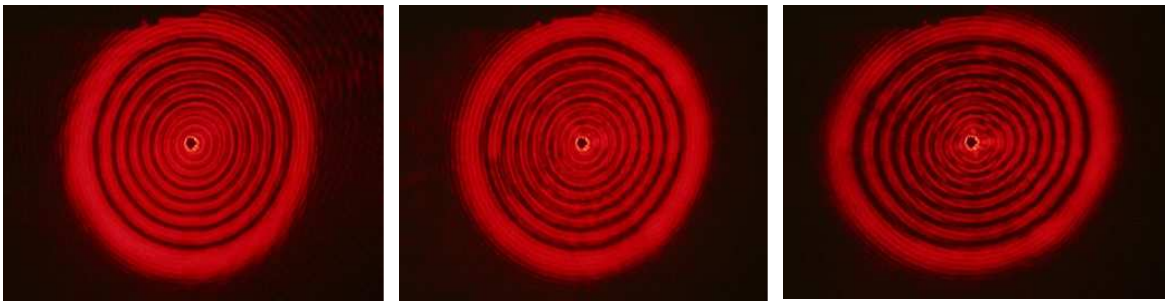

0° incident angle 20° incident angle 40° incident angle

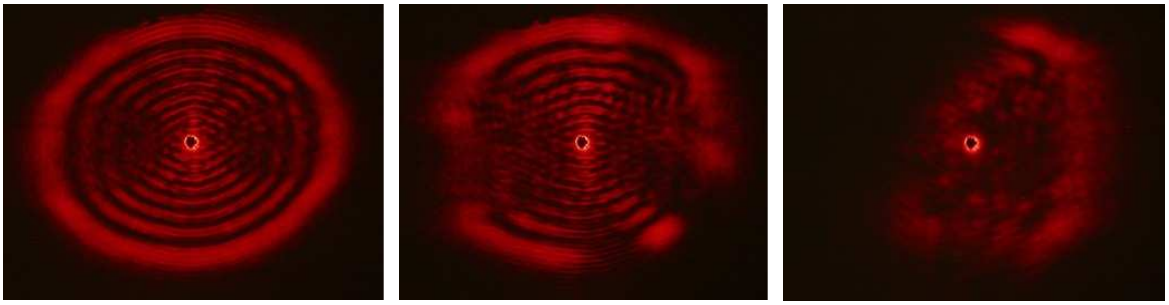

50° incident angle 55° incident angle 60° incident angle

Figure 2.17 Spot images of reflected beam at different incident angle

These spot images proved that this retroreflector has a full FOV of 120 degrees. However, at extreme angles, the reflected beam suffers from astigmatism in the direction of rotation, which agrees with the simulation results. Astigmatism and spherical aberration are the largest contributing aberrations for this device. This aberration in spot images shows an increase in beam divergence and consequently degradation in the reflected light intensity. Figure 2.18 supports such correlation between spot size, divergence angle and the received signal intensity. In these experiments a photo-detector was connected to a Tektronix Oscilloscope to obtain the *Vpp* value of the received signal. *Vpp* value is a good measure for signal contrast when dealing with binary data in communication link.

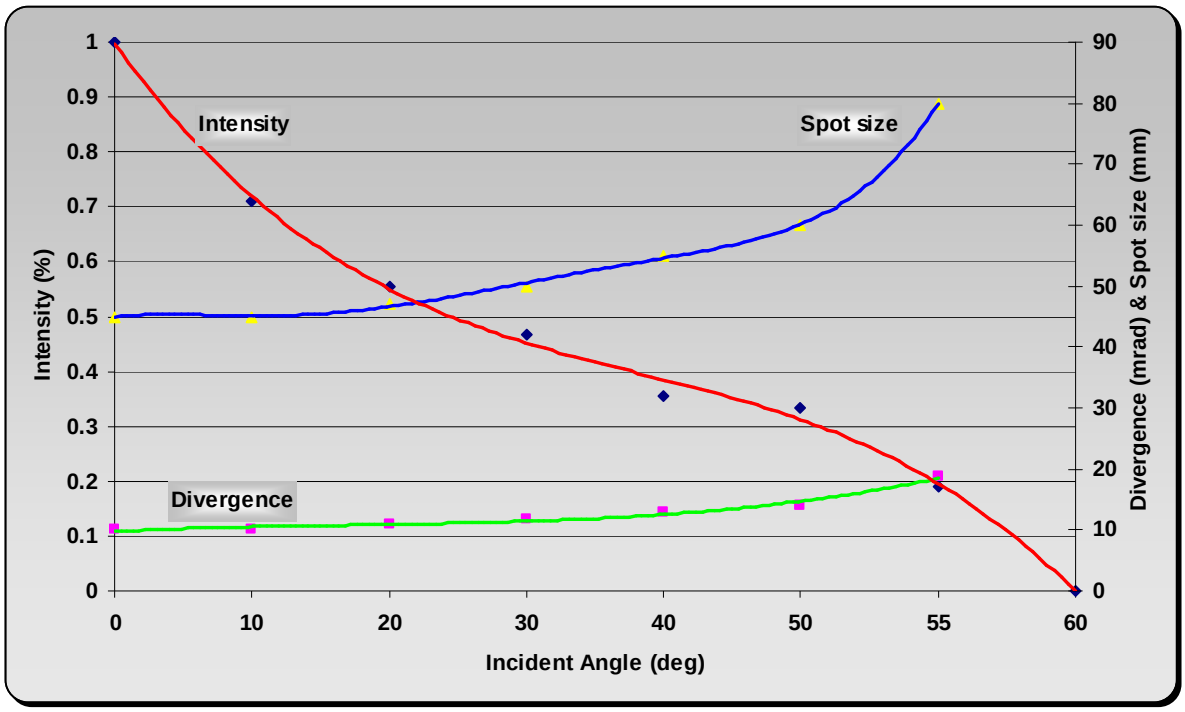

Figure 2.18 Effect of beam incident angle on spot size, received signal and divergence angle

The intensity measurements of the reflected beam were taken using an optical power meter. Figure 2.19 shows a bill shape curve of a retroreflected beam intensity caused by changing the beam incident angle. Because the power meter was not sensitive enough to detect the optical power of a very low light intensity, the detection at high incident angle (50 degrees) was almost zero. Therefore, the graph indicates that the retroreflector has a full FOV of near 100 degree.

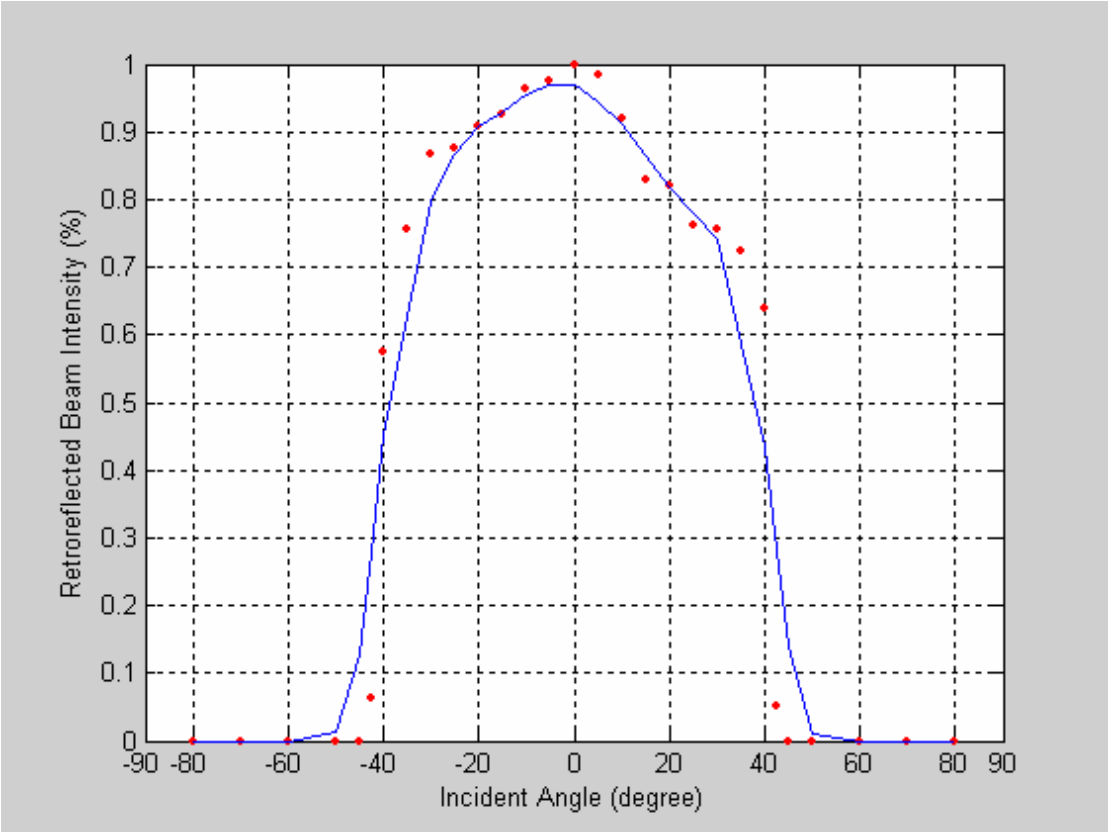

Figure 2.19 Effect of changing beam incident angle on the retroreflected beam intensity

Theoretically, the retroreflected beam intensity curve should maintain symmetry around the zero incident-angle. However, the intensity curve obtained experimentally is not exactly symmetric. This asymmetric result is due to the intensity of the retroreflected light, detected by a power meter, being very sensitive to any scattering of light. Major sources of light scattering are small dusts on lens's surfaces, imperfection in lens fabrication and inhomogeneous coating of Cat's-eye lens. Therefore, different reflections around the center of rotation of the retroreflector would result in asymmetric curve.

2.5.2 Range experiment

The effective distance of the retroreflector device was found using range experiments. A series of experiments was carried out to obtain the maximum working distance for the retroreflector device. The retroreflector device was mounted on a moving cart and the light incident angle was fixed at zero-angle. The effect of increasing the separation distance between the laser source and the target (retroreflector) on the intensity of the received signal is given in Figure 2.20. The plotted curve proves that the retroreflected light was detectable over a distance of 25 feet. In fact, the device range could go further than 25 feet if the experiment range was not limited by the laboratory space. The slope of the range curve between 20 and 25 feet gives an indication that the received signal could be traced at longer distance.

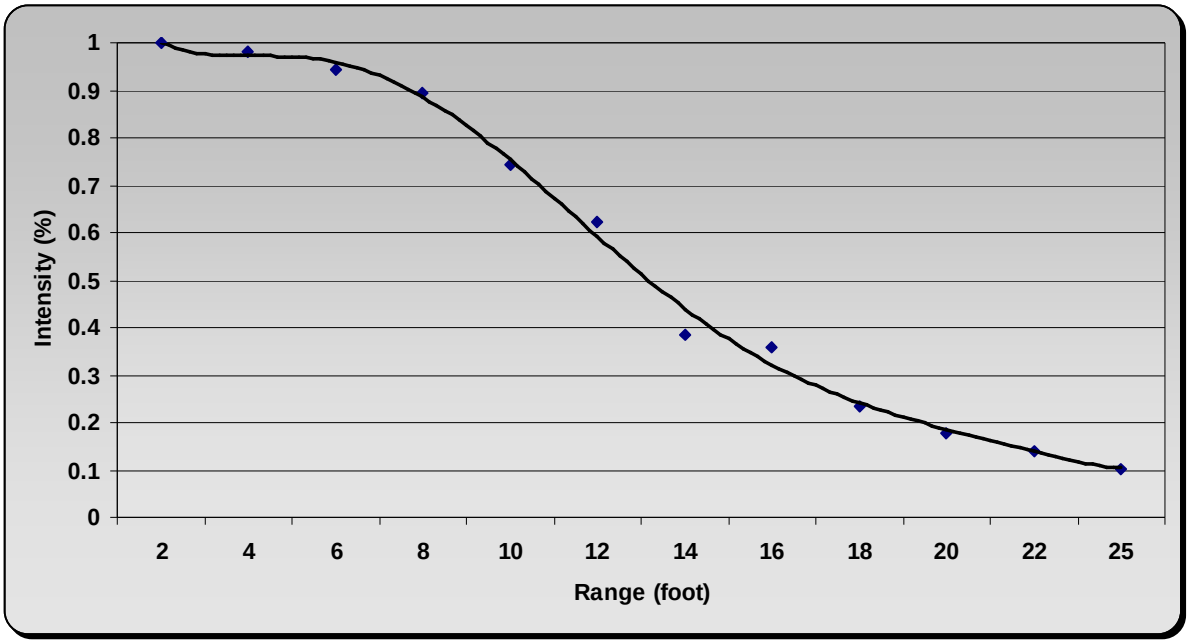

Figure 2.20 Range experiment with laser pointer

2.6 Experiment Power Budget

Intensity of the retroreflected light is inversely proportional to the working range and beam incident angle. To improve the system efficiency, the transmission factor of every element in the optical path needs to be investigated. A simple retroreflector device consists of one meniscus lens and a spherical Cat's-eye. At each uncoated lens surface, the incident light loses 4 to 5% of its power due to the unwanted reflections. Hence, the efficiency of the retroreflector device is

$$T_{retro} = (0.95)^6 \; R$$

where R is the reflectivity of the coated material at the back side of the spherical lens. Assume the coated material has a reflectivity of R = 98% and all the incident light go through the Cat's-eye lens, then the retroreflector device retroreflects 72% of the incident light.

In these experiments, a 50% beam splitter and a focusing lens were used to direct and collect the retroreflected light onto a photo-detector. The net transmission of the beam splitter after double passes is 25% of the transmitted light. The focusing lens allows for 90% light transmission. When power losses due to surface reflection of the detector, lens absorption, and light scattering, are ignored, the final percentage of the incident light received by the detector is

$$\eta = T_{retro}\, T_{splitter}\, T_{focus} = (72\%)(25\%)(90\%) \approx 16\%$$

It is important to enhance the overall system efficiency by minimizing the losses and maximizing the intensity of the retroreflected beam. With the current setup, the system lost approximately 85% of its transmitted light. The main source of this large loss is due to the beam splitter (75% loss). Other procedures that can be considered to minimize the unwanted surface reflection (blue rays in Figure 2.13) is the use of anti-reflection coating on every surface in the design especially the meniscus lens. In these experiments, none of the lens surfaces were coated. Furthermore, Cat's-eye lens should be replaced with a GRIN lens to

eliminate lens aberrations, as suggested in section 2.2.2. These modifications in the retroreflector design should improve the device efficiency for use in mid-range applications or even long-range applications.

In conclusion, this research presented a new wide FOV retroreflector device that was designed and implemented. The device was experimentally tested and initial results were presented. This research addresses the problem of expanding the FOV of retroreflectors. In addition, Cat's-eye lens limitations and the advantages of spherical gradient index lens in improving the retroreflectivity efficiency were explored and discussed.

2.7 *References*

[2.1] Toshiyuki Takatsuji, Mitsuo Goto, Sonko Osawa, Ruimin Yin and Tomizo Kurosawa, "Whole-viewing-angle Cat's-eye retroreflector as a target of laser trackers". *Measurement Science and Technology* 10 (1999) N87-N90. Printed in the UK.

[2.2] Yang, B., Friedsam, H., "Ray-tracing studies for a whole-viewing-angle retroreflector", *International Workshop on Accelerator Alignment* 1999, Grenoble (FR), 10/18/1999-10/22/1999 ; PBD: 2 Feb 2000.

[2.3] Lin Yongbing, Zhang Guoxiong and Li Zhen, "An improved cat's-eye retroreflector used in a laser tracking interferometer system", *Measurement Science and Technology*, Vol. 14 Issue 6 Article 404 (2003).

[2.4] Lin PD, Lu CH. "Analysis and design of optical systems by use of sensitivity analysis of skew ray tracing", *Applied Optics,* 43(4):796-807, Feb 1 (2004).

[2.5] Liao TT, Lin PD., "Analysis of optical elements with flat boundary surfaces", *Applied*

Optics, 42(7):1191-202, Mar 1 (2003).

[2.6] Yasuhiro Koike, Yuji Sumi, and Yasuji Ohtsuka, "Spherical gradient-index sphere lens", *Applied Optics,* vol. 25, pp. 3356-3363 (1968).

[2.7] Yasuhiro Koike, Akiyoshi Kanemitsu, Yoshimi Shioda, Eisuke Nihei, and Yasuji Ohtsuka, "Spherical gradient-index polymer lens with low spherical aberration", *Applied Optics*, vol. 33, pp. 3394-3400 (1996).

[2.8] D. Hamblen, "Miniature aspheric lenses with spherical index gradients" *Applied Optics*, vol. 33, pp. 561-564 (1996).

[2.9] Team Products International Inc. <www.teamproducts.com>.

Chapter 3

Optical Modulator Design

Modulators are optical devices that can operate as electrically controlled switches: that is, a beam of light passing through a modulator can be turned ON/OFF. Modulators are important to optical communication systems because they encode the desired information onto a beam of light. The information is then transported from one location to another as an on/off sequence of light pulses.

In this research, two types of modulator were tested: (1) a Liquid Crystal Display (LCD), and (2) a Liquid Crystal Polarization Grating (LCPG). Although, they can be operated by the same drive signal, every modulator has its unique way of modulating light. In the following sections, a brief description of the two modulator types is given and their characteristics are discussed.

3.1 LCD Optical Modulator

3.1.1 Modulator structure and modulation principle

An LCD modulator consists of liquid crystal molecules suspended between two transparent electrodes, and two polarizing filters. The axes of polarity of the polarizing filters are perpendicular to one another. Polarizers possess a unique property; they only pass light if it is oriented in a specific direction. Without the liquid crystals between them, light passing through one would be blocked by the other, as illustrated in Figure 3.1. The liquid crystal twists the polarization of light entering one filter to allow it to pass through the other.

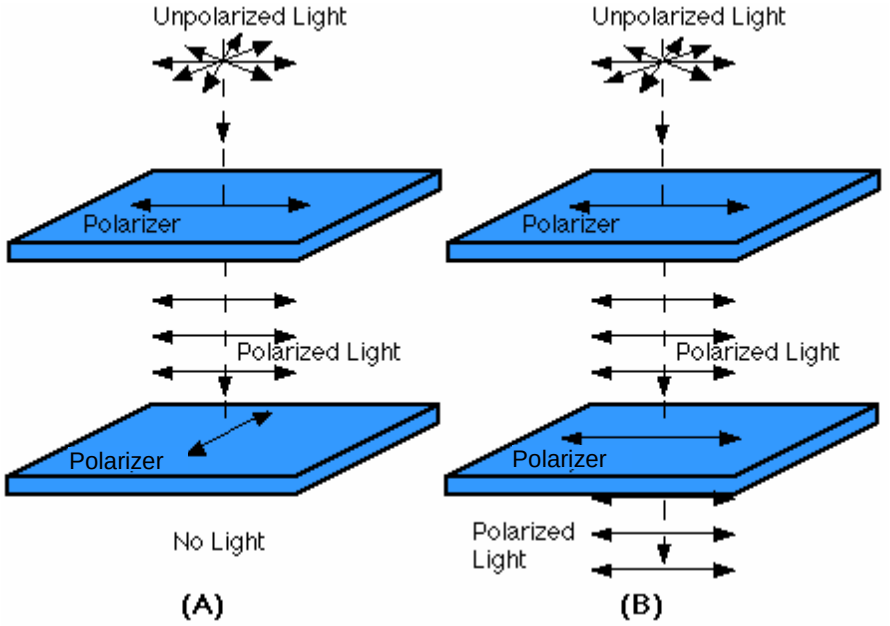

Figure 3.1 Illustration of two polarizers modulating an unpolarized light

Liquid crystals are affected by electric current. A particular sort of nematic liquid crystal, called twisted nematics (TN), produces a 90-degree shift in the polarization of the light passing through it in the absence of an electric field [3.1]. When a voltage is applied, an electric field is produced in the liquid, affecting the orientation of the molecules. This causes the polarization shift to be reduced slightly at low voltages, and greatly as the voltage (and the resulting field strength) increases. When the applied voltage reaches a certain level, the polarization shift disappears entirely. In other words, the LCD operates as a light shutter based on voltage being applied, or removed. A schematic illustration of an LCD before and after subjected to electric field is given in Figure 3.2. The observer plane in the left part of the diagram sees the incident light when no voltage is applied. Alternatively, when voltage is applied across the modulator electrodes, the light is blocked from the observer.

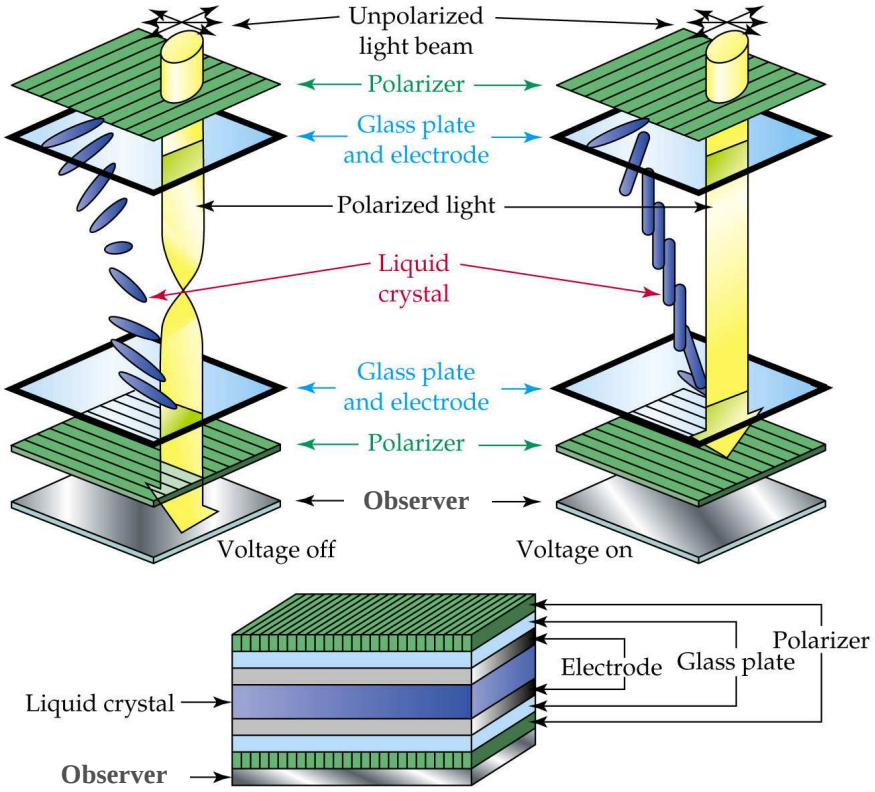

Figure 3.2 Schematic of LCD behavior under voltage application [3.1]

3.1.2 Characterization test

An LCD modulator was tested to characterize its operating parameters. Since the modulation mechanism of this device primary depends on the light polarization, the orientation of the front and back polarizers must match the nematic liquid crystal polarization axes. In addition, to maximize the transmission of the light, the orientation of the LCD front polarizer must be adjusted to match the linearly polarized laser beam. Below is a plot that shows the effect of LCD polarization orientation on the transmitted light power. The graph clearly signifies the importance of matching polarization axes of each component to achieve maximum efficiency. This experiment was carried out by shining a laser beam from (633 nm) HeNe source on an LCD and recording the power of the light intensity from other side. No voltage was applied across the LCD modulator.

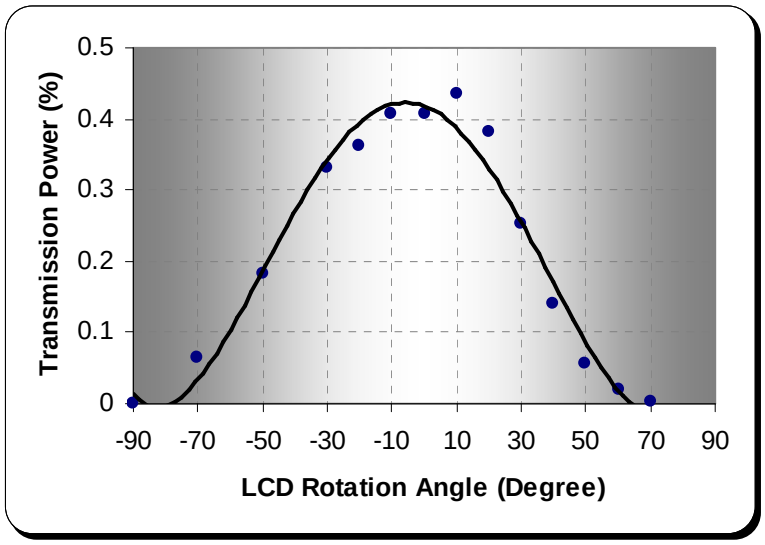

Figure 3.3 Effect of LCD rotation on transmitted power

Once the orientation angle of the device was determined, a second experiment was curried out to obtain the correct driving voltage for the device. Since the device will be employed in an application where a microcontroller unit controls the driving voltage, the LCD was first connected to a logic signal, one that alternates between 0 and 5 volts to determine its operating range. Although the device worked well, it was noted that it started to darken and attenuate the transmitted light after a long period of operation. It turns out that polling the polarization of the crystal molecules to one side pushes some of the molecules to be oriented in one direction permanently. Over time the device became opaque even in its idle state. Figure 3.4 shows pictures of a damaged LCD resulting from such a buildup process. The dark area at the center of the damaged LCD blocked more than 45% of the transmitted light.

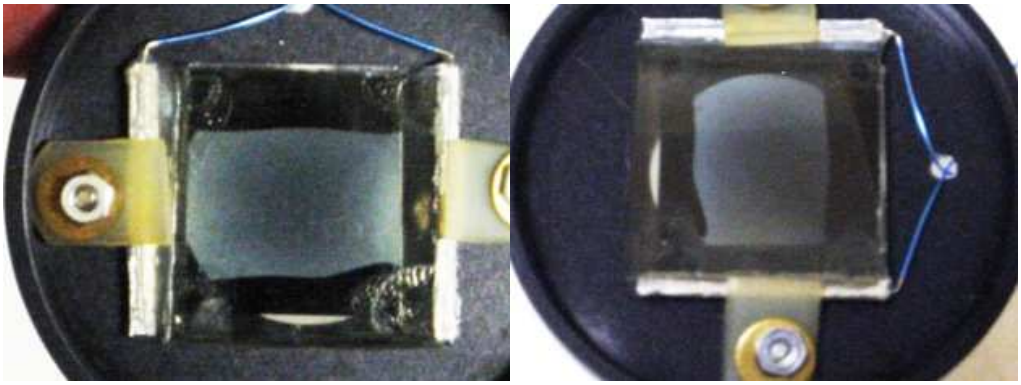

Figure 3.4 Damaged LCD due to 0-5 switching voltages

To over come this problem, the driving voltage of the LCD was modulated. An AM modulation was used to turn the LCD ON/OFF. Hence, when the LCD is on, i.e., energized, the carrier frequency alternates between positive and negative voltage levels at a high frequency (5kHz) and thus prevents the crystal molecules from being damaged. It is extremely important, when using an AM modulation signal, to keep the DC level of the driving voltage at zero level. Otherwise, drifting will once again effect on crystal molecules but at a slower rate than previously.

Having established that an AM modulated voltage is required to drive an LCD; an experiment was conducted to obtain its optimized driving voltage. LCD transmission power as a function of the applied voltage is shown in Figure 3.5. There is a voltage threshold associated with most LCDs. No change in transmission occurs until the threshold voltage, V_{th}, is passed. Light transmission then decreases as the applied voltage increases until a saturation state is reached. This experiment revealed that the threshold voltage of the modulator tested was 1.5 RMS volts, and saturation occurred at 2.5volts. Between these two values, transmission power attenuated as applied voltage increased. The graph also reveals that the LCD modulator allows less than 45% of incident light to pass through. Considering that transmission efficiency is essential for optical communication, experiments were conducted to investigate the source of losses in this device, and whether it is useful for optical communication.

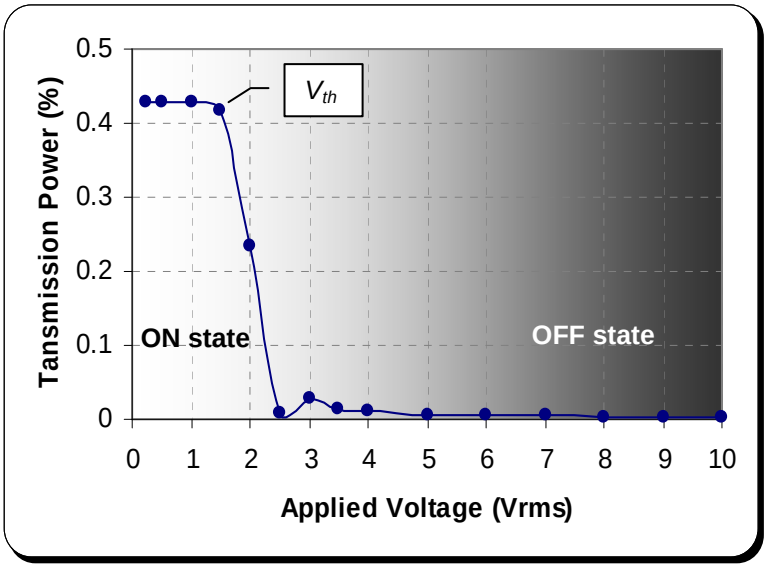

Figure 3.5 LCD switching behavior due to applied voltage changes

Since this modulator was to be integrated into a retroreflector device, ensuring that maximum light is essential. This is because the transmitted light passes through the modulator twice, so artifacts of the modulator will have a double impact on the light intensity. Table 3.1 shows the percentage losses of the transmitted light in each part of the LCD

Table 3.1 Light loss due LCD components for one pass

LCD Component	**Light Loss**	
Liquid Crystal	15%	(1.24dB)
Polarizer	28% (each)	(0.7dB)
LCD device	57% (total)	(3.54dB)

From Table1 it can be seen that only 43% of the light passes through the modulator and hits the retroreflector. If only the losses due the LCD are considered, then about 19% of the transmitted light is retroreflected and captured by the receiver. This means that more than 81% of light intensity loss is attributed to this LCD modulator.

What makes the situation worse is the effect that the retroreflector has on the polarization of the incident light. Figure 3.6 shows that Cat's-eye retroreflector changes a linearly polarized light into a circularly polarized light. And, since LCD's are polarization-dependent modulators, they block more than 50% of circularly polarized light retroreflected from Cat's-eye reflectors. So the net received signal will be less than 10% of the original transmitted light.

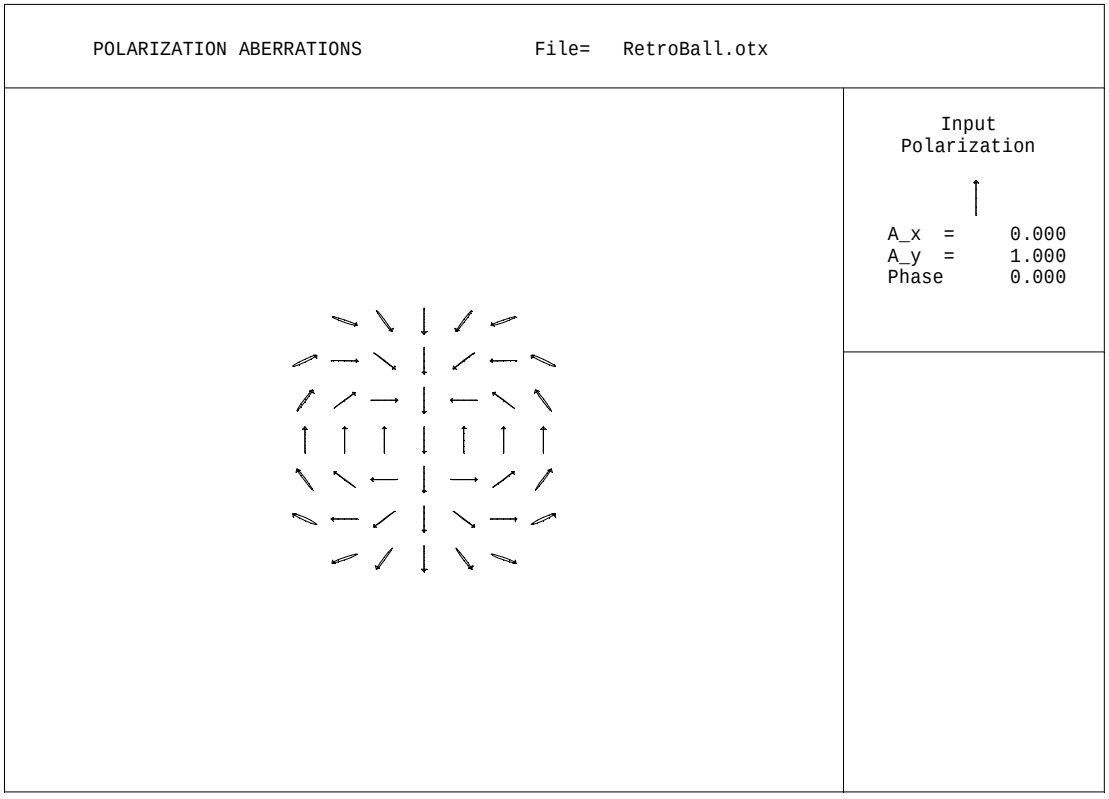

Figure 3.6 Cat's-eye retroreflector polarization effect on a linearly polarized light

To summarize the results, there are two major drawbacks with this type of modulator. First, the two polarizers and the liquid crystal materials absorb and scatter more than 57% of the incident light. Second, the polarization-dependent property of the LCD modulator accounts for additional 50% loss when it is integrated into a retroreflector system. As a result, the optical efficiency of the retroreflector modulator is less than 10%. Therefore, this particular optical modulator is not suited for applications that employ retroreflector devices.

3.2 Liquid Crystal Polarization Grating (LCPG) Modulator

3.2.1 Modulator structure and modulation principle

Conventional diffraction gratings operate by periodically modulating the phase or the amplitude of light propagating through them. Polarization gratings (PGs), by contrast, generally operate by modulating the state of polarization of the light passing through. PGs with 100% diffraction efficiency could be achieved with thin-grating regardless of input polarization [3.2, 3.3]. By carefully balancing the choice of the liquid crystal (LC) and photo-alignment materials with cell geometry, Escuti [3.4, 3.6] at NC State University developed a novel liquid crystal polarization grating (LCPG) technology that operates on unpolarized light with diffraction efficiency into the first order at > 99%. With this technology, up to 600:1 contrast ratio was achieved for monochromatic light. The device has a switching time near 2ms for nematic LCs and a threshold voltage of 1.65Vrms.

The liquid crystal polarization gratings (LCPGs) are polarization-independent and have only three orders of diffraction (0, ±1). Other gratings have a large number of diffraction orders, as illustrated in Figure 3.7. The diffraction efficiency for unpolarized light is given by the following equations:

$$\eta_o = \cos^2\left(\frac{\pi \Delta n\, d}{\lambda}\right)$$
$$\eta_{\pm 1} = \frac{1}{2}\left[1 \pm S_3'\right] \sin^2\left(\frac{\pi \Delta n\, d}{\lambda}\right) \qquad \textbf{(3-1)}$$

where η_0 and $\eta_{\pm 1}$ are the diffraction efficiencies of the 0^{th}- and $\pm 1^{st}$-orders, λ is the wavelength of incident light, Δn is the birefringence, d is the thickness of the PG, and $S'_3 = S_3/S_0$ is the normalized Stokes parameter corresponding to ellipticity of the incident light.

Two main features of this technology over the conventional diffraction gratings are:

1. The 0^{th}-order diffraction efficiency does not depend on the polarization of incident light and reaches a minimum (0%) when the retardation is half-wave ($\Delta nd = \lambda/2$).
2. The sum $\eta_{+1} + \eta_{-1}$ is also polarization-independent of the incident light, even though the individual diffraction efficiencies are not. For example, when $\Delta nd = \lambda/2$, then η_{+1}=100% and η_{-1}=0% if the input polarization is right-circularly polarized (Figure 3.7c), and $\eta_{+1} = \eta_{-1}$=50% if the input is linear or unpolarized (Figure 3.7b).

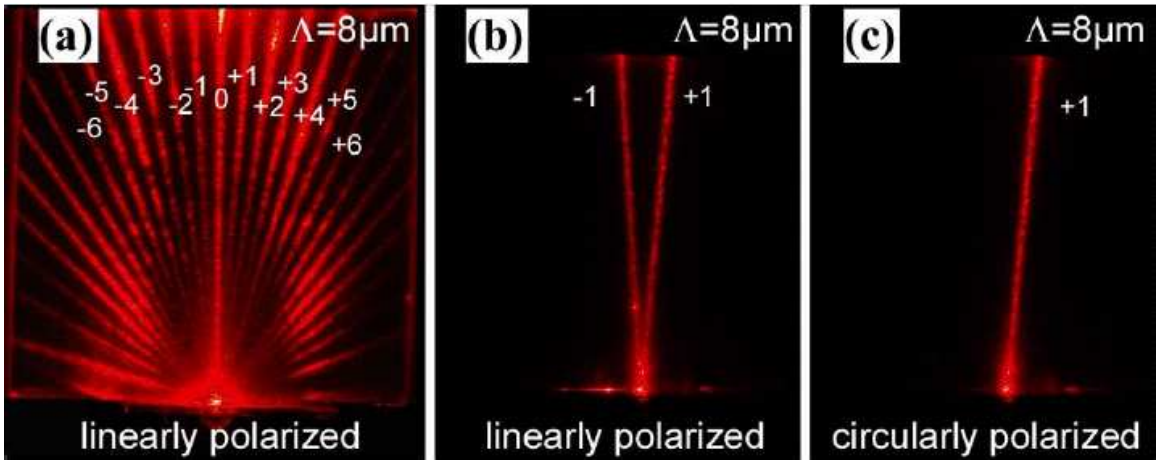

Figure 3.7 (a) conventional phase grating; (b) and (c) polymerized reactive LC polarization gratings with 633 nm light of various polarizations incident (notice (b) and (c) both have η_0=~0% regardless of incident polarization) [3.4]

The LCPG cell consists of two glass substrates with transparent conducting electrodes such as indium-tin-oxide (ITO). The substrates are coated with a UV-sensitive photo-alignment layer. The space between the substrates is filled with liquid crystal. Figure 3.8 describes the structure of a single-pixel LCPG element and the modulation principle of a light passing through.

The essence of this type of modulator is that an applied voltage reduces the effective birefringence (Δn) and tunes the transmission spectrum. The birefringence is voltage controlled and the 0^{th}-order is directed to the viewer achieving polarization-independent

operation. Electro-optic switching occurs when an applied field orients the nematic director out of plane, decreasing the effective retardation and allowing energy to couple from $\pm 1^{st}$-orders into 0^{th}-order. Therefore, by directing the incident light that passes through the 0^{th}-order to a retroreflector lens, one can modulate the incident light for free-space optical communication.

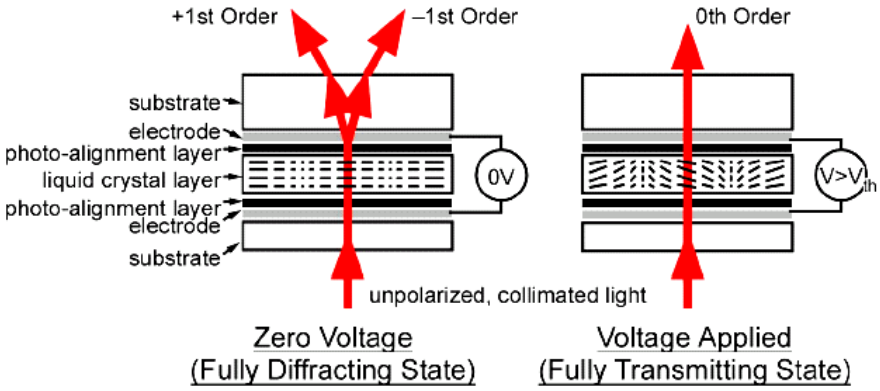

Figure 3.8 Structure and modulation principle of LCPG [3.5]

3.2.2 Characterization Test

The electro-optical performance of a single LCPG cell is based on the critical thickness of the LC layer, threshold voltage and the switching times. Theoretically, when LCPG thickness approaches the critical thickness, the applied voltage threshold decreases to zero. Then, as the applied voltage increases the switching time decreases [3.4].

The characterization method for the LCPG cell was similar to the one described in the preceding section 3.1.2. An electrical drive signal was applied to the cell under test and the optical output signal was detected to extract the envelope waveform and compare it with the drive signal. The objective was to maximize the modulator optical efficiency and switching

rate by adjusting driving voltage parameters such as carrier power and frequency, index of modulation and modulation frequency.

In these experiments, a single-pixel LCPG element was placed between a HeNe laser source and a photo-detector. The radiometric power of the incident light that passes through the LCPG element was recorded by a photodiode or power meter.

Transmittance (T) is defined as $T=I_{MOD}/I_{REF}$, where I_{MOD} is the modulated intensity of the LCPG cell and I_{REF} is reference intensity with the LCPG cell removed. This normalized measure includes the effect of the cell reflections and any absorption. All electro-optic measurements were done with a 5kHz square wave.

Basic switching behavior is shown in Figure 3.9(a) for the HeNe (633nm) laser source. The projected intensity for a range of applied voltages was measured using a power meter. The transmittance curve for the 0^{th}-Order revealed that a 1.55Vrms acts as a threshold for the LCPG modulator to turn it on. At this voltage, light intensity has its minimum value; 0.7% of the transmitted power presented in the dark (off) field. The maximum optical efficiency at 0^{th}-order is about 87% in the bright (on) field. Losses due to air-glass interfaces and scattering, ITO absorptions contributed to about 1% loss of optical power. Primary source of losses is the coupling between diffraction orders due to imperfections in fabricating the LCPG cell. This optical coupling or light-leakage is very clear from the spot images in Figure 3.9(b). The 0^{th}-order in the top view should be the only visible order. In contrast, the bottom view should show only the $\pm 1^{st}$-orders of diffraction. This light-leakage contributed to 10% loss of transmitted optical power. In addition, this leakage varies from one spot to another on the same cell due to inhomogeneous distribution of the cell's structure.

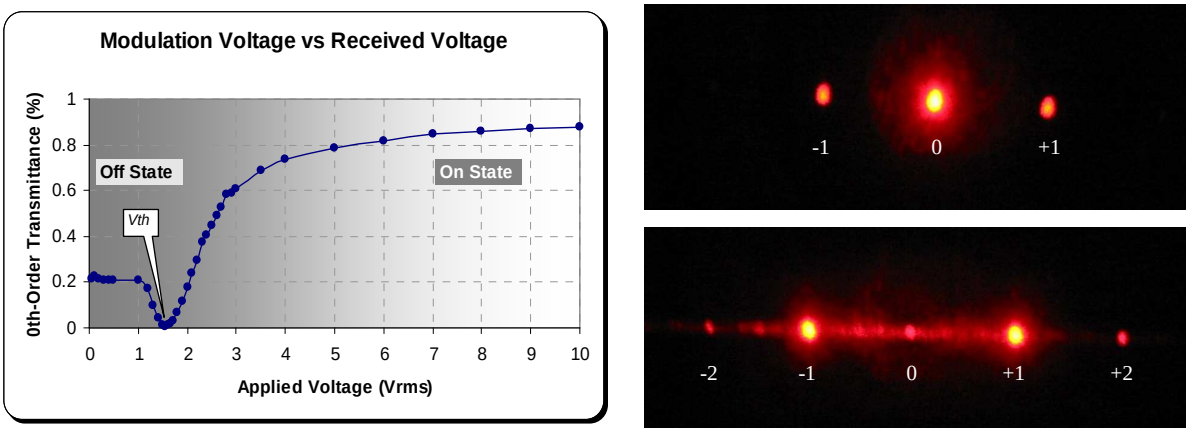

(a) **(b)**

Figure 3.9 (a) Transmission behavior of LCPG cell when subjected to different voltage levels, (b) LCPG diffraction for 0^{th}- and $\pm1^{st}$-orders. Note that there are other diffractions than the desired one due to fabrication imperfection

At 6Vrms applied voltages, 80% of the transmitted power reaches the detector. Although, it is reliable to work at this voltage level, the rise-time curve, shown in Figure 3.10b, suggests that the modulation voltage should be as high as 10Vrms to achieve better switching time.

The full-contrast switching times of the 0^{th}-order intensity were measured with the HeNe laser and a modulated drive signal. Figure 3.10(a) shows a screenshot of an LCPG element responding to a 10Vrms square wave of a 30Hz modulation frequency. A summary of the 10%-90% rise and fall times vs. applied voltage is shown in Figure 3.10(b). The switching times are all on the order of ~10ms. This indicates that this sample can modulate light at 100Hz.

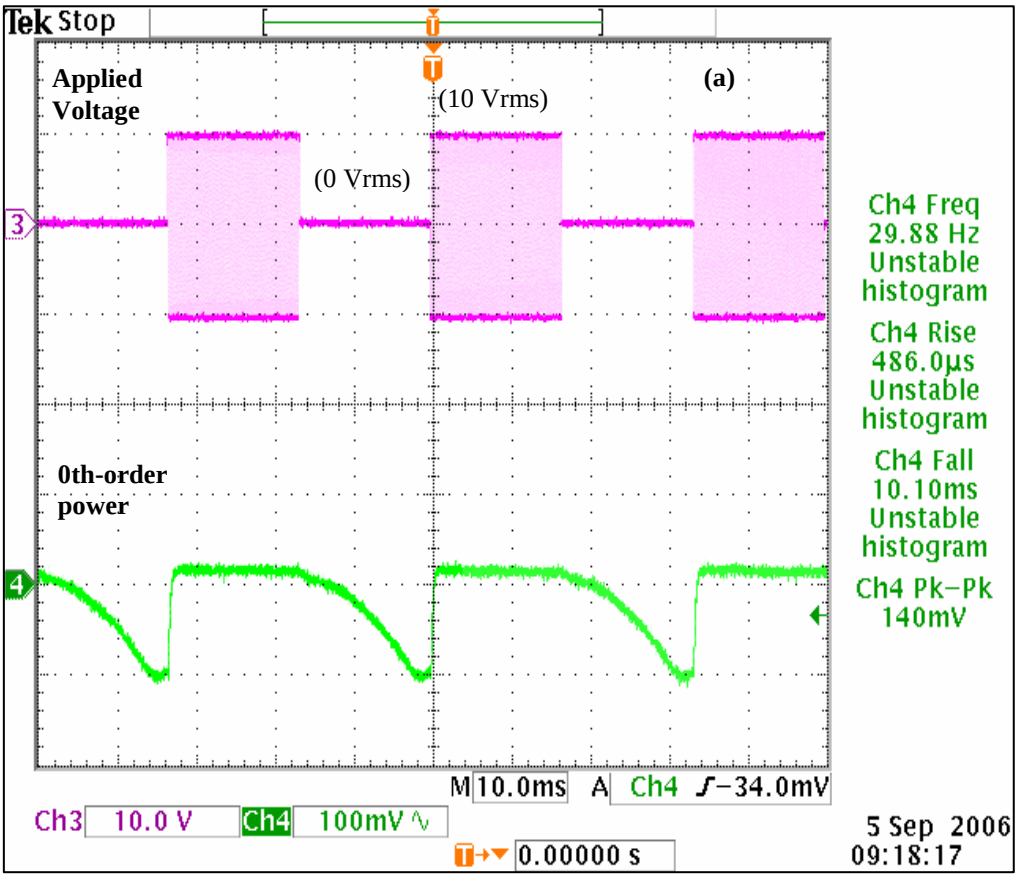

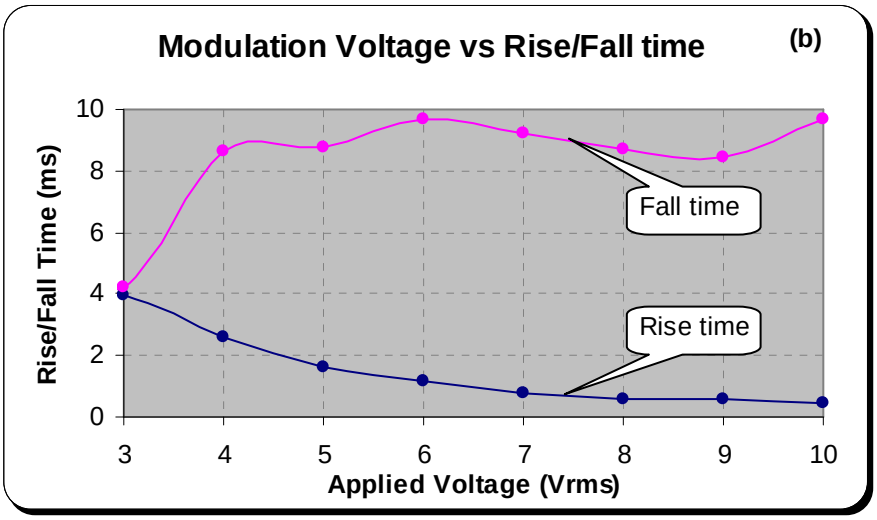

Figure 3.10 Effect of applied voltage on modulator switching time: a) screenshot for modulator response to 30Hz modulated signal, b) switching times at different applied voltages

The next experiment studied the effect of power intensity attenuation on the contrast of the received power. Signal contrast study gives an indication of how an optical communication system will perform. By definition, contrast is the difference in intensity between dark (OFF) and bright (ON). The greater the difference in intensity, the better the contrast:

$$\%\,Contrast = \frac{I_{\max} - I_{\min}}{I_{\max} + I_{\min}} \times 100$$

where I_{max} is the maximum intensity and I_{min} is the minimum intensity.

Normally, a transmitted signal through a wireless communication channel should be modulated using a data stream. Therefore, modulation frequency is another factor that should be considered when using this type of modulator. Here, LCPG element was driven by 5kHz carrier frequency. It turns on the modulator when the applied voltage is 10Vrms and turns it off at the threshold voltage (1.55Vrms). The modulation frequency carrying the data varies from 5 to 500Hz. Figure 3.11 indicates that as the modulation frequency is increased, the response will drop off and the detected peak-to-peak voltage, i.e., signal contrast is decreased.

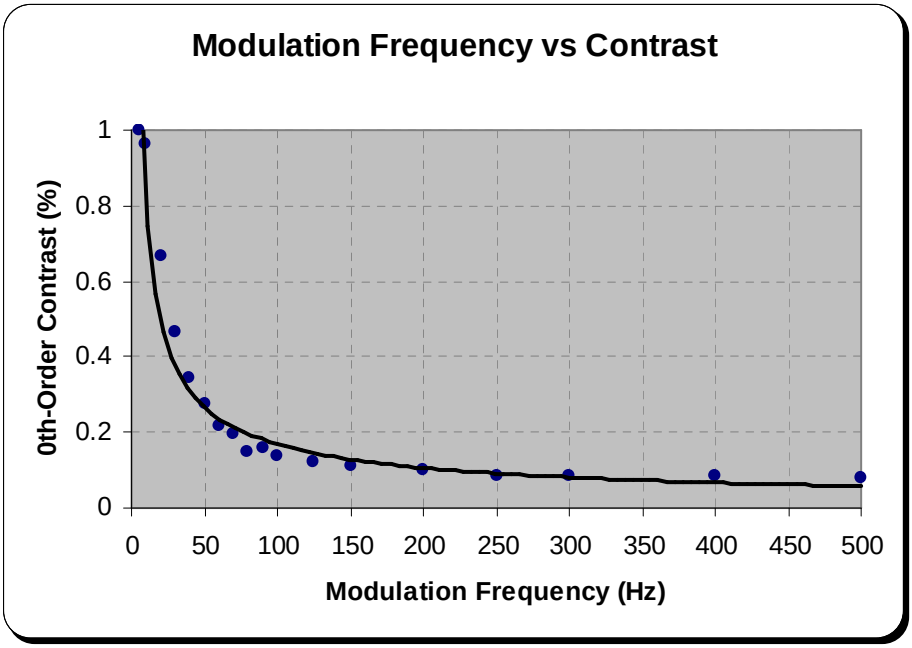

Figure 3.11 LCPG response to increase in modulation frequency

The contrast curve indicates that this modulator has low contrast at high modulation rates. Although detection at higher rates can be achieved at the expense of circuit detection complexity. This complexity arises from the fact that not only were the peak values of the received voltage decreased, but the shape of the pulses was distorted too. Figure 3.12 shows screenshots of the LCPG responding to a 10Vrms square wave of varies modulation frequency. The deformation in pulse shape is obvious and it is proportional to the increase of modulation frequency. Also, as it is common in optical communication receivers, output signals always accompany DC signals. For this signal to be reliable in digital communications these pulses need to be sharpened and the DC signal should be filtered out in the receiver circuit. This should be done before the signal is sampled for data processing.

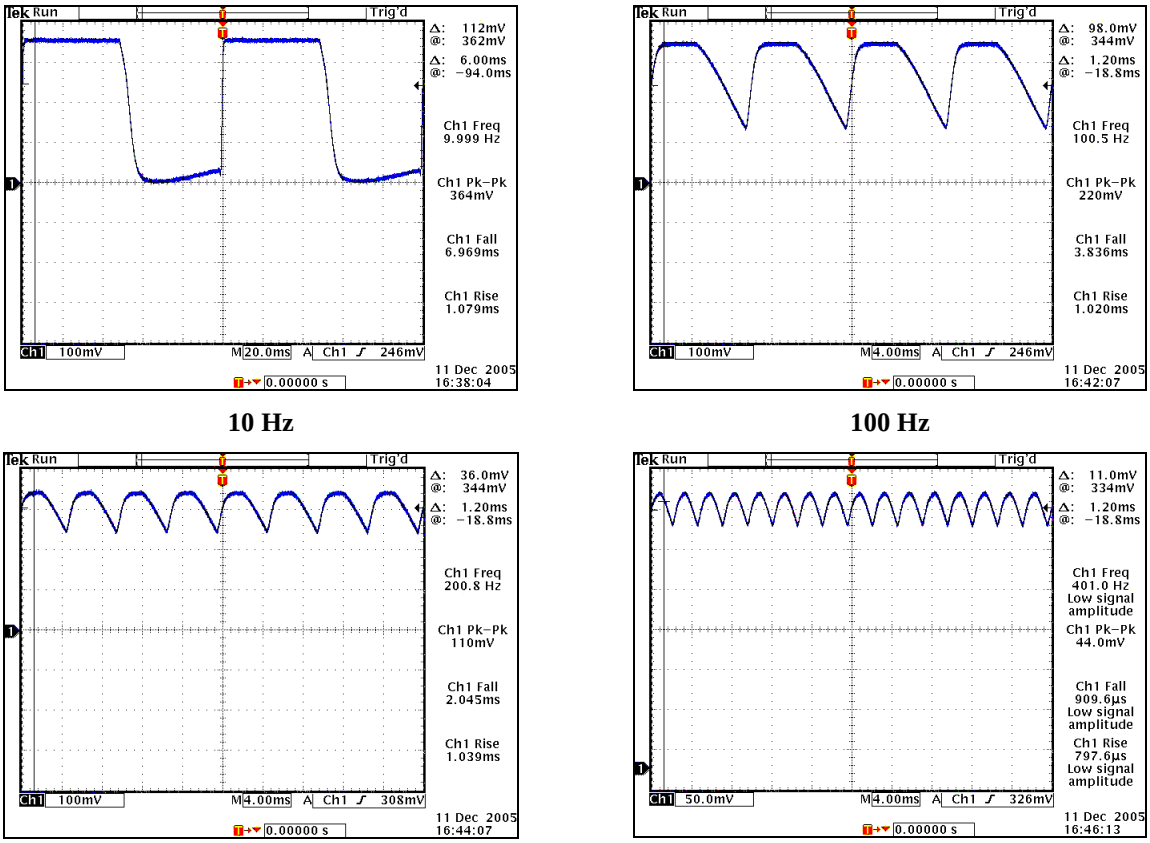

Figure 3.12 Effect of modulation frequency on pulse shape and DC level of received signal

When combined with retroreflectors, the most important diffraction order of the LCPG modulator is the 0^{th}-order diffraction, because it retroreflects modulated light back to the light source. Fortunately, the small separation distance between the LCPG modulator and the Cat's-eye retroreflector prevents high-order diffractions from shining at the center of the reflector aperture. Even when a portion of the diffracted light enters the retroreflector aperture, it enters with a diffraction angle of 60mrad, which causes it to be reflected away from its emitting source. Therefore, other diffraction orders will not interfere with the communication performance. Although, these higher orders are reflected back in the same plane of the incident light, they should be blocked for safety considerations.

The transmission rate of any optical communication system is dominated by the efficiency of its modulation capability. Alternatively, transmission range is solely determined by the strength of the received signal. Therefore, as a start point, a 50Hz modulation rate was used to determine the maximum transmission range for the retroreflector modulator device. A range experiment was carried out after characterizing the device and obtaining its optimal parameters. In this experiment, the LCPG modulator was attached to a retroreflector lens and a laser source was moving away from the modulator. A photo-detector attached to the laser source recorded the retroreflected signal every 2 feet. The range curve in Figure 3.13 indicates that this modulator is reliable for optical communication in short range applications. The low signal contrast after 6 feet was mainly due to beam divergence. In moving target systems, beam spot is proportionally increases with range distance. Inversely, beam intensity decreases when its spot increases.

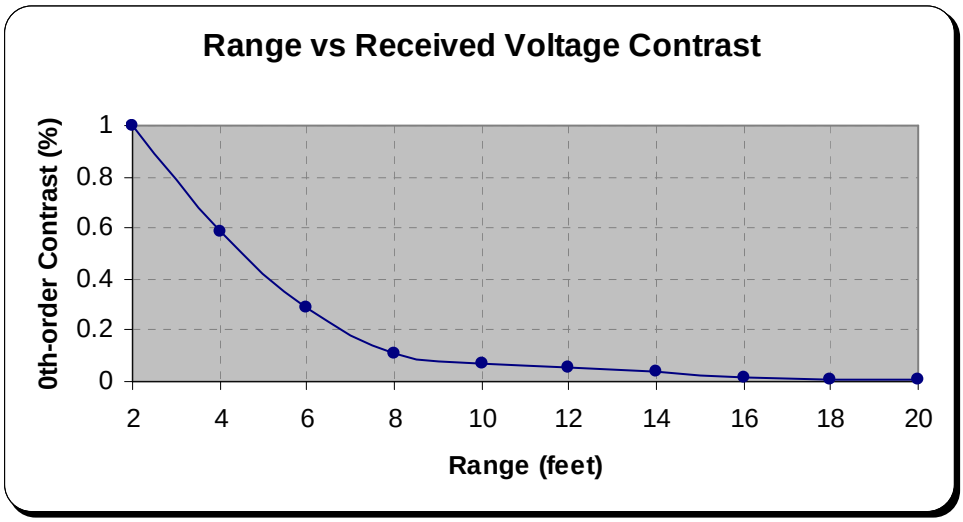

Figure 3.13 Detected voltage signal as a function of target distance

In conclusion, LCPG modulator performance supersedes the LCD modulator. The tested sample has higher optical efficiency (90%) even though it was not designed for optical communication systems. Despite the imperfection in fabricating the modulator cell and power losses due to light-leakage, the modulator performed well at short ranges without any electronic circuits. Therefore, the decision was made to integrate the LCPG cell in the retroreflector modulator device for free-space optical communication.

3.3 *References*

[3.1] John McMurry, Robert C. Fay, "Chemistry" *Cornell University*, ISBN: 0-13-140208-0, Prentice Hall (2004).

[3.2] L. Nikolova, T. Todorov. "Diffraction Efficiency and Selectivity of Polarization Holographic Recording." Optica Acta, vol. 31pp. 579-588 (1984).

[3.3] J. Tervo, J. Turunen. "Paraxial-Domain Diffractive Elements with 100% Efficiency Based on Polarization Grating." Opt. Lett., vol. 25, pp. 785-786 (2000).

[3.4] M.J. Escuti and W.M. Jones. ”Polarization independent switching with high contrast from a liquid crystal polarization grating”, *SID Symposium Digest*, 2006, vol. 37, paper 39.4.

[3.5] W.M. Jones and B.L. Conover and M.J. Escuti. ”Evaluation of Projection Schemes for the Liquid Crystal Polarization Grating Operating on Unpolarized Light”, *SID Symposium Digest*, 2006, vol. 37, poster P209.

[3.6] M.J. Escuti and W.M. Jones. “A Polarization-Independent Liquid Crystal Spatial-Light-Modulator”, *SPIE Optics & Photonics Conference*, 2006, paper 6332-22.

Chapter 4

Optical Communication System Design

The laser communication experiments demonstrated the feasibility of designing and constructing a compact robotic communication link, on a small budget, using retroreflector modulator technology. The design provided a solution for transmitting data from one mobile robot to another, using a Manchester encoded signal, that decodes the data to perform locomotion tasks. Manchester Encoding has been used to reduce the complexity of the receiver design, and in particular symbol synchronization.

Flexibility and scalability of the test hardware was strongly emphasized in the design of the first prototype. To test the basic functionality of the transceiver hardware, a computer program was written, to transmit, receive, and to carryout the instructions contained within the received data.

4.1 Transceiver Circuit Design

A transceiver board receives and transmits data, although not at the same time. In this research, the transceiver is designed to perform dual tasks: 1) communicating locally with the mobile robot base and 2) communicating optically with other robots. Figure 4.1 illustrates the high level design of the system.

The microcontroller unit (MCU) in the transceiver communicates with the MCU (BasicX) on the mobile robot base through RS232 link (UART0). The BasicX receives commands and

moves the robot to a desired location by controlling two DC motors. Any discrepancies in the robot's position and orientation are adjusted using the optical encoders on each motor. Optical communication between robots is the center focus of this research. It consists of a transmitter circuit for light modulation and receiver circuit for light detection. An ATmega128 MCU is the processor that controls both tasks through a UART1. The laser would essentially constitute the "wire" in this link connecting the two UARTs. An On-Off Keying system was chosen for data transmission where the oscillator at the carrier frequency is switched directly by the data to be transmitted.

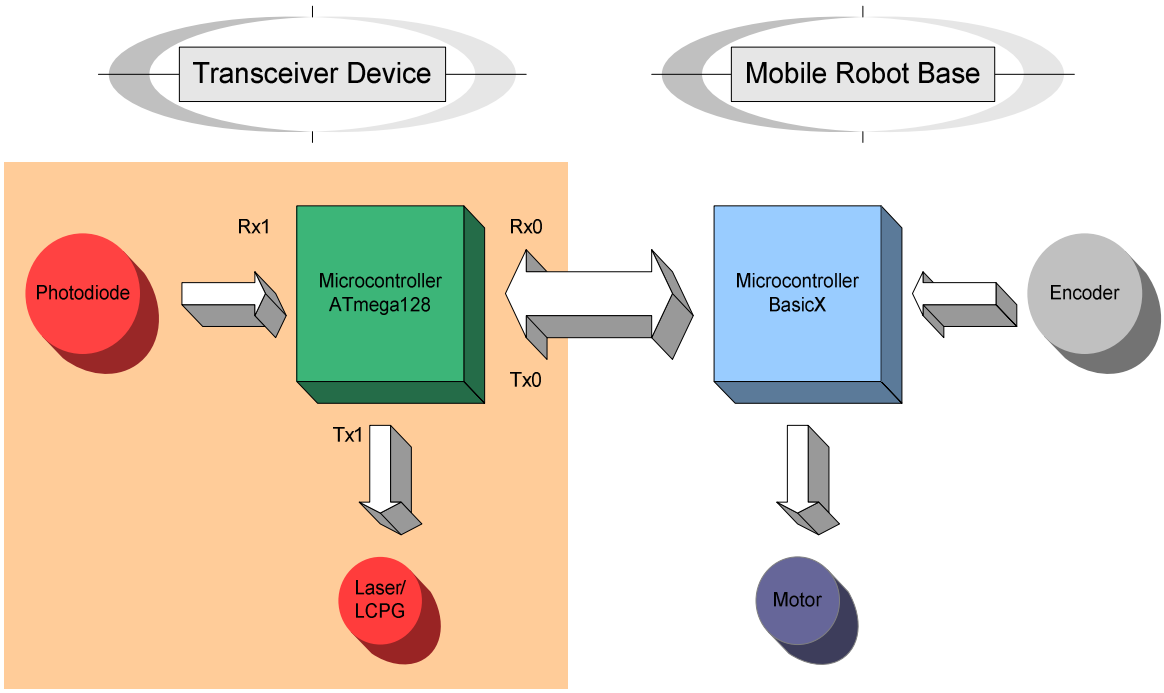

Figure 4.1 High level structure of the communication system design

The input/output of the transceiver circuits is connected directly to the microcontroller pins after signal conditioning. The circuit design was optimized to minimize noise and maximize transmitter baud rate. Figure 4.2 shows a schematic diagram of the transceiver design. A detail explanation of every circuit in the schematic is discussed next.

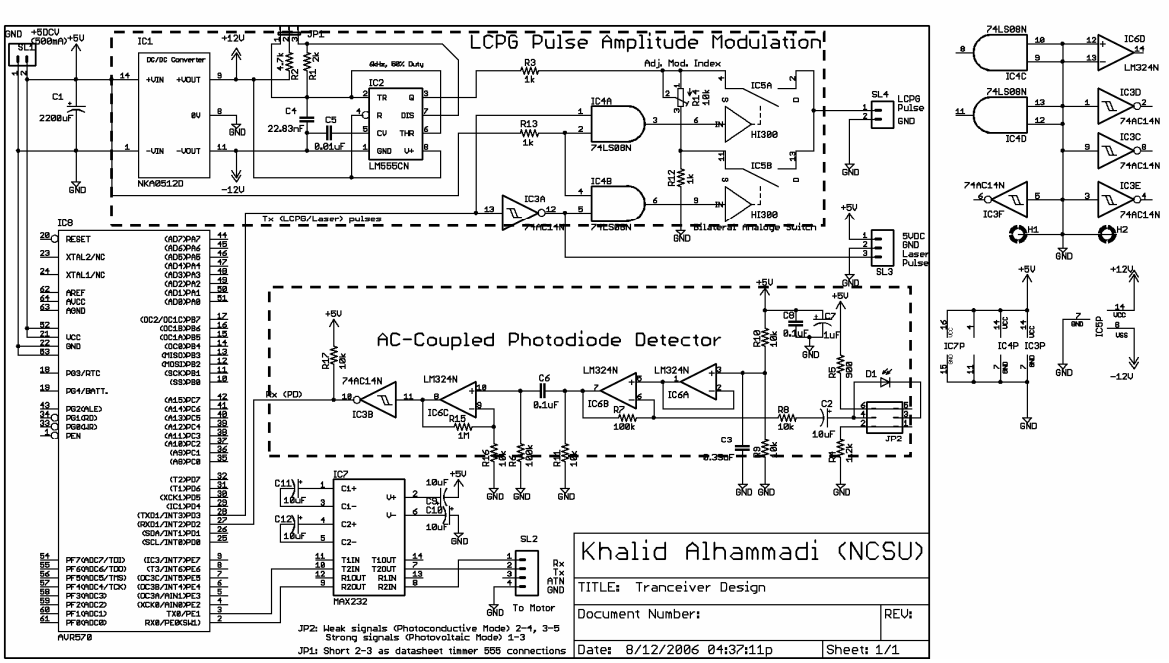

Figure 4.2 Transceiver circuit design

4.1.1 Transmitter (optical modulator) design

In transmission mode, the MCU passes the signal to UART1. The UART sets a transmit pin high or low according to the serial protocol. Two types of data transmission were conducted in this research: (1) direct transmission by pulsing the laser driver circuit, and (2) indirect transmission by pulsing the retroreflector modulator carrying LCPG.

a) *Laser pulsing circuit*:

A laser modulator board (YWP-G) was used to pulse a 15mw laser diode (DL7147-201). The board contains a semiconductor laser diode driver (M66510FP) that drives a semiconductor laser of the type whose cathode and anode of monitor photodiode are connected to the stem. It operates from a 5V single power supply, allowing switching of

laser driving current at a speed of 20M bits/sec. Figure 4.3 shows a picture of the board. More information can be found in the producer datasheet reference [4.1].

Figure 4.3 Laser driver board with laser diode attached to it

b) ***LCPG pulse amplitude modulation circuit*:**

The efficiency of the modulation/demodulation process determines the accuracy of the data coming from the receiver. Therefore, careful consideration must be given to the selection of an appropriate modulation-demodulation scheme. Amplitude Modulation (AM) is perhaps the oldest technique for impressing information onto a carrier signal. With normal amplitude modulation, the amplitude of a carrier frequency is raised and lowered in harmony with the modulation source. This modulation technique is very simple, inexpensive to implement and the transmitter draws virtually no power (2-3mA). On the other hand, it is limited to less than 10k bit/second due to the start-up time of the oscillator and poor noise immunity. Since cost, operating distance and power efficiency are the overriding concerns of the research, amplitude modulation was the preferred technique.

In the case of pulse amplitude modulation, the transmitter turns the carrier frequency on and off. If the carrier frequency is present, then a '1' is being sent. If the carrier frequency is absent, then a '0' is being sent. However, to achieve high contrast, at off state the carrier frequency should be turned off completely; a small voltage (1.55Vrms) across LCPG terminals should be applied.

As proven experimentally in the previous chapter, the amplitude of the carrier frequency should be approximately 10Vrms. Therefore, since the maximum voltage of the supply is 5V, a DC/DC converter was included in the circuit to boost the source voltage to ±12V. A 555timer IC provided the high frequency signal (7kHz), and the bilateral analog switch turns the carrier frequency on and off at 1kbps data rate according to the input modulation signal. In order to control the modulation index of the circuit, a 10kΩ variable resistor was used. This is very useful for testing or when replacing the modulator with different type.

The output of the circuit is shown in Figure 4.4. It is similar to the result obtained in the previous chapter during the characterization process of the LCPG modulator. It was easy to achieve the maximum contrast by adjusting the modulation index using the variable resistor.

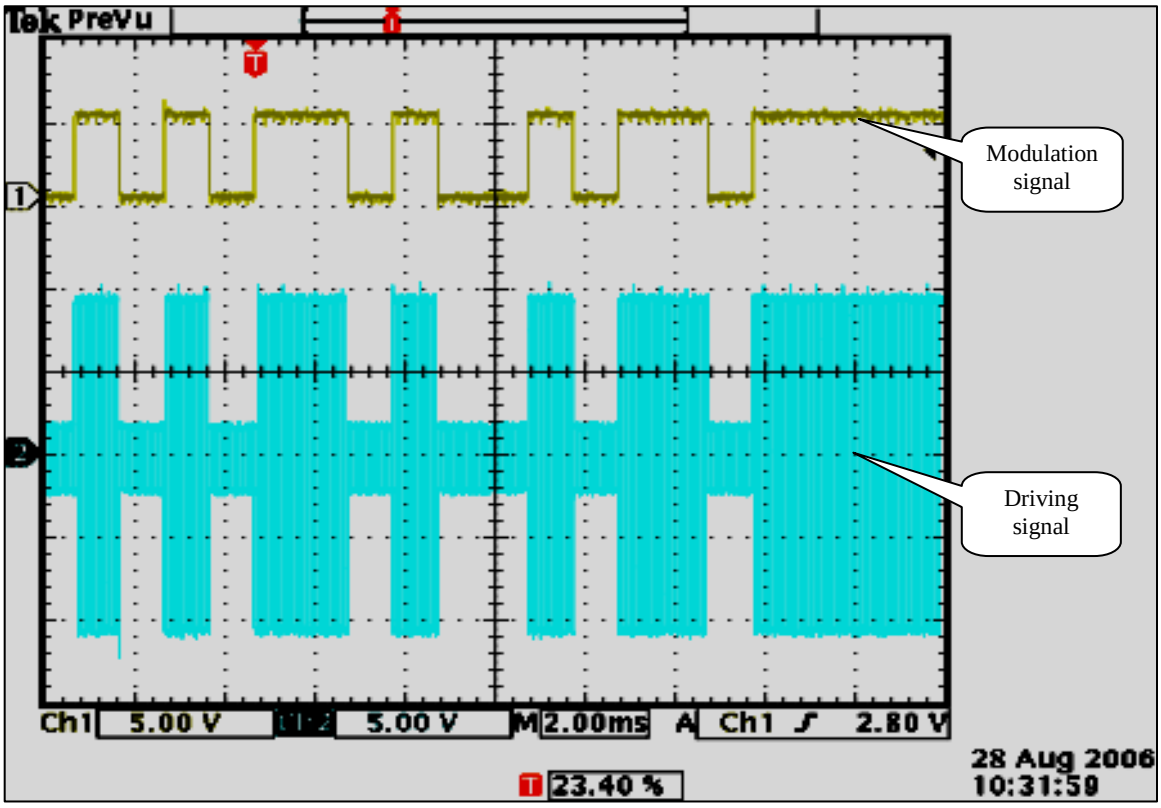

Figure 4.4 Modulation signal and carrier signal after modulation

4.1.2 Receiver (AC-coupled photodiode detector) design:

On the receiver side, the signal is read by a photodiode. The signal coming off the photodiode circuit is passed through an AC-coupled circuit to generate the required high and low signals. UART1 reads these signals and generates a byte according to the serial protocol. This section addresses two main topics: (1) the photodiode connections, and (2) the design of the AC-coupling circuit.

a) *Photodiode operation modes*:

Photodiodes are ideal for measuring both pulsed and CW light sources, by converting the optical power to an electrical current. For most devices this relationship is linear over a

120dB (1 million to one) span, ranging from tens of milliwatts to nanowatts. Many photo detectors are available that suit the specifications of this project. In particular, there is a wide array of Silicone PIN photo diodes used in the communication industry that are both fast and precise enough to light intensity from a laser diode source. The silicon photodiode (S2386-5K) was selected for this project. Its properties are presented in Table 4. Note that the device's response drops to about 45% its peak at the visible red wavelength (633nm).

Table 4.1 Photodiode Key Specifications

Part Number	S2386-5K
Type	Si photodiode
Package	TO-5
Active Dia./ L [mm]	2.4mm
Active Height	2.4mm
Min λ	320nm
Max λ	1100nm
Peak λ	960nm
Peak Sensitivity.	0.6A/W
Max I_D	5.0E-03nA
Rsh	50GΩ
T_R	1.8us
C_T	730pF

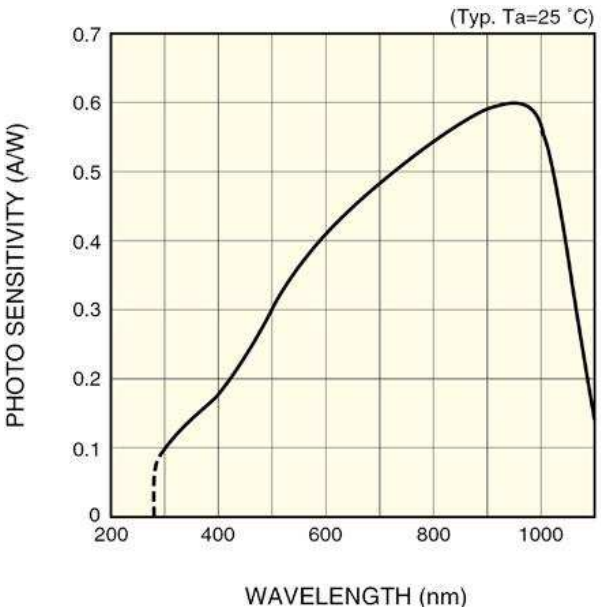

Figure 4.5 Photodiode Spectral Response

The photodiode anode produces current, which is a function of the incident light power P and the wavelength. The photodiode sensitivity *S(λ)* can be read from Figure 4.5 to estimate the amount of photocurrent I_{pd} to expect. Thus the photocurrent is given by

$$I_{pd} = P * S(\lambda) \quad \textbf{(4-1)}$$

This photocurrent can be converted to a voltage by placing a load resistor R_{LOAD} from the photodiode anode to the circuit ground. The output voltage is given as:

$$Vo = P * S(\lambda) * R_{LOAD} \quad \textbf{(4-2)}$$

In case of using op-amp circuit, the photocurrent flows only in the feedback resistor R_f. Thus the previous equation is still applied by replacing R_{LOAD} with R_f with attention to the output voltage sign.

Ideally, a 15mW laser diode of a 630nm wavelength across 100kΩ load resistor will produce output voltage of 675V. Unfortunately, there are tremendous losses of the light intensity in the optical path due to beam divergence, unwanted reflections, absorptions, etc. that dramatically attenuates the incident light and produce output voltage in the milli-range. These losses effect on the received power will be very clear later in the power budget study section. It is common to apply anti-reflection coatings to enhance the response at the required wavelength.

The bandwidth, f_{BW}(-3dB) is determined from the diode capacitance, C_T, and the load resistance, R_{LOAD} [4.2] as:

$$f_{BW} = \frac{1}{2\pi R_{LOAD} C_T} \quad \textbf{(4-3)}$$

Having 100kΩ load resistor and 730μF diode capacitance, the bandwidth of the photodiode will be 2kHz. Although, 2kHz bandwidth is sufficient, higher value is necessary for very weak signals. This gives 175μs rise time according to the approximate formula [4.3]:

$$T_R\,(10\%\text{-}90\%) * f_{BW}\,(\text{-}3\ \text{dB}) = 0.35 \qquad \textbf{(4-4)}$$

There is direct correlation between the active area and the total capacitance, which has an effect on the detector's speed. However, the capacitance is not a fixed value. Placing a bias voltage at the photodiode cathode lowers the photodiode capacitance, and simultaneously increases the photodiode bandwidth and improves the circuit performance.

According to cathode biasing there are two operation modes for photodiodes: Photovoltaic and Photoconductive modes. Due to the photovoltaic effect, photodiodes can generate a power and operate without the need for an external power source (Photovoltaic mode). However, frequency response and linearity can be improved over six or more orders of magnitude of the light power by using an external reverse voltage (Photoconductive mode) [4.4]. Diodes usually have extremely high resistance when reverse-biased. This resistance is reduced when light of an appropriate frequency shines on the junction. Hence, a reverse-biased diode can be used as a detector by monitoring the current running through it. Circuits based on this effect are more sensitive to light than ones based on the photovoltaic effect. Although, the magnitude of the reverse voltage has nearly no influence on the photocurrent, care is required to maintain the reverse voltage within the maximum ratings and to ensure that the cathode is maintained at a positive potential with respect to the anode. Typical circuits for the two modes are shown in Figure 4.6.

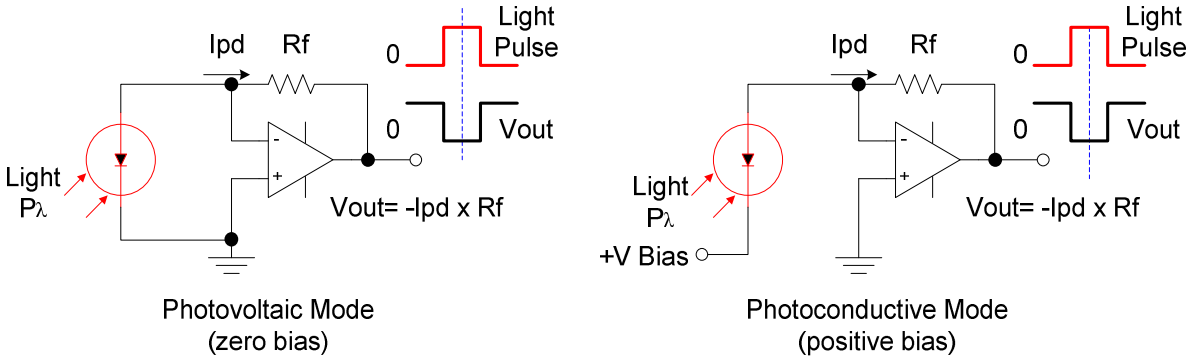

Figure 4.6 Photodiode operation modes

Utilizing the two operation modes, Photovoltaic Mode was used for the photodiode detector circuit at the retroreflector unit. With this circuit configuration, the photodiode was less sensitive to unwanted high frequency noise introduced by the carrier frequency of the LCPG modulator. Conversely, the detector circuit of the laser unit was of Photoconductive Mode type so to be very sensitive to weak signal coming from LCPG modulator.

b) *AC-coupling circuit*

Unlike fiber optic communications, free-space optical communication systems collect additional light from the environment. Light from the sun, street lights and car head lights can all be focused onto the detector. The stray light competes with the modulated light from the distant transmitter. If the environmental light is sufficiently strong it can interfere with light from the light transmitter. As long as there is extra light focused onto a detector there will always be noise. The noise has the effect of reducing the sensitivity of the detector, during high ambient light conditions. Therefore it essential in applications where large amounts of DC offset are expected on the input, the input stage of the receiver can be AC-coupled with an RC filter. The low-pass RC filter acts to remove the carrier and leaves only the original data intact. Typically, capacitors are inserted at the inputs and outputs of amplifiers to “block” DC signals, as long as they are large enough to "look like shorts" in the frequency range of interest. Amplification is used on the output of the detector to limit and shape the data back to its original form. However, since the circuit is powered from a single polarity supply, additional passive components in each stage are required and, if not properly specified, can lead to serious instability problems.

Single supply applications have inherent problems that are not usually found in dual supply op-amp circuits. The fundamental problem is that an op-amp is a dual supply device and so some type of biasing, using external components, must be used to center the op-amp’s output voltage at mid-supply. This allows the maximum input and output voltage swing for a given supply voltage.

The AC-coupled circuit of Figure 2 uses single supply biasing method. It is a modified version of a circuit borrowed from Analog Devices application note [4.5]. This inverting, AC-coupled, amplifier circuit uses a resistor divider with two biasing resistors, R9 and R10, to set the voltage on the inverting equal to $V_s/2$. As shown, the input signal is capacitively coupled to the inverting input terminal. A voltage follower is inserted in between to reject any change in supply voltage that could directly change the $V_s/2$ biasing voltage set by the resistor divider. Power Supply Rejection (PSR) is a very important op-amp characteristic.

The tap point on the voltage divider is bypassed for AC signals by capacitor C3, to improve AC PSR. The –3dB bandwidth of this network is set by the parallel combination of R9 and R10 and Capacitor C3 and is equal to:

$$f_{cutoff} = \frac{1}{2\pi\left(\frac{1}{2}R_9\right)C_3} = 96\,Hz \qquad \textbf{(4-5)}$$

This means that a pulse with duration longer than 10ms will be considered as a DC level and will be grounded gradually. The circuit acts as a band-pass filter with a lower limit of 100Hz and a higher limit of 2kHz.

Low noise amplifier circuits require low resistance values in the signal path. Johnson (resistor) noise equals 4nV times the square root of the resistance value in kΩ. While the Johnson noise of a 1kΩ resistor is only $4\,nV/\sqrt{Hz}$, this increases to $40\,nV/\sqrt{Hz}$ for a 100kΩ resistor. Even though the R9/R10 resistor divider is bypassed to ground with a capacitor (C3), these resistors set a limit on the minimum value that can be used for the op-amp's feedback resistor and, the larger this is, the greater the Johnson noise. So low noise applications need to use much smaller op-amp biasing resistor values than the 100kΩ specified here. However, lower value resistors in the divider mean higher power supply current and reduced battery life. Therefore, two 10kΩ voltage divider resistors were used. In addition, the use of a linear voltage regulator provides very low noise and output impedance.

One final issue that needs to be considered is circuit start-up time. The approximate start-up time equals the RC time constant of the lowest BW filter being used. The circuit is designed for the R9/R10, C3 voltage divider network to have a 10 times longer time constant than that of the input or output circuit. This long time constant helps keeping the biasing network from "turning on" before the op amp's input and output networks, thus, the op-amp's output gradually climbs from zero volts to $V_s/2$ without "railing" to the positive supply line.

Five thousand ohms (the parallel combination of R9 and R10) times 0.3μF equals an RC time constant of 1.5ms. So the op-amp's output will take 1.5ms (approximately) to settle to $V_{supply}/2$. The input and output RC networks will charge up ten times faster.

4.2 Microcontroller Unit (MCU)

An ATmega128 microcontroller was chosen for this project primarily because its dual UART feature. UART operates on the premise that one can transmit an 8-bit (sometimes 9-bit) data message through a single wire link without time synchronization between source and destination. The resultant single wire link is known as a Serial Data Link because the bits of the 8-bit message are transmitted in series. The asynchronous part of the UART is achieved by sending known bits to denote the beginning and end of the data message. In the hardware implementation of the UART on most Atmel chips the UART samples received bits 3 times in the middle of the bit and uses a "majority rule" process to determine the value of the bit.

Unlike many microcontrollers, the ATMEL ATmega series were designed explicitly for support high-level languages. The ATmega128 is a low power CMOS 8-bit microcontroller based on the AVR enhanced RISC architecture. By executing powerful instructions in a single clock cycle, the ATmega128 achieves throughputs approaching 1 MIPS per MHz allowing the system designer to optimize power consumption versus processing speed [4.6]. The layout of the processor is shown in Appendix B1.

Fortunately, AVR570 is a plug-in module holding a surface mounted ATmega128 CPU, and its associated components, e.g. the crystal, capacitors, reset generator, and ISP programming connector. The module is mass-produced by JED [4.7] and has 64 pins in a square pattern to plug into socket strips on the user's base board. Figure 4.7 shows a picture of the module.

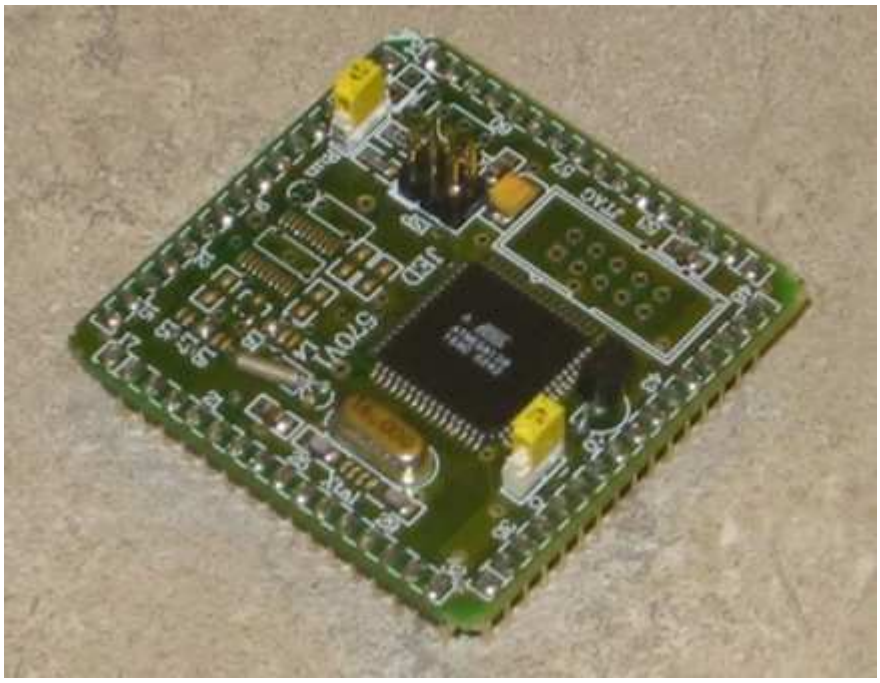

Figure 4.7 AVR570 ATmega128 CPU module

The ATmega128 is the central device in the microcontroller implementation. In order to get a functional test system some peripheral components were needed. The RS232 communication was established via a MAX232 circuit which converts the TLL/CMOS levels of the ATmega128 to RS-232 signal levels and vice versa. A 74AC14N Schmitt trigger IC was chosen to reshape and prepare incoming signal as a square pulse for the microcontroller input ports.

4.3 Software Design

In ideal conditions, free-space optical communications work greatly by transmitting and receiving modulated light. Unfortunately, transmission of data across a noisy communication channel requires some manner of separating the valid data from the background noise. The most common way to accomplish this is to modulate the data at the transmission side and to demodulate the data on the reception side, so that the data coming from the receiver are the same as the data being presented to the transmitter. There are two major problems related to free-space optical communications: (1) the serial data being transmitted must be 'balanced', and (2) the receiver does not like "bursty" communications.

When a very long duration square wave pulse is passed through an AC-coupled circuit, the top line of the pulse will eventually decay exponentially back down to zero. This can happen in a digital system with a Non Return to Zero (NRZ) digital code whenever a long string of either 0's or 1's occurs. Simply sending binary or ASCII signals over the serial link obviously won't meet this requirement, and some method must be employed to encode the serial stream. There are several options, ranging from look up tables to ensure that everything is balanced to sophisticated CPU intensive encoding schemes. Somewhere in the middle of that range lies a technique named Manchester Encoding (ME) that has an alternating 1's and 0's pattern in every byte to balance the signal. The next section briefly describes the Manchester Encoding algorithm and highlights its useful features.

An AC-coupled circuit is not immediately ready to receive data when an incoming transmission begins. It takes some 'start-up' time to charge the capacitors and to filter out the DC signal. Therefore, some preamble bytes are appended at the beginning of the Manchester encoded data packet before transmission. This solves the "bursty" communication problem and enables each stage in the data path to properly synchronize with the start of the transmitted packet.

There are many ways to detect bit errors in a serial transmission. Some methods are even able to correct the bit errors without requiring a retransmission. Obviously, the more sophisticated a solution becomes, the more code space and CPU time it requires. Fortunately, the optical communications were extremely reliable, so no error check schemes were implemented, e.g., parity checking, cyclic redundancy check, etc. A simple Manchester decoding check was enough to check for bit errors. The microcontroller receiver onboard each robot synchronizes on the first two bytes received and decodes the next bytes into data. The receiving microcontroller performs error checking on the data. If any of the transmitted bytes fails Manchester decoding check, a flag is raised to indicate that the packet is bad. If the packet is bad, then it is rejected.

4.3.1 Manchester encoding

IEEE Standard 802.3 uses a scheme called Manchester Encoding instead of straight binary encoding with 0 volts for a 0 bit and 5 volts for a 1 bit, as in NRZ. This because it leads to ambiguities caused by the fact that nodes cannot tell the difference between the idle state (0 volts) and a 0 bit being sent. The encoding of digital data in Manchester format defines the binary states of "1" and "0" to be transitions rather than static values. The transition at the middle of each bit period serves as a clocking mechanism and also as data. Manchester encodes ‘1’ into ‘10’ and ‘0’ into ‘01’; hence it can be viewed as 1B/2B encoding or bi-phase encoding [4.8-4.10]. Given that a 0 encodes to 01 and 1 encodes to 10, it follows that 00 and 11 are illegal sequences or codes. These codes are used to error check the data. An example of Manchester Encoding for data bits is shown below in Figure 4.8.

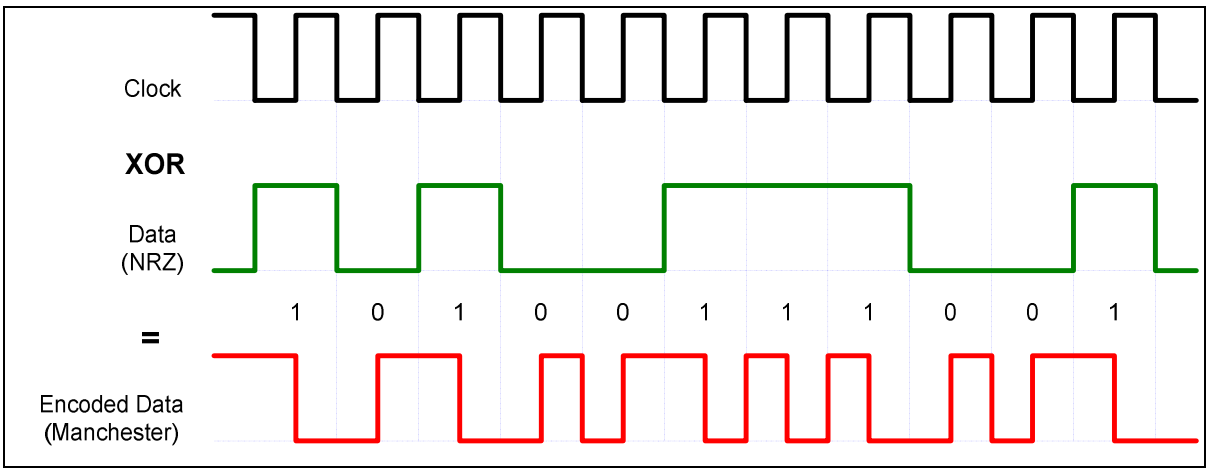

Figure 4.8 NRZ and Manchester encoded waveforms

It is easy to maintain synchronization between transmitter and receiver, as during every bit interval there is a transition so it is easy to distinguish between an idle period and a transmission of a 0 bit. Manchester Encoding was ideal for this project, because of its self-clocking quality, and because of its low cost of implementation. The main advantages of using Manchester Encoding in free-space optical communications are:

1. The encoded signal never produces frequency components near DC, regardless of the data, which is useful for transmission over channels that require AC-coupling.
2. Simple to encode, decode and has good error detection negating the need for 'check-summed' data.
3. Can be transported using standard RS232 software /hardware.
4. Practical and easy to implement on target devices and fast to perform.

Since there are two bits of Manchester encoded data for each bit of original data, the one clear disadvantage to Manchester Encoding is its substantial bandwidth consumption; it halves the data rate. However, since high data rates were not a design constraint, the other advantages of Manchester Encoding easily outweighed the bandwidth inefficiency.

4.3.2 Program description

The main program flow is shown in the flowchart of Figure 4.9. The program is divided into two routines; Transmitter and Receiver. Both of them are interrupt-driven. The program initializes the ports, sets up the UARTs and enables interrupts. UART0 is set to communicate with BasicX at 19200 bits per second (bps). And UART1 is to pulse the optical modulators (laser/LCPG) at 1000bps. Setting the data rate is important for two reasons: it determines how long the transmitting UART must maintain a bit's value on the wire, and it determines how long the receiving UART must wait between sampling bits. Communicating with BasicX is straight forward through serial RS232 link. In contrast, communicating with optical modulators needs more codes and data manipulation to successfully transmit/receive data through light.

RS232 is used as a carrier for Manchester Encoding provided that bytes of RS232 are transmitted end-to-end. RS232 has a start bit, logical '0', and a stop bit, logical '1'. All that's required is to insert Manchester encoded data into the RS232 data bits. There are 4 Manchester encoded bits in each RS232 byte.

The communication code was written as a serial transmission routine that is interrupt driven in the ATmega128. Interrupts are used for two reasons: (1) the robot software does not need to actively handle transmitting/receiving data; it simply works in the background, and (2) the incoming data needs to be used to synchronize the data. As data is received on the other end using a second ATmega128, baud rates do not need to be standard baud rates, but they are required to be the same baud rates on both the transmitter and receiver MCU's.

In transmitting mode, the program keeps transmitting the same data packet repeatedly until acknowledgement is received indicating that the package is delivered. Then the program continues with task executing and loops back to the beginning of the program. However, in

the receiver mode, the program executes the received task when the received data is error free. Otherwise, the program rejects received data and loops back again.

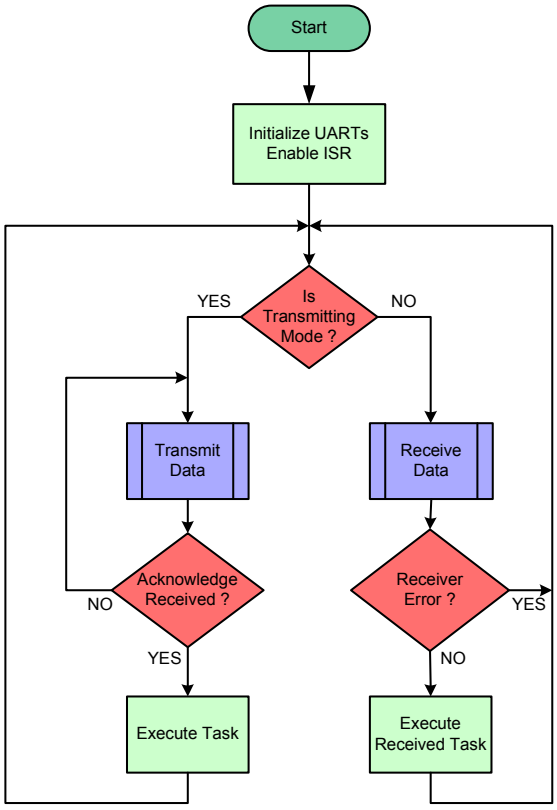

Figure 4.9 Main loop flowchart

The transmission routine is simple, as shown in Figure 4.10a. Since the MCU receiver is connected to a photodiode detector through an interrupt service routine, any change in the light intensity triggers the receiver. To overcome this artifact the receiver is disabled during data transmission; else the receiver will pick up reflections from its own transmitted data. Next, bytes are encoded with the Manchester Encoding scheme and transmitted through UART1. The program returns from this routine when all data bytes are transmitted. Note that the transmitted data is inverted compared to the actual data (i.e., the data is idle high).

The data frame is started by transmitting a preamble of high/lows patterns (UU) to the serial link. The number of UU patterns depends on the characteristics of the receiver. In general, enough UU patterns are needed to:

1. Initialize the receiver demodulator
2. Allow the RS232 decoder to synchronize to the start bits of each RS232 byte.
3. Indicate to the software communications handler that an UU pattern has been received and data is expected to follow.

Receiver is a device that receives the encoded bit stream is responsible for decoding the bit stream by extracting the data from the received signal. In most cases, the receiver must retrieve the original data stream by using the encoded signal without any additional information about the transmit clock. Unfortunately, in asynchronous communication and with this type of encoding scheme, it is common that the receiver decodes two consecutive bytes that did not originate from the same encoded byte. This Manchester Decoding error causes the rest of the received data to be corrupted. In order for the receiver to synchronize with the incoming data, symbols '(' and ')' were selected identify the boundaries of data frame. They have unique Manchester Encoding characters that distinguish them from any alphabetic and numeric symbol. These unique representations improve synchronization and simplify receiving process. In addition it looks more natural to enclose a data packet with some type of brackets or parentheses.

Therefore, when the receiver routine is called, it first enables the receiver and waits for the Start Byte symbol '(' to synchronize with the transmitter. The Start Byte is easily distinguished from the 'U' character of high/lows pattern that keeps the line active before transmitting the real data. Hence, the routine can only continue once a start byte has been detected. Upon receiving the start byte, data is acquired and decoded. An acknowledgment will be sent indicating command is received if Stop Byte was received and no decoding error was detected. Otherwise, receiver error flag will be set and the routine returns. During data

packet transmission, synchronization is not required. Figure 4.10b illustrates the program flow of the receiver routine in a flowchart diagram.

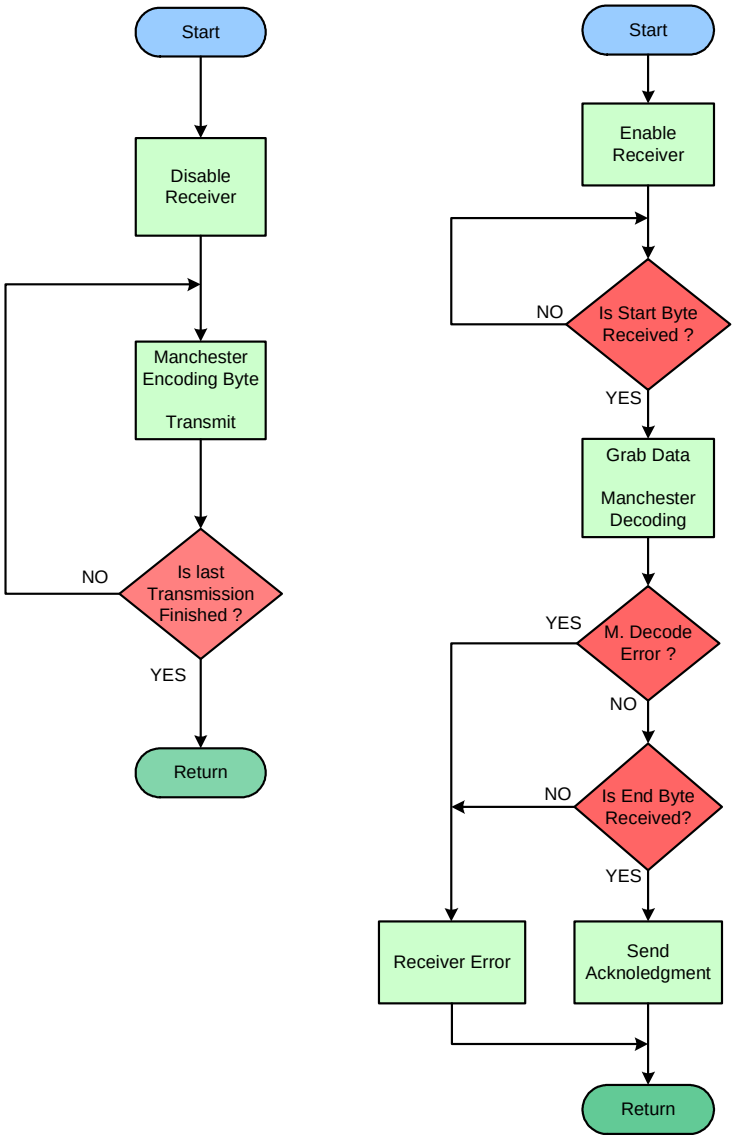

Figure 4.10 Transmitter flowchart (a) and receiver flowchart (b)

As far as physical communications are concerned, the most difficult and technically challenging part is data reception. While some thought had to be put into the design of the transmission software, the Manchester Encoding algorithm is simple to implement. The algorithm is slightly different from the traditional Manchester Encoding algorithm to avoid unnecessary bit manipulation [4.11]. It is faster to encode odd bits (7,5,3,1) into the most significant 8 bits and the even bits (6,4,2,0) into the least significant 8 bits in each byte with no downside. Only shift, mask, complement and OR the bits together are needed to get an encoded byte. Converting Manchester encoded data back to original data is straight forward and error checking may be carried out at the same time. Since data arrives as 4 bit-pairs of Manchester encoded data a simple shift and test algorithm can be implemented to retrieve the original data.

Since all software development was undertaken using C++, a software tool called WinAVR was used because it includes the GNU GCC compiler for C and C++. WinAVR is a suite of executable, open source software development tools for the Atmel AVR series of RISC microprocessors hosted on the Windows platform. The full code demonstrating the transmitter/receiver is almost 500 lines long, and its C code is given in Appendix C2.

In summary, there are two challenges to working with serial optical communication. The first challenge is that the serial data must be balanced. Manchester Encoding is the easiest way to overcome this, but it has a penalty of cutting the bit rate in half. The second challenge is that many AC-coupled receivers require certain amount of startup time before reliably detecting data. This can be overcome by transmitting a short burst of meaningless data prior to sending the true data.

4.4 Optics Design

Laser beam alignment from the laser's end window to some terminal target is quite a challenge. It requires work with an open beam and involves directing the beam toward a

series of reflective or partially reflective surfaces, such as mirrors or lenses, so that the beam follows some predetermined path.

The design goal was to build the retroreflector modulator and laser transceiver units with minimum components for simplicity and robustness and maximum efficiency for long range communication. The first design trial was consist of beam splitter and focusing lens to direct and collect reflected light from the retroreflector to the detector. Although the design worked with acceptable performance, the optical power loss was high and the packaging was quit challenging and heavy for a small mobile robot to carry.

Off-axis parabolic (OAP) mirror was the solution to these problems. It simplified the alignment focusing and reduced optical components for the system. A brief description for OAP is given next followed by Solid Works design model for the retroreflector and laser bases.

4.4.1 Off-axis parabolic (OAP) mirror

Off-axis parabolic mirrors are only a section of the parabola form. These mirrors have the advantage of directing and focusing incident collimated light at a specific angle, allowing unrestricted access to the focal point as shown in Figure 4.11. There are no shadowing problems if a detector or source is placed at the focus. In addition, OAP mirrors are free from spherical aberrations, and thus focus the parallel beam to a point or point source to infinity. Therefore, a 90-degree off-axis parabolic reflector from Edmund Optics [4.12] was used in this study. It has 2 inches focal length and 2 inches open aperture. Reflector specifications were selected carefully to fit design parameters such as aperture size, weight and focusing length and angle.

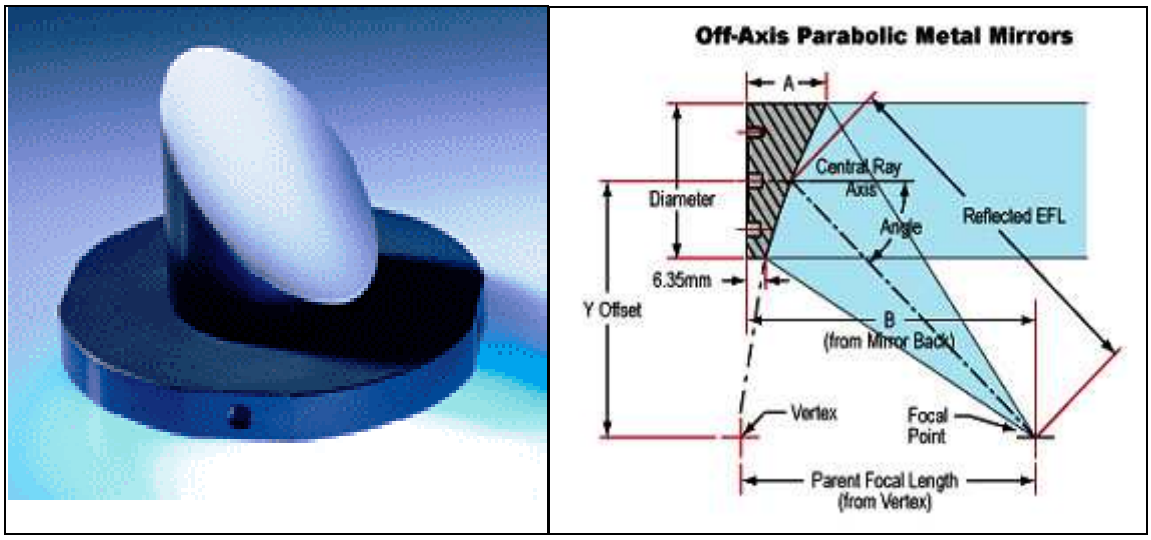

Figure 4.11 Off-Axis Parabolic Reflector [4.12]

To utilize the advantages of OAP mirror, a hole was made at the center of the OAP mirror so that a laser beam can pass through. Then, when a transmitted light hits a retroreflector target, a modulator modulates light beam and retroreflects it back to the source. The modulated light is then collected by the OAP mirror and focused down onto a photo-detector. This communication scenario using OAP reflector was simulated and is presented in Figure 4.12.

The expectation of this arrangement is high. Eliminating the need for a deflecting mirror or a beam splitter, and a focusing lens will enhance the system efficiency. In addition it simplifies the design and reduces the weight and the cost.

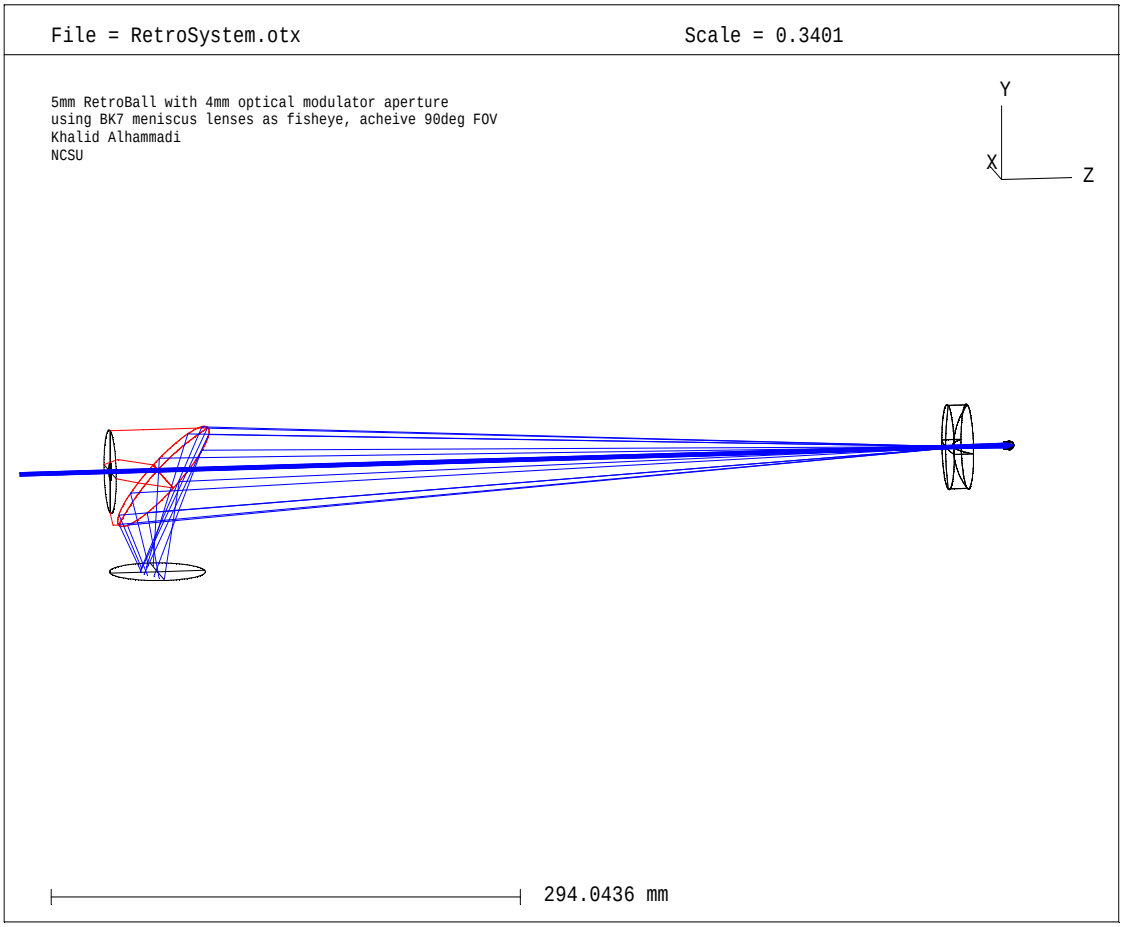

Figure 4.12 Overall optical system design: Laser transceiver (left) and Retroreflector modulator (right)

4.4.2 Retroreflector and laser base structural design

The proposed optical system consists of two major devices: laser transceiver and retroreflector modulator. Laser transceiver was made of three components:

1. Laser diode as a light source,
2. Off-axis parabolic mirror to collect and focus incident light and
3. Photodiode as a light sensor and placed at the focal point of the OAP mirror.

On the other end of the communication link is the retromodulator, which also has three components:

1. Fisheye lens to expand FOV of the retromodulator,
2. Liquid Crystal Polarization Grating (LCPG) device to act as an optical modulator and
3. High reflection coated ball lens to retroreflecte incident light.

Solid Works software package was used to design every components of the laser transceiver and retroreflector modulator as a single part. Then these parts were matted together to form the final design model. Figure 4.13 shows a 3D CAD model of the two devices without their transceiver circuits. Schematic drawing for the two bases are provided in Appendix B2.

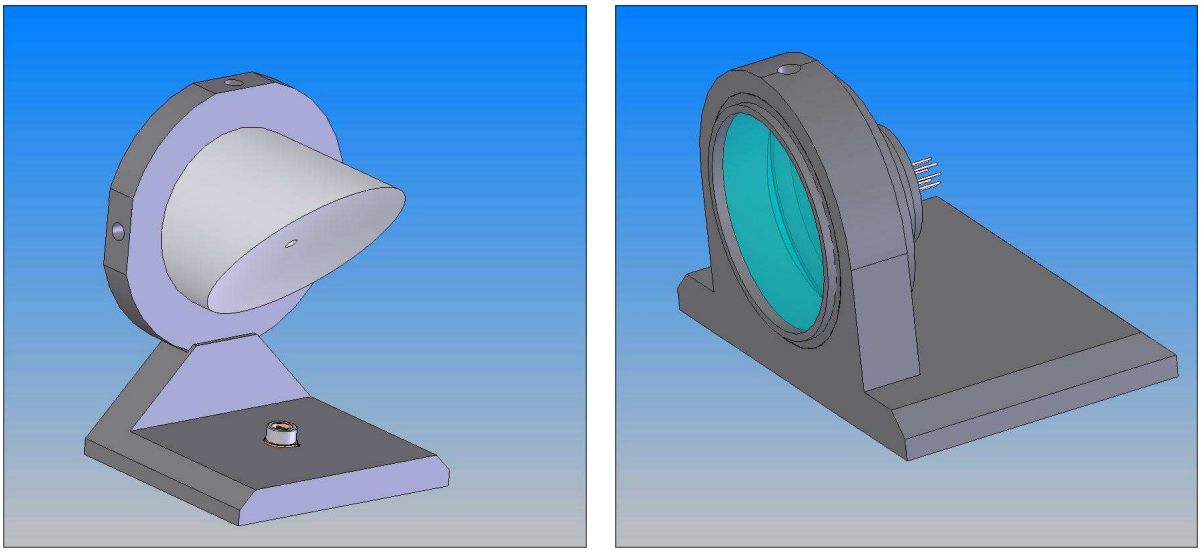

Figure 4.13 3D CAD model for: laser transceiver (left) and retroreflector modulator (right)

All parts were bought from Thorlab and Edmund Optics except for the device base. The base was fabricated in the university machine shop. It was designed to be a stand alone unit that holds all device components in one unit. It is portable and easy to be mounted on a mobile robot. The components are destined to be as easy to plug in or removed for cleaning or debugging. Figure 4.14 shows a SolidWorks drawing for the expected behavior of the two devices when placed in action.

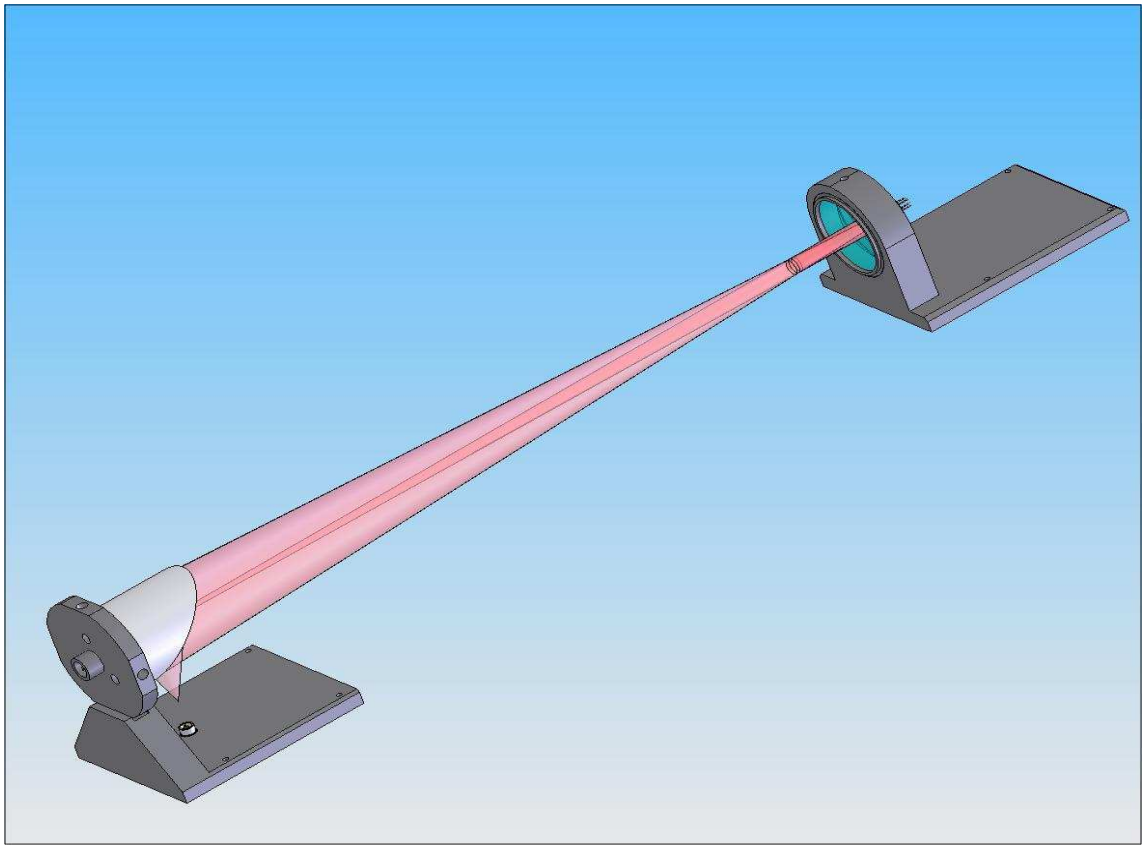

Figure 4.14 SolidWorks drawing of laser transceiver and retroreflector modulator in action

4.5 Reflected Power Efficiency (Optical Power Budget)

Laser is a powerful tool for distance communication. However, many variables can affect laser intensity at the receiving end: the power of the laser, its wavelength and spot size; intensity of the background illumination; and position of the observer relative to the target. It is utmost important determine the losses that an optical signal undergoes between the source and the receiver. This section describes the transmitter/receiver power in a retroreflector optical system.

Retroreflectors such as Corner cube or Cat's-eye reflectors are types of cooperative target for which the reflectivity of the laser beam is enhanced to give a higher return signal to the

receiver. When using them, alignment is not a critical issue because they give a return beam independent of the exact orientation of the reflector.

In a typical wireless optical system, laser beam first goes through transmitting optical system to reduce the divergence angle of the transmitted beam and to aim the beam at the target. Then, at the target, the receiver optical system collects part of the beam and focuses it into the detector/retroreflector. However when operating at small beamwidths and divergence angles better pointing and tracking techniques are required. Link budget include pointing losses where transmitter and receiver are not stationary.

In the literature, several authors discussed the geometrical factors that affect the relation between transmitted power and received power [4.13, 4.14]. However, the Laser Electro-Optics Technology (LEOT) [4.15] discussion was most pertained to this research. Here, a summary of their work is presented. Appendix A3 contains step by step derivation of the final formula.

A laser beam with an aperture diameter d_t and divergence angle θ_t (radians) radiates a target at a distance R and illuminates an area A_{tar} at the target plane. Assuming the transmitted beam completely covers the entire area of the target that retroreflects the beam back to the source, Figure 4.15 illustrates this radiation pattern of the transmitter-to-target geometry.

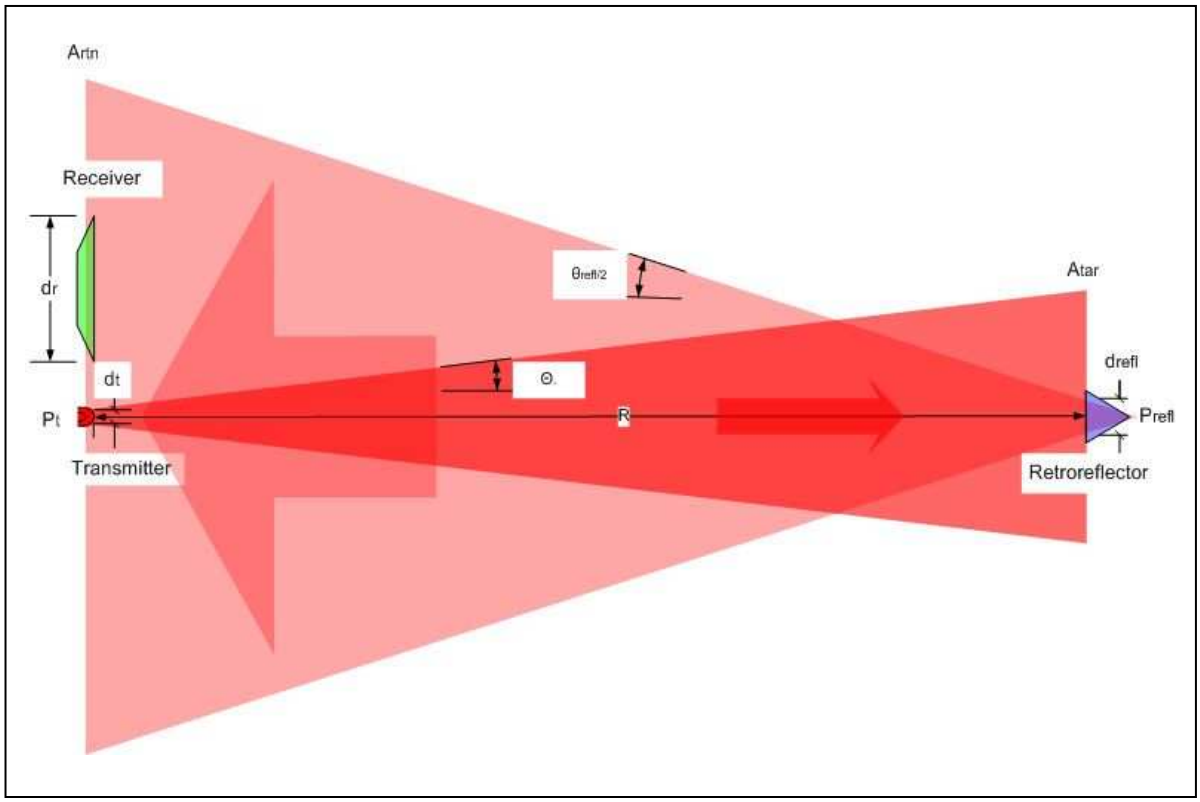

Figure 4.15 Radiation pattern of the transmitter-to-target geometry for efficiency computation

The emerging beam from the reflector with d_{refl} effective diameter will have a divergence angle θ_{refl} equals to the divergence of the transmitted beam plus diffraction effects due to the limited size of the reflector. Assuming 100% surface reflectivity for the reflector and account for atmospheric attenuation factor T, the general formula of the received power by the detector surface d_r is given as:

$$P_r = P_t \left(\frac{d_{refl}\, d_r T}{(\theta_t R + d_t)\left(2d_{refl} + \frac{2.44\lambda R}{d_{refl}} \right)} \right)^2 \qquad \textbf{(4-6)}$$

It is clear that the range has significant effect on the received power. At short-range measurements, such that $2d_{refl} >> \frac{2.44\lambda R}{d_{refl}}$, the received power is dependent on the inverse square value of the range and independent of the reflector area. In contrast, at very long-range measurements, such that $\theta_t R >> d_t$ and $\frac{2.44\lambda R}{d_{refl}} >> 2d_{refl}$, the received power is dependent on the inverse fourth power of the range and on the fourth power of the reflector diameter. And it is quite possible, at this range, for the atmospheric transmission to be the dominant factor. However, equation (4-6) can be simplified by letting *T* has a value of 1 and keeping the term θ_{refl} in the formula which can be measured experimentally. Thus the formula deduced to:

$$P_r = P_t \left(\frac{d_r \, d_{refl}}{(\theta_t R + d_t)(\theta_{refl} R + d_{refl})} \right)^2 \qquad \textbf{(4-7)}$$

Applying the values in the Table 4.2, one can estimate the amount of the received power by the detector. The calculation shows that at 1m distance the received power is 1% of the transmitted power. When using a 15mW laser source, 0.15mW will be seen by the laser transceiver detector. This low power requires a good receiver with high gain and low noise.

Table 4.2 Power budget parameters

Rang (*R*)	1 m
Detector Receiver diameter (d_r)	2 mm
Retroreflector diameter (d_{refl})	6 mm
Reflected beam divergence (θ_{refl})	17 mrad
Transmitted beam divergence (θ_t)	3 mrad
Transmitted beam diameter (d_t)	2 mm

The calculation revealed that this device works for short range applications. However, the retroreflector aperture will receive 21% of the transmitted power. This indicates the

possibility of employing this device for long range applications on one way transmission, i.e., laser transmission. Power calculation does not include losses due to unwanted lens surface reflections, glass absorptions, or parabolic mirror hole; it merely shows the upper limit of the device performance.

4.6 *References*

[4.1] M66510P/FP Laser diode deriver, MITSUBISHI
http://www.ortodoxism.ro/datasheets/MitsubishiElectricCorporation/mXssrzs.pdf

[4.2] Hamamatsu Photodiode Technical Guide
http://www.usa.hamamatsu.com/assets/html/ssd/si-photodiode/index.htm

[4.3] J. Palais, "Fiber Optic Communications". 4th ed. Pg. 183, 219 (Prentice Hall, 1998).

[4.4] Encyclopedia of Laser Physics and Technology. www.rp-photonics.com/photodiodes.html

[4.5] C. Kitchin, "Biasing and Decoupling Op Amps in Single Supply Applications". *Analog Devices Inc.*, Application Note: AN-581, (2002)

[4.6] Atmel Corporation http://www.atmel.com/dyn/products/product_card.asp?part_id=2018

[4.7] JED Microprocessors Pty. Ltd. http://www.jedmicro.com.au/avr.htm

[4.8] Wikipedia encyclopedia < http://en.wikipedia.org/wiki/Manchester_encoding>, August 2006.

[4.9] "Manchester Data Encoding for Radio Communications", *Maxim Integrated*

Products, Inc. APPLICATION NOTE 3435.

[4.10] "Background on Manchester encoding", *The MathWorks, Inc.*

[4.11] Aaron Ramsey, "RF Communications Primer". www.ottawarobotics.org

[4.12] Edmund Optics Inc., http://www.edmundoptics.com/onlinecatalog/displayproduct.cfm?productID=2307

[4.13] M. Last, S. Patel, B. Fisher, C. Ezekwe, S. Hollar, B. Leibowitz and K. S. J. Pister, "Video Semaphore Decoding for Free-Space Optical Communication," *Proceedings of the SPIE - The International Society for Optical Engineering*, vol.4303 (Electronic Imaging `01), San Jose, CA, 21-26 January 2001.

[4.14] M. Achour, "Free-Space optical communication by retro-modulation: concept, technologies, and challenges", *Modus Technologies*, Inc.

[4.15] Laser Electro-Optics Technology (LEOT) curriculum materials from the Center for Occupational Research and Development (CORD) in Waco, Texas.

Chapter 5

Optical Communications for Robotics and Other Potential Applications

Laser communication systems use wireless transmission through free space. The carrier used for the transmission signal is generated by a laser diode. Although, the transmitter and receiver must require line-of-sight to function correctly, such, laser communication systems are easily deployed since they are inexpensive, small, low power and do not suffer from radio interference. It is an attractive solution for the demands on increasing communication bandwidth. With possible transmit speeds of up to a gigabit per second, this is an exciting area. Bandwidth could be distributed in neighborhoods by putting laser communication systems on top of homes and pointing them towards a common transceiver with a fast link to the Internet. Other applications for this technology include temporary connectivity needs (e.g. sporting events, disaster scenes, or conventions), or space based communications.

Here, the application of retroreflector communication technology, this researches autonomous mobile robotic communication and underwater communication. Hence, the chapter covers two main topics. First, a description of the transceiver board layout and a discussion of its performance and limitations are presented. Second, experimental results from the laser transceiver and retroreflector modulator units are presented for two applications: (1) autonomous mobile robot communication, and (2) underwater communication.

5.1 Transceiver Implementation

The transceiver board layout was designed using EAGLE (Easily Applicable Graphical Layout Editor) light software, reference [5.1]. As shown in Figure 5.1, the circuit board consists mainly of three sub-circuits: (1) a pulse amplitude modulation as a transmitter, (2) an AC-coupled photodiode detector as a receiver, and (3) an ATmega128 microcontroller, that is the microcontroller of choice. In addition to these circuits, an MAX232 IC was used as RS232 serial communication interface to the onboard MCU (the AVR570 discussed later). The main design feature of the board is that it can switch between photodiode modes (photovoltaic and photoconductive) simply by using jumper2 (JP2). That is, the same board can be used as either a laser transceiver unit or as a retroreflector modulator unit by simply switching the JP2 connections. AVR570 (MCU) has its own reset switch making it easy to reboot the MCU after a new program has been downloaded into the MCU memory. All the circuitry needed for optical communication system are contained on this single board design. Once it was fabricated and tested the board showed that it consumed a current less than 170mA when it was powered from low voltage source (regulated 5VDC). Figure 5.2 shows a true image of the transceiver board.

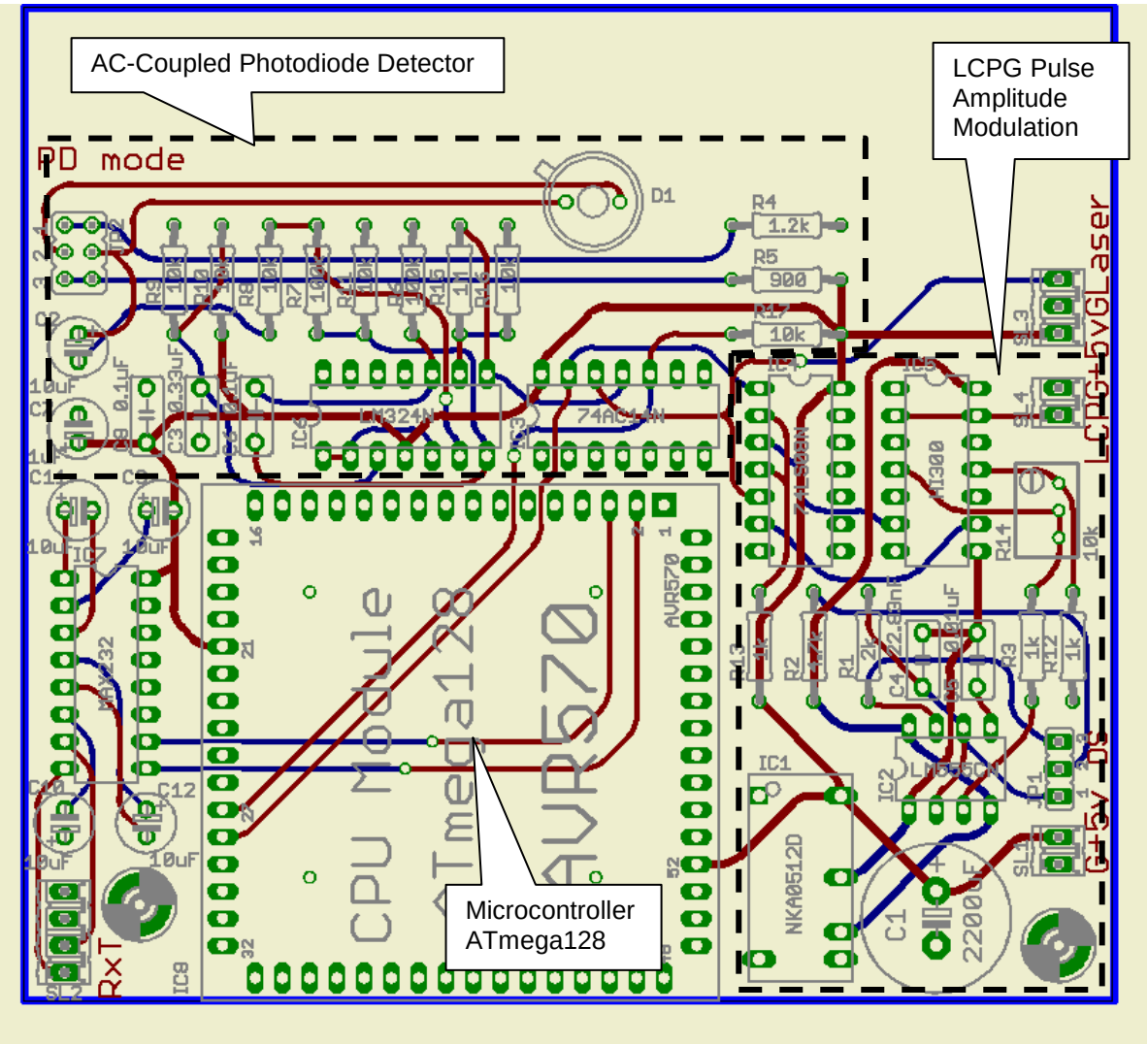

Figure 5.1 Board layout for the transceiver circuit

The AC-coupled circuit has a wide bandwidth, one that is stable in the range 100Hz to 1kHz. The upper limit represents the maximum permissible baud rate of the circuit. The lower limit is important because it indicates the longest bit period that the circuit permits without significant attenuation in the received signal. The 100Hz means a bit of less than 10ms period will be considered a bit in the data stream and not a DC signal.

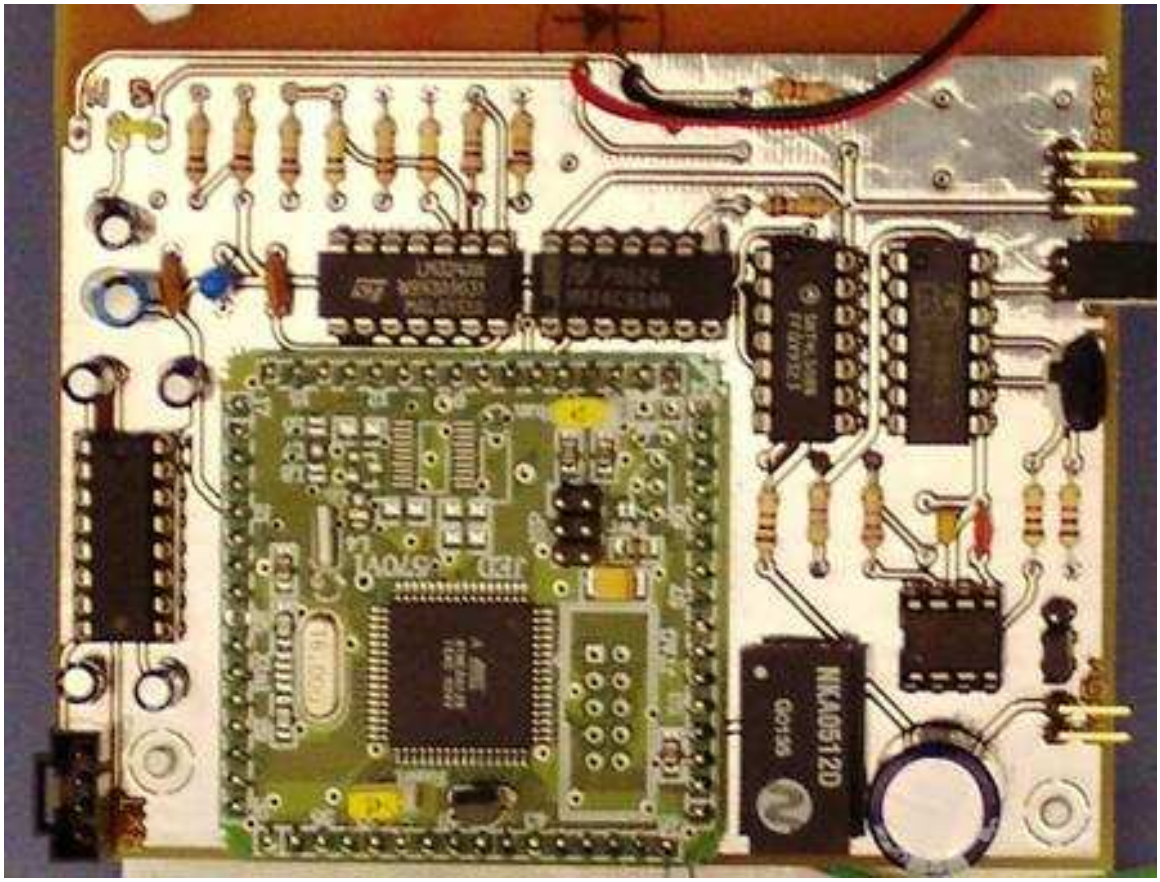

Figure 5.2 Image of the transceiver board

The transceiver takes about 30µs to 'start-up' before it is able to receive the transmission. Start-up is inversely proportional to the received signal strength, i.e., light intensity. At the beginning of data transmission some erroneous data is transmitted, this must be dealt with prior to dealing with the true data being communicated. To ensure data integrity a stream of 1's and 0's represented by ‘U’ symbol was transmitted prior to the channel transmitting real data. Because the transmission is bursts of data rather than a continuous stream of data, this pre-transmission signal is used before every data transmission. In addition to the preceding, a synchronization symbol ‘(‘ is also transmitted. These pre-transmission bytes, four bytes when using Manchester encoding, reduces the number of bits per second being transmitted by adding a total of 40ms overhead to data transmission period. Figure 5.3 shows a screenshot for 3 channels representing the transmitted data, the retroreflector modulated

signal and the received data. This start-up time will increase rapidly with presence of weak received signals.

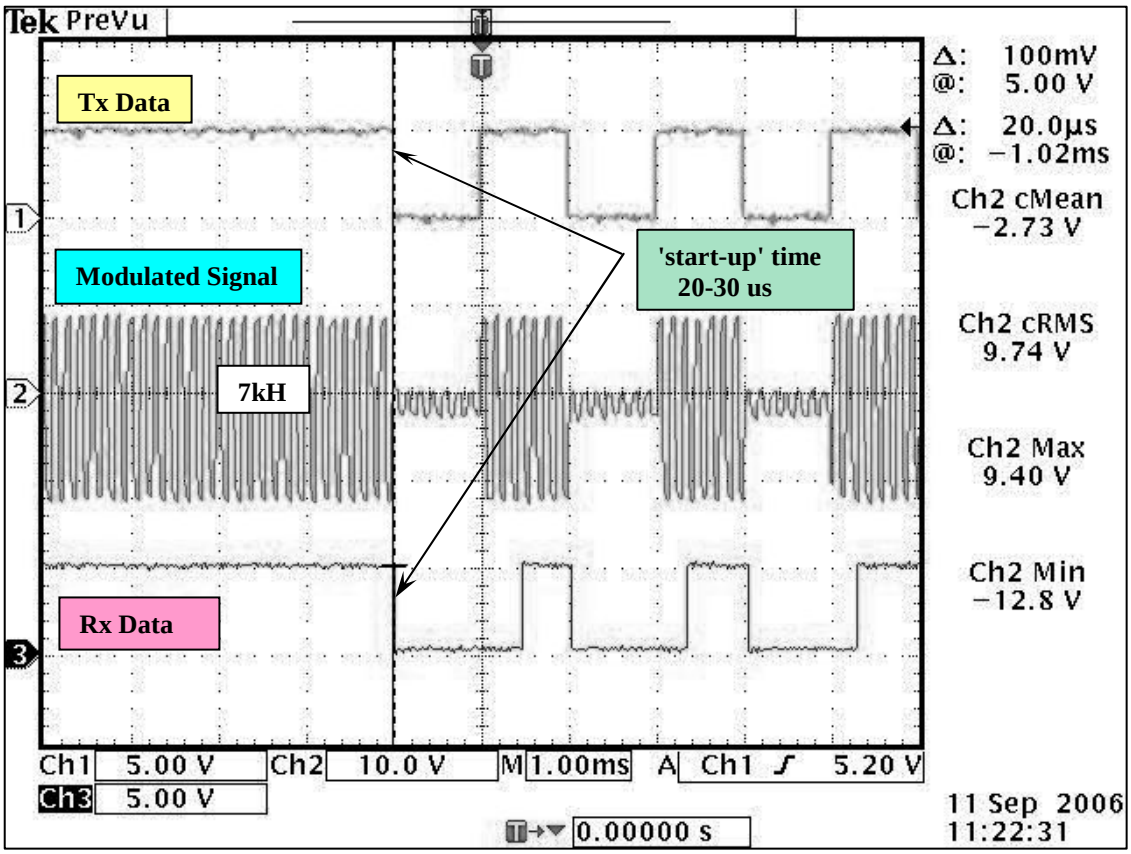

Figure 5.3 Screenshot for transmitted data, modulated signal and received data

Noise is very problematic when working with sensitive communication circuits. The PD circuit was very sensitive to high frequency signals. It picked up the carrier frequency of the LCPG modulator when not illuminated which destabilized the receiver circuit operation. Turning off the LCPG did not solve the problem as the receiver still picked up noise from other sources in the surrounding area. The solution was to lower the amplification gain of the AC-coupled circuit, which then compromises the detector sensitivity.

Focusing a laser beam emitted from a laser diode turned out to be quite a challenge. Laser diode device has a large beam divergence, as specified in manufacture datasheet given in Appendix B3. Basically, the laser diode requires focusing optics. Fortunately, the LT230A collimation tube from THORLABS is a simple and compact module that uses an aspheric lens to focus the laser beam manually. Aiming the laser beam at a target was another problem, especially at long ranges. No aiming or tracking system was implemented for this project; rather any adjustment was made manually. The lack of an optical tracking system is one of the major performance limitations of the device.

The laser transceiver and retroreflector modulator devices were assembled as a stand alone unit. The two units, shown in Figure 5.4, need only two connectors to operate; connection to a 5V from a regulated DC power source and RS232 serial cable to the mobile robot MCU or to a PC's Hyper-terminal for debugging.

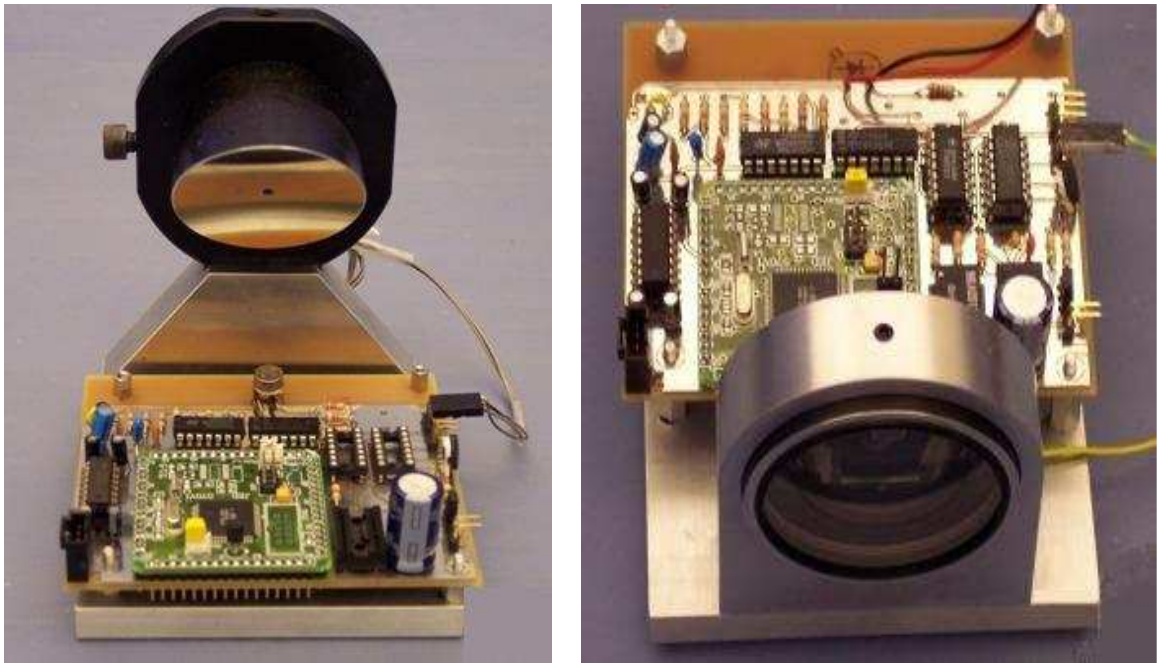

(a) **(b)**

Figure 5.4 a) Laser transceiver unit, b) Retroreflector modulator unit

The system that has been designed and implemented has several attractive features. One board is responsible for transmitting, receiving, and decoding the laser signal. Using UART0 to communicate with hyper terminal on a PC, the two transceivers were tested to optically transmit text through UART1 at 1 kbps data rate. At this rate it is entirely error free. The system can likely transmit much faster (2.4kbps), but for communication stability and optimality anything faster is overkill.

5.2 Mobile Robot Communication

Commonly in autonomous mobile robotics, robots cooperate to solve complex tasks, tasks that would take more than a single robot to solve. In essence, the robots were meant to be autonomous and would need to coordinate themselves without some sort of master. Exchanging information such as the position, speed, braking, turning, dimensions and destination of the robot is essential in robotic applications. Obviously, some way of communication is needed between the robots in order for them to coordinate their movements. A two-way communication system using a laser emitter and retroreflector was proposed by Aoki et al. [5.2]. Wireless optical communication is one way of simple, clean communication. The laser emitter system transmits a modulated laser beam and the reflector modulates the beam and returns it toward the emitter system. For the purpose of this research, EvBot mobile robots (named EvBot II) were used as the platform to host transceiver devices for wireless communication, as shown in Figure 5.5.

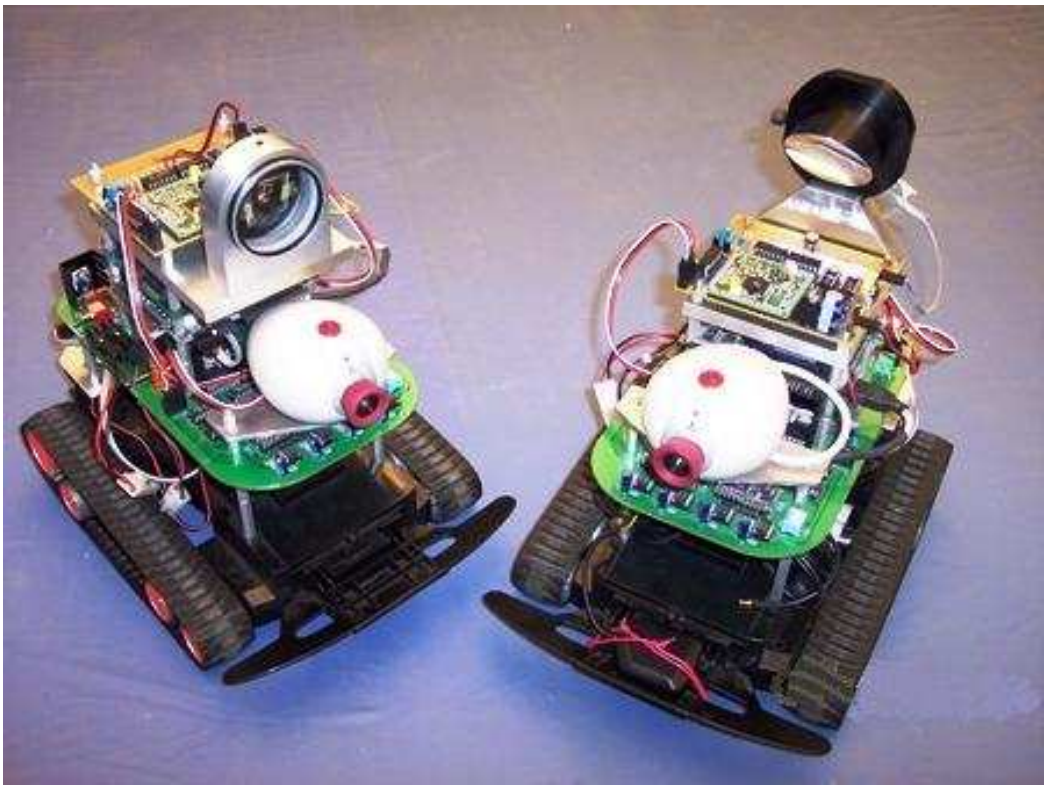

Figure 5.5 EvBots mounted with Laser transceiver (right) and Retroreflector modulator (left)

Galeotti [5.3] developed and built the EvBot robotic platform to be small and inexpensive and yet robust and powerful. Mattos [5.4] expanded Galeotti's work and developed the EvBot II, the next generation of autonomous robots for distributed robot-colony research. His design expanded the sensing capabilities and performance capabilities by using two microcontroller units, shaft encoders and a complete acoustic array system for tracking and navigation purposes. The EvBot II is a small, and more computationally powerful and robust evolutionary robotics platform than the original EvBot's. It uses a PC104 stack equipped with a Pentium class processor, and it also features low power consumption, being able to continuously operate for more than two hours on a single 7.2V/3000mAh Ni-MH battery. The CRIM's EvBot II has the advantage of reduced size (twelve by ten inches) and low price (about $1400.00 for parts per unit).

In order to test the communication system (hardware and software) and to prove the research concept, 3 simple program subroutines were written. The first two programs were to test and obtain the ultimate range of the implemented system at which data can be transmitted and received. This includes obtaining the maximum FOV and operation range for the system. The third program was to test how the mobile robots coordinated with each other in a cooperative movement using the retroreflector communication system.

5.2.1 Maximum FOV experiment with EvBot II

The mobile robots (EvBots) were tested for their FOV ranges in two setups. In these setups, once a robot gets the request, it compiles the requested data, replies back to the transmitter and performs the requested action. The two arrangements are shown in Figure 5.6 including illustration of the angle of incident light and the direction of robot movement.

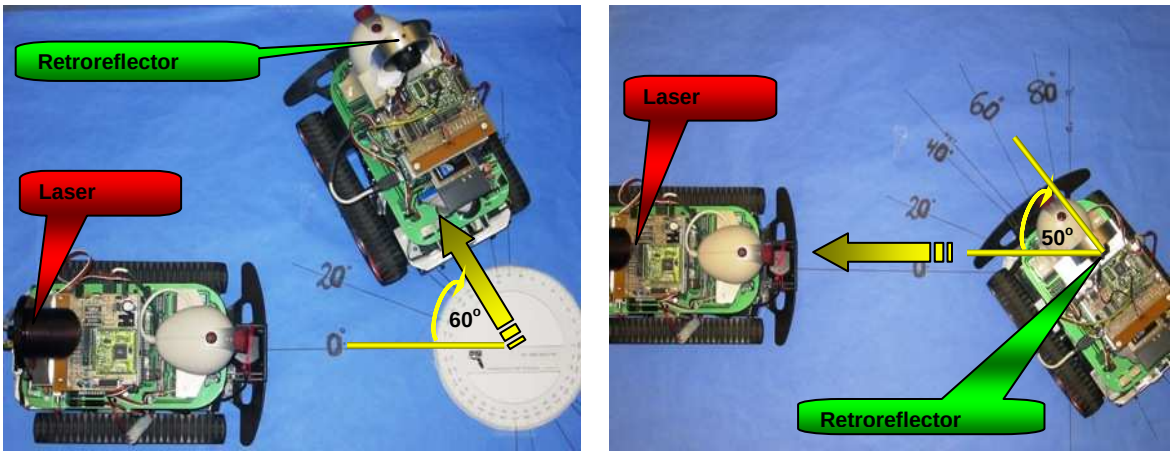

Figure 5.6 FOV test with direct transmission (left) and retroreflected transmission (right)

In the first arrangement (left), the robot carrying the laser device, name the Laser Evbot, transmitted a “move forward” command to the robot carrying the retroreflector device, name the Retroreflector EvBot. It was found that the maximum incident angle of the Retroreflector

EvBot to execute the transmitted command was 60 degrees. This indicates that the full field of view angle of the retroreflector device as a receiver is 130 degrees.

In the second setup (right), the Retroreflector EvBot modulated the retroreflected laser beam to command the Laser EvBot to move backward. Laser EvBot was able to receive the transmitted data with 100% fidelity at a maximum incident angle of 50 degrees. However, traces of retroreflected light can be observed at a higher incident angle. Near 60 degrees tilt angle, light still was detected but with higher bit error rate (BER). Nonetheless, the device performance was very good under indoor ambient light conditions.

5.2.2 Range experiment with EvBot II

The range finding experiment was interesting and testing. The mobile robot in Figure 5.7 at its stationary location commanded the other robot to move backward one foot. This command was repeated continuously and the other robot performed the requested action until it was out of the receiving range. Again, each robot commanded the other robot in two different sets until the communications failed, which was an indication that, the maximum operation range had been determined.

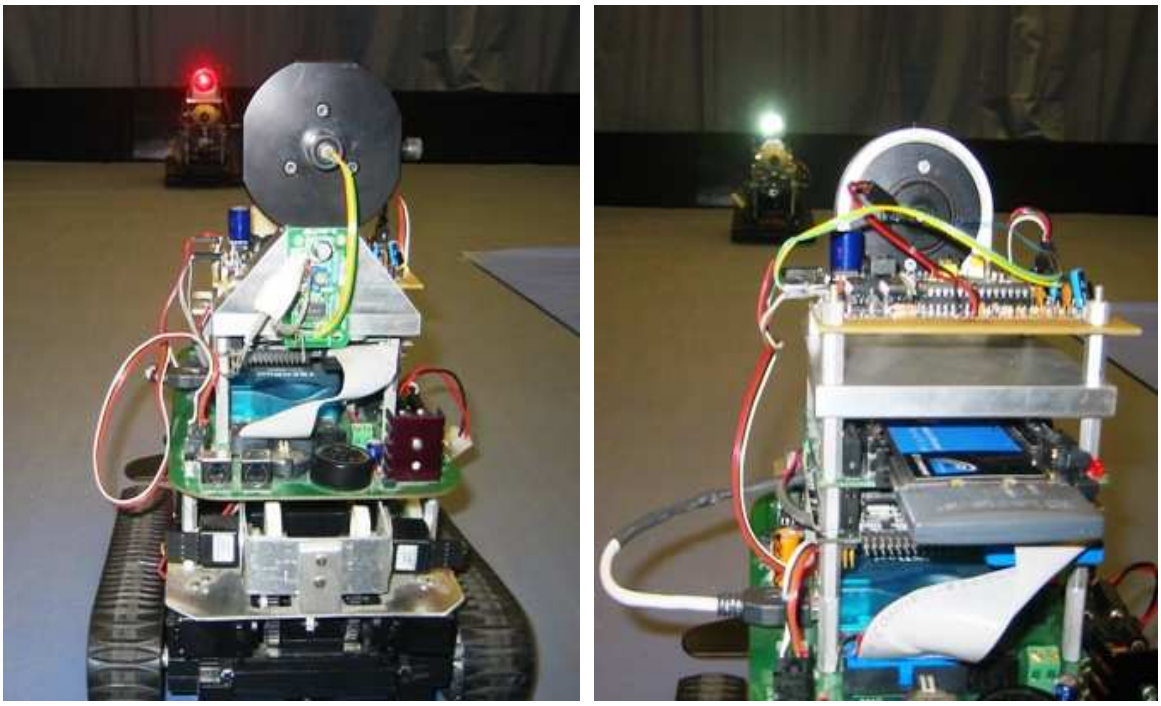

(a) **(b)**

Figure 5.7 a) Laser EvBot is command unit, b) Retroreflector EvBot is the command unit

It was found when the laser was properly aimed at the target; the bit stream was received perfectly. Transmission worked flawlessly at the largest test distance within the CRIM lab. However, it was very hard to test the system at larger distance without an aiming and focusing mechanism. Therefore, the maximum range for direct laser transmissions by Laser EvBot could not be determined exactly with the current setup. The transmission worked flawlessly at a range of 150 feet, which is the maximum distance available in the corridor of the engineering building. On the other hand, the maximum communication range achieved by the Retroreflector EvBot was 60 feet. This range test proved that the retroreflector communication system functioned perfectly for short range applications. Without additional control and focusing mechanisms on the optical systems the maximum range cannot be determined at this time.

It is worth mentioning here some observations from the experimental tests. First, parabolic mirrors are designed to focuses light coming from infinity at a focal point, i.e., the detector in this case. This focusing point moves away from the designed focal point when incoming light is emitted from close ranges. Therefore, with respect to detector's window and focusing spot, the longer the distance between the two EvBots the better the beam is focused. Second, unlike the 5mm lens, the 8mm ball lens improved the retroreflected light significantly. The detection and the communication limits were enhanced significantly, which strongly confirms the results obtained in the retroreflector analysis chapter, Chapter 2, section 2.3. Finally, by adjusting the focusing lens of the laser beam, both the retroreflector FOV and the communication range are enhanced. It is the reflected light intensity that limits device performance because at large incident angles or distance; astigmatism and beam divergence weakens the light intensity. A study of the optical power budget, in Chapter 4, section 4.5, revealed that there would be system limitations due to beam divergence angle.

5.2.3 Cooperative movement experiment

The most difficult and essential in cooperative movements using optical communication system was aiming the laser beam at the retroreflector device. After every movement, the two robots must be in line-of-sight to communicate optically. Adjusting robot's orientation to be in line-of-sight with other robots requires tracking and pointing system that is not implemented yet. Therefore the next experiment was merely to prove the concept of this research goal.

In this experiment, one of the robots commanded the other robot to move on a specific trajectory and meet at certain location. Figure 5.8 shows the trajectory that both robots should follow. To show that the communication works in both transceiver units (laser and retroreflector), the experiment was conducted twice so the commander position was alternated between them.

The robot was ordered to move in ‘U’ shape trajectory and stop at a specific location waiting for the next command. The commander robot, after receiving the acknowledgment, should move to the meeting location. The commands were received correctly and the two robots carried out the mission successfully. However due to optical encoder errors and tread slippages, discrepancies in robots motions occurred. The two robots should meet at the “end” point apart by an equal distance as they were at the “start” point. Instead, they ended miss-aligned with different separation distance and some times they crashed into each other. This experiment shows the need for a better speed controller unit for the EvBot II and an optical tracking system for the communication system.

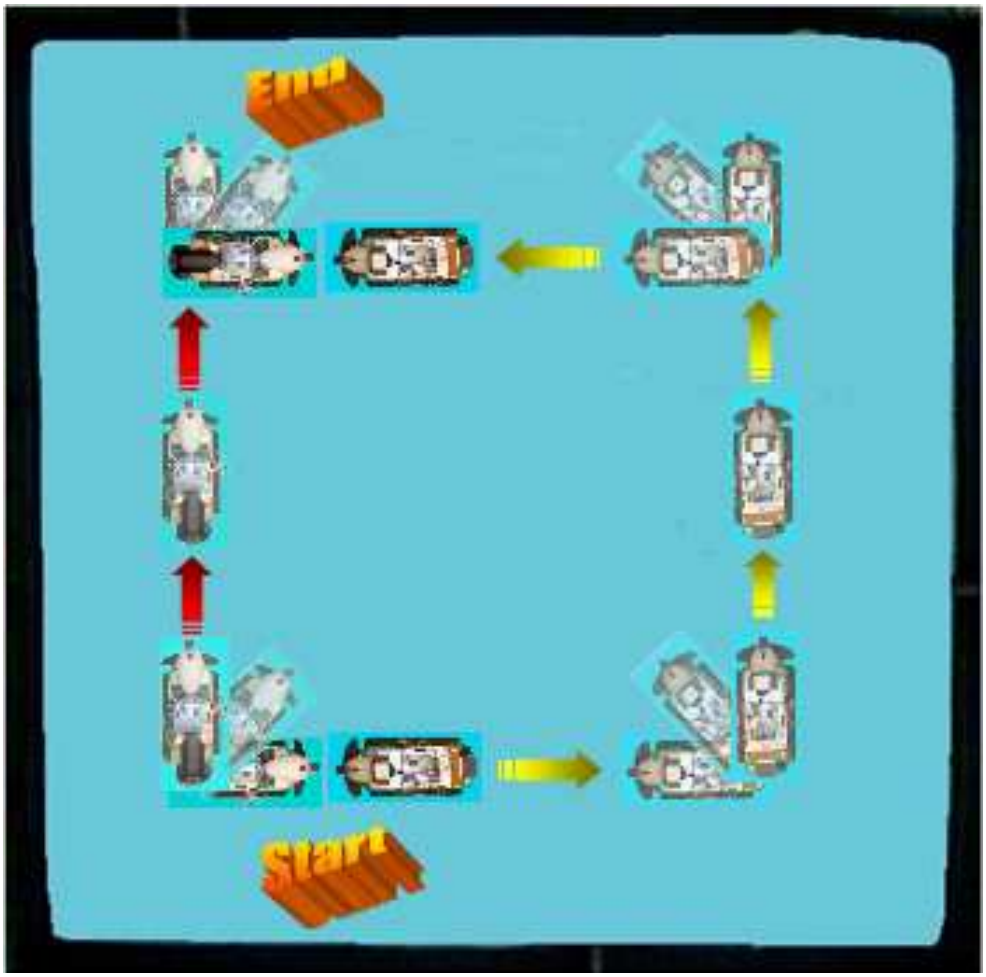

Figure 5.8 Trajectory movement for the two robots in cooperative task (U shape experiment)

Two main concerns when dealing with laser communication systems: obstruction and safety. Obviously if such laser communication systems are to ever become widely used they will have to be placed where they will not be obstructed for reliable communication. Laser light can be very harmful to the eye if shined directly into it and so no one accidentally should look into the laser beam or any of its reflections.

5.3 Underwater Communication

Recent interest in robotic communication for underwater application has been growing. Water is a complex medium for optical communication. In order to investigate the performance of our system for underwater applications, a simple experiment was constructed to test and measure modulated signals being received under different water conditions. The different water conditions were created by adding a commercial antacid product, Maalox® [5.5], into the water. In measured quantities this causes an increase in the turbidity of the water leading to high attenuation of the light signal.

These increased concentrations of Maalox® are assumed to be different regions in the water mass. This is similar to having the most turbid medium as harbor waters and clearest medium as open ocean waters. Figure 5.9 and Figure 5.10 are metrics for modulated signals in water as the medium. The experimental setup includes a glass water tank of dimensions 1m x 0.3m x 0.4m completely filled with 60L of clear tap water. The laser transceiver (15mW operating at 633nm) was placed in line-of-sight with the retroreflector device at either ends of the tank. This particular arrangement includes all the reflections from the glass surfaces of the tank and is considered as the ground-level measurement for the setup.

Figure 5.9 Underwater experiment tank filled with 5mL of Maalox® liquid (side view)

Increased quantities of Liquid Maalox® lead to turbidity in the water, which led to increased the scattering and absorption of laser beam. Greater effects were observed since the measured voltage from the reflected light signal traveled twice the length of the tank and propagated through glass and air. Figure 5.10 shows these effects of decreasing laser beam intensity at the retroreflector side.

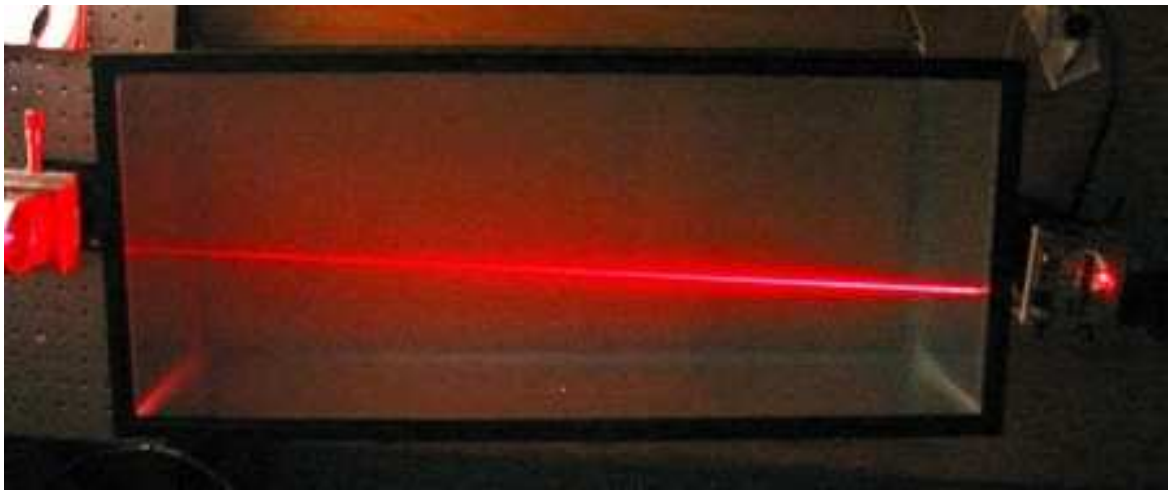

Figure 5.10 Red laser propagating in water with 5mL of Maalox® liquid (Top view)

It is hard to compare water turbidity with Maalox and natural sea water. Table 5.1 gives the concentrations used for these experiments, and includes an assessment of what the natural waters would be with such concentrations.

Table 5.1 Maalox concentrations compared to natural water

Concentration of Maalox® (mL) in 60 Liters of water	Natural Water
0 mL	Clear water
1 mL	Costal water
2 mL	Harbor water
3 mL	Turbid water
4 mL	Very turbid

Voltage readings of the photodiode were taken for various water conditions. Liquid Maalox® was added to water in measured quantities and the received voltage power was measured from the photo-detector circuit. The detector circuit has a 1000 amplification gain, thus it is very sensitive to low signals strength. On the other hand, using high laser intensity produces strong signals that reach the amplifier maximum rails so the voltage received was clipped.

The FOV of the retroreflector was tested under these different water conditions. Figure 5.11 shows curves of the received power, for a 1kHz modulated signals, at different Maalox® concentrations. It is obvious that there is an inverse relationship between retroreflector FOV and water turbidity. Thus, when this device is to be used for underwater communications, the more the water is turbid the more the two transceivers need to be aligned. The peeks of the curves are skewed toward -20 degrees rotation angle. This is due to imperfection in retroreflector's lenses and coated surface.

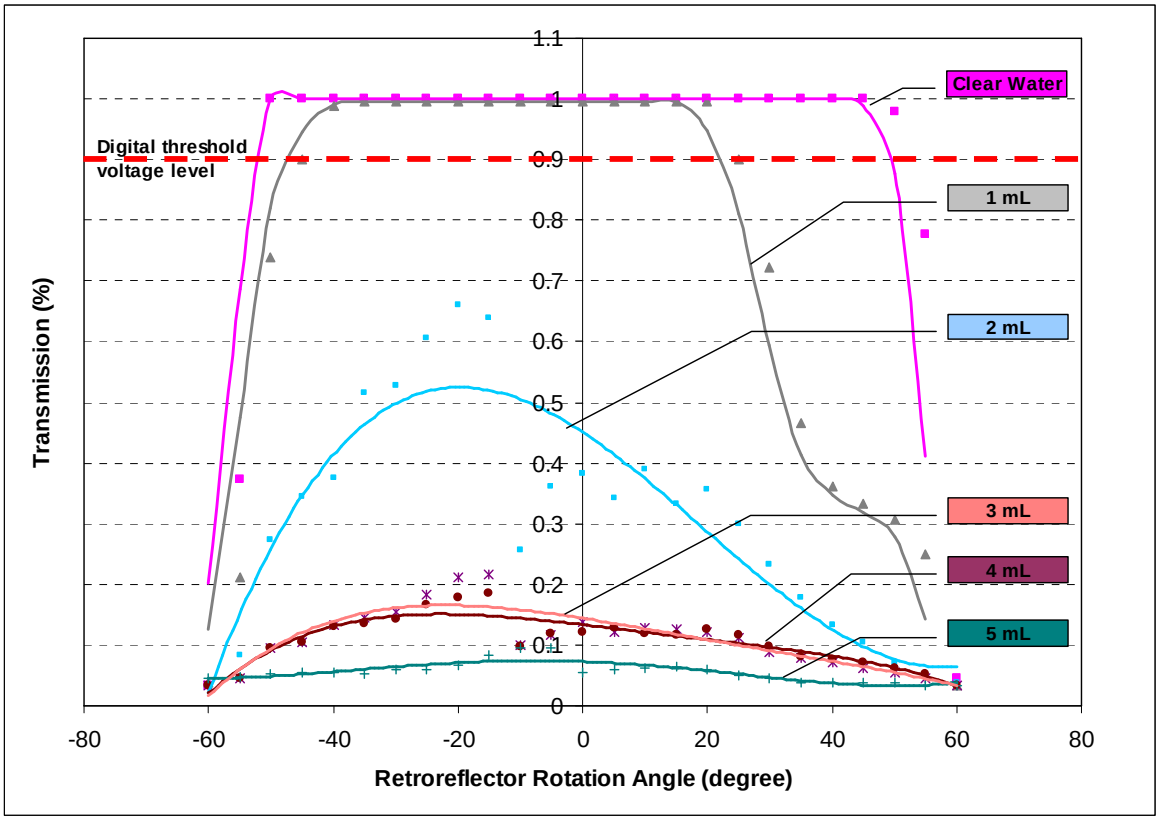

Figure 5.11 Received modulated voltage at (1kHz) with increased Liquid Maalox® concentrations

So, it is important for the received voltages to cross the receiver threshold level to ensure reliable digital communication. The receiver circuit Schmitt trigger considers voltages greater than 3V as logical '1' and logical '0' for voltages less than 0.7V. With this system, the curves in Figure 5.11 indicate that digital signals cannot be detected in turbid water with Maalox® concentration greater than 1mL. At a 6mL concentration, the attenuation was so severe that it was hard to detect any change in the received signal.

To improve system detection at high Maalox® concentrations, the modulation was decreased to 100Hz. Surprisingly, the detection improved significantly and the received signal was able to cross the digital threshold level in water with a 3mL concentration. Figure 5.12 shows a comparison of the detected signal for both modulation frequencies.

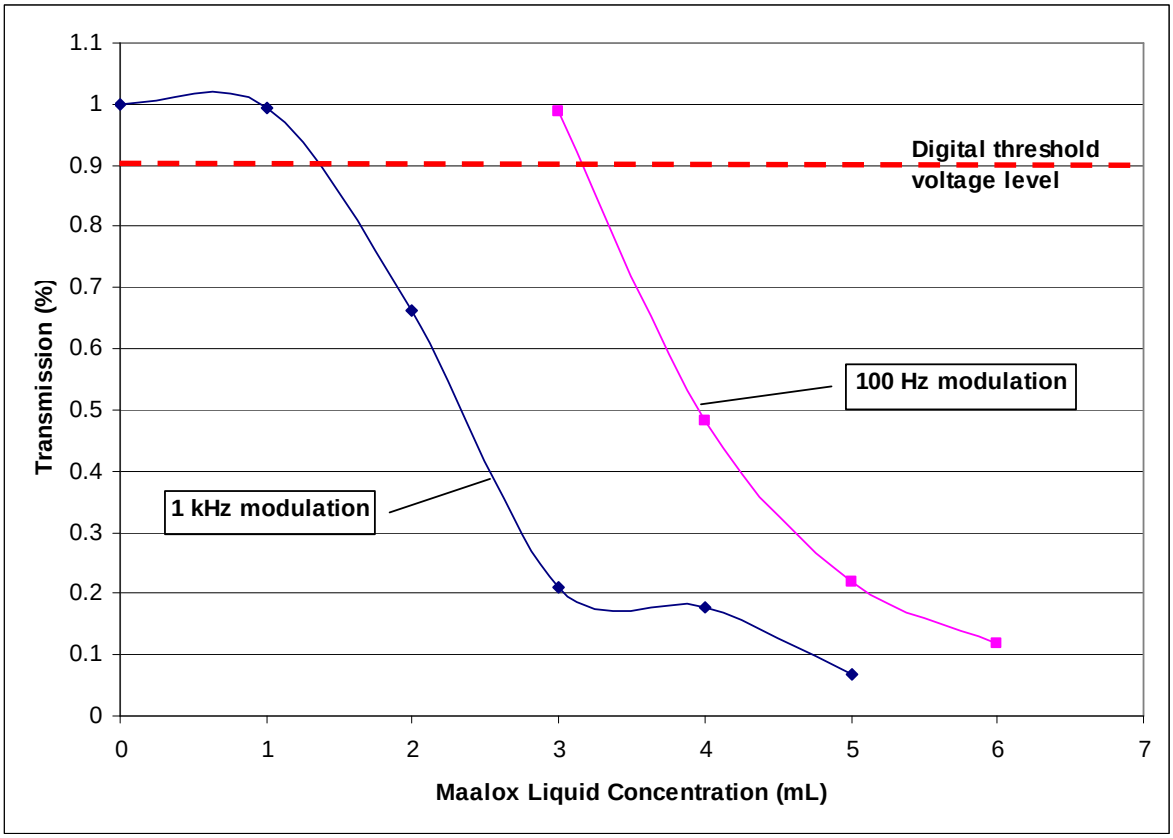

Figure 5.12 Transmission of 100Hz and 1kHz modulated signal at different Maalox concentrations

In conclusion, the wide FOV retroreflector device performed well in free space communication as well as in underwater communication. Lacking of tracking and pointing system in robotic experiments was the main obstacle for a complex navigation experiments. On the other hand, the device performed well in turbid water although it was not designed for underwater communication. In very turbid water (5mL) the receiver was able to detect 20% of the transmitted power passing through the water tank twice, a total distance of 2m. To improve the system performance in order that it can be used for data communication, the receiver circuit will have to be redesigned to ensure higher sensitivity and noise immunity. However the modulator (LCPG in this system) was the major factor in system efficiency. At high modulation frequency, the LCPG attenuates transmitted power; as was proved in section

3.2.2. Certainly, a modulator that is free from this attenuation problem would improve the system performance and efficiency significantly.

5.4 *References*

[5.1] EAGLE Freeware Light Edition, http://www.cadsoft.de/info.htm

[5.2] Aoki, N., N. Komatsu, and T. Tsumura. "Vehicle to Vehicle Optical Two Way Communication by Use of Laser and Corner Cube." *IEEE International Conference on Intelligent Transportation System* (1997). 787-790.

[5.3] Galeotti, J. 'The EvBot: a Small Autonomous Mobile Robot for the Study of Evolutionary Algorithms in Distributed Robotics." Master Thesis in Electrical and Computer Engineering. North Carolina State University, 2002.

[5.4] Mattos, L. S. "The EvBot II: An Enhanced Evolutionary Robotics Platform Equipped with Integrated Sensing for Control." Master Thesis in Electrical and Computer Engineering. North Carolina State University, 2003.

[5.5] Liquid Maalox®, Novartis Consumer Health Inc., Parsippany NJ-07054-0622 ©2005

Chapter 6

Conclusion and Future Research

In this research a new wide field of view retroreflector device was designed, fabricated, tested, and finally applied in autonomous robotics communication and control. The results obtained from researching into the field of wide field of view retroreflector are presented, as are the results obtained from exploring into the problems associated with expanding the field of view of retroreflectors. By experimenting in the physical world it is proved that the final device benefits autonomous robot navigation and underwater optical communication. The former application shows potential for security, and search and rescue applications, while the latter application shows potential for underwater robotics.

Cat's-eye retroreflectors have a small field of view, especially when a modulator is placed in front of its aperture, which limits its applicability in autonomous mobile robot applications. A Fisheye lens when combined with a suitable compensating lens set on the other hand offers a solution to the small field of view limitation of the Cat's-eye retroreflector, and expands a retroreflectors field of view significantly up to 180 degrees. Since both of these lenses interact with incident light differently, meaning there is an engineering trade-off, an in-depth study was conducted to explore the performance and the limitations of these lenses. On the basis of that in-depth study recommendations are made in the section of this chapter that deals with future research.

The designed and fabricated laser transceiver unit consists of a laser diode module; transceiver circuit board for detecting and processing received data; detection optics. The detection optics ware formed from a single photodiode and an off-axis parabolic mirror. The

design and the use of a parabolic mirror, for directing and focusing reflected light, simplified the detection optics and improved system performance; by reducing optical losses. The overall size of this unit is 11.5x9.5x12 cm.

The retroreflector modulator unit is bulkier, since it consists of: Cat's-eye and fisheye lenses; a transceiver board with photodiode detector and a light modulator. The size of the retroreflector modulator module is only 11.08 cm diameter and 2.54 cm thick. The overall unit size is 13x10x9 cm.

When the transceiver and retroreflector units were integrated they produced an effective and efficient optical communication for robots and other applications. The retroreflector modulator device was tested for optical communication: (1) robot to robot communication, for navigation and localization, between two collaborating robots; (2) for experimenting with underwater optical communication in turbid water, with the potential application being communications between underwater robots.

Employing the new modulator technology (LCPG) in the retroreflector device enhanced the power of the retroreflected transmitted signal greatly. The LCPG modulator performance supersedes the LCD modulator in the tested sample, and it displayed an optical efficiency higher than 90%. Despite the fabrication imperfection of the modulator cell and power losses due to light-leakage, the modulator performed well. Currently, the device is useful for short range applications.

Based on the results obtained from this first demonstration of principle unit, the first prototype, the limitations that can be sighted for improvement in future work includes: (1) optimizing the fisheye lens design is required to obtain optimal parameters to produce a maximum FOV and a minimum light divergence, (2) minimizing the unwanted surface reflection. This can be achieved by applying an anti-reflection coating on every surface in the system; especially the fisheye lens. In the current system, none of the lens surfaces were

coated during any of the experiments, (3) the Cat's-eye lens could potentially be replaced with a GRIN lens to minimize lens aberrations. The power budget computations revealed that this device works well for short range applications. The retroreflector aperture receives near 21% of the transmitted power. Much of the range limitation arose from the simplicity of the receiver circuit used.

The liquid crystal polarization grating was limited in bandwidth and at the upper range of its modulation frequencies, experiments showed that the LCPG attenuated transmitted power. A modulator were free from this attenuation problem the device would be more efficient. A recommendation for the future is to apply Multiple Quantum Well modulators (MQW); since these are faster modulators that can be easily integrated to retroreflector unit. These modulators have modulation rates in MHz without displaying significant attenuation effects; as such they are suited to the applications under consideration. Appendix A4 gives a brief description of MQW modulators and their eye safety range operation.

In conclusion, the wide field of view retroreflector device performed well showing the potential for free space communications between robots and potentially underwater communications between autonomous underwater vehicles.

APPENDICES

Appendix A

A1 Optical Aberrations

In paraxial approximations, lenses are viewed as perfect optical devices; however lenses do not form perfect images. There is always some degree of distortion or *aberration* introduced by the lens which causes the image to be an imperfect replica of the object being viewed. Among several different types of aberration that affect image quality, three types of aberrations are presented in this section: spherical aberration, coma, astigmatism and chromatic. Information in this section obtained mainly from Wikipedia encyclopedia [A1.1] and Olympus America [A1.2].

A1.1 Spherical Aberration

Spherical aberrations occur for lenses that have spherical surfaces such that the edges of a lens refract more light than the center resulting in the production of different focal points along the optical axis. At the area where most of the optical rays focus together, an image forms a disc - the circle of "least confusion". The effect of spherical aberration is that an image of a point source will have a diffuse halo around it, as illustrated in Figure A1.1.

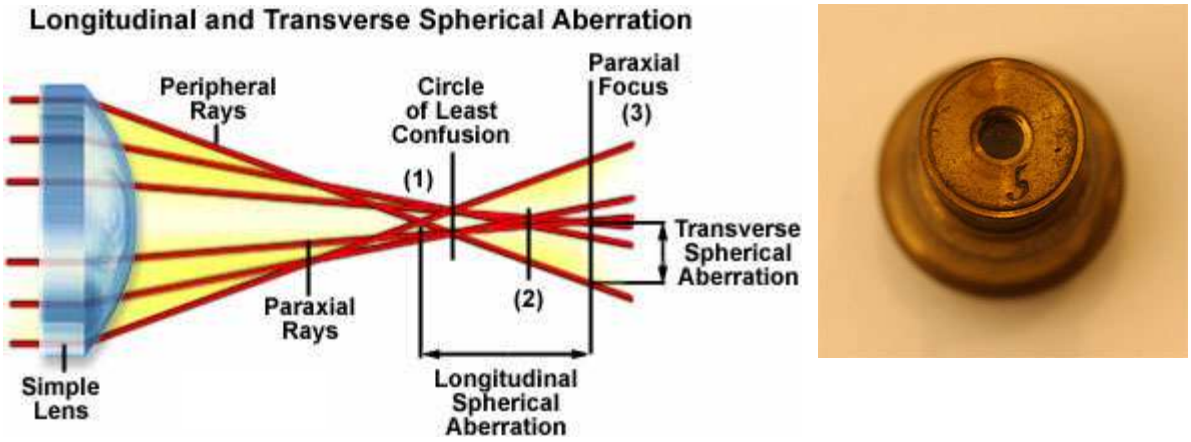

Figure A1.1 Spherical Aberration

A1.2 Coma

Comatic aberrations are similar to spherical aberrations, but they are only encountered with off-axis objects. In this instance, the image of a point is asymmetrical, resulting in a comet-like (hence, the term coma) shape. The distinct shape displayed by images with comatic aberration results in refraction differences in light rays passing through the various lens zones as the incident angle increases, as illustrated in Figure A1.2.

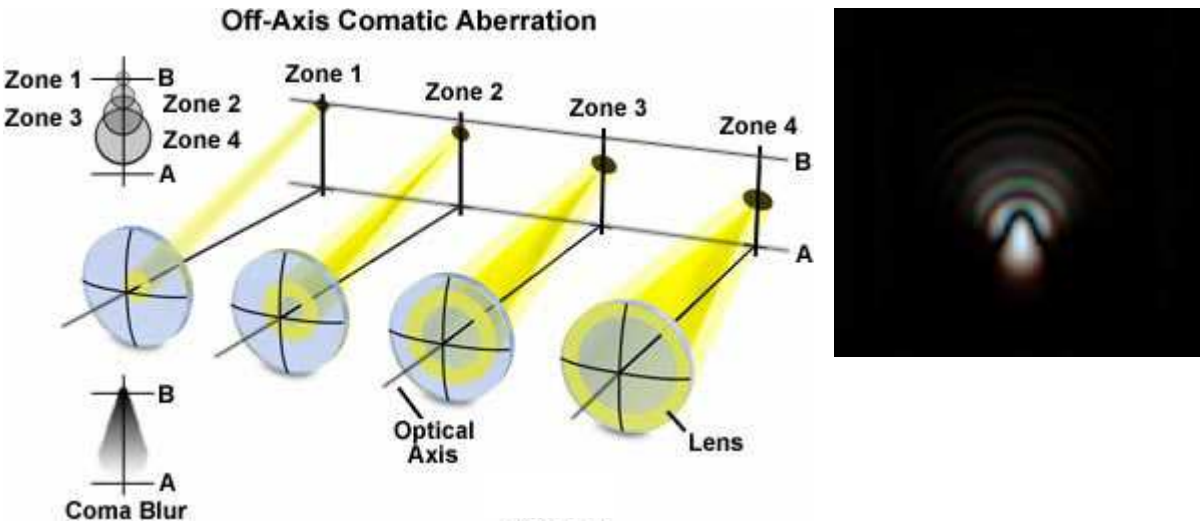

Figure A1.2 Comatic Aberration

Spherical aberration and coma can be minimized by choosing the curvature of the two lens surfaces to match the application. Lenses in which both spherical aberration and coma are minimized are called *bestform* lenses.

A1.3 Astigmatism

In optics, astigmatism is when an optical system has different foci for rays that propagate in two perpendicular planes, tangentially (meridionally) or sagittally (equatorially). Depending on the angle of the off-axis rays entering the lens, the contrast will be lost as the distance from the center is increased. Figure A1.3 shows an illustration of astigmatism aberration in spherical lens and a blurred text due to astigmatism.

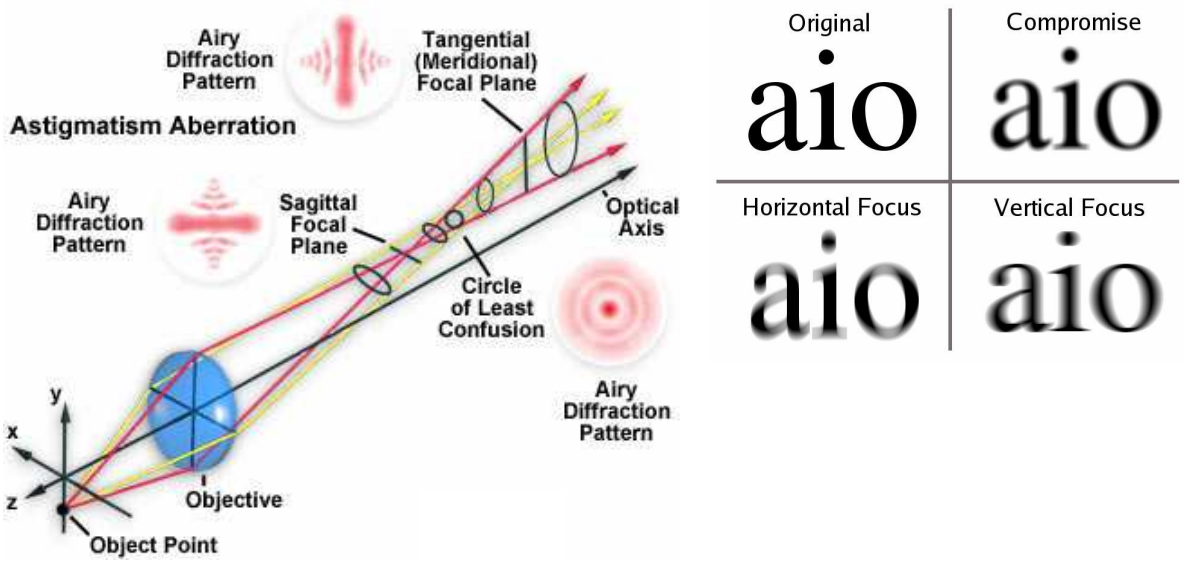

Figure A1.3 Astigmatism Aberration (left) and Text blurred by different focal positions of an astigmatic lens (right)

With care, an optical system can be designed to reduce or eliminate astigmatism. Such systems are called anastigmats.

A1.4 Chromatic Aberration

Chromatic aberration is caused by a lens having a different refractive index for different wavelengths of light. The amount of chromatic aberration depends on the dispersion of the lens. Longitudinal and lateral chromatic aberration of a lens is seen as "fringes" of color around the image, because each color in the optical spectrum cannot be focused at a single common point on the optical axis. Figure A1.4 illustrates this type of aberration and its effect on a real image.

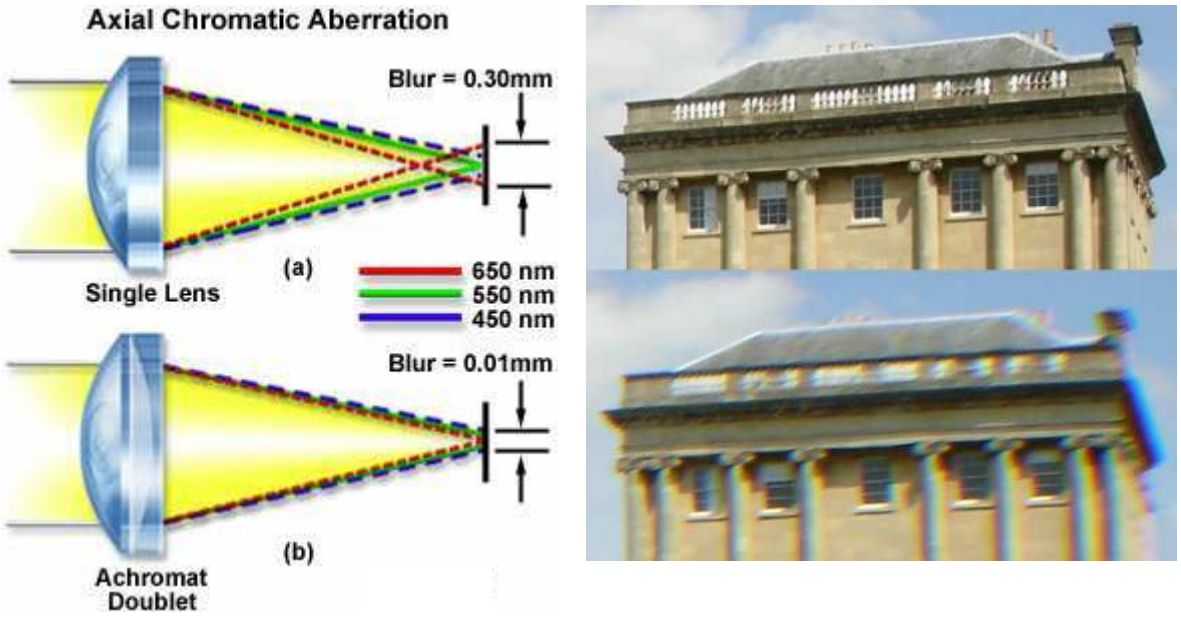

Figure A1.4 Chromatic Aberration

This aberration can be corrected by using lenses cemented together (e.g., *doublet, triplet),* where each lens has a different refractive index and dispersive properties. Lens doublets and triplets are also known as *achromatic and apochromatic* lenses respectively.

A2 RMS Calculation

To obtain the RMS spot radius of rays distributed in a square grid structure, the coordinates x_o and y_o of a spot center are computed by averaging the intersection coordinates [A2.1],

$$x_o = \frac{1}{N}\sum_{i=1}^{N} x_i, \qquad y_o = \frac{1}{N}\sum_{i=1}^{N} y_i \tag{A2-1}$$

Then,

$$RMS\ spot\ radius = \sqrt{\frac{\sum_{i=1}^{N} R_i^2}{N}} \tag{A2-2}$$

where $R_i^2 = (x_i - x_o)^2 + (y_i - y_o)^2$.

As the number of rays is increased, the RMS spot radius is generally decreased, and approach a definite lower limit as the number of rays becomes very large. A decision must be made as to how many rays are traced to obtain an RMS spot radius that is within certain accuracy, a limiting value for $N \to \infty$. Foreman [A2.1] found that if the error is to be reduced to less than 1%, N must exceed 20, according to the following formulas;

$$error = \frac{\alpha_N - \alpha_\infty}{\alpha_\infty} \tag{A2-3}$$

Where

$$\alpha_N = \sqrt{\frac{(2N-1)}{6(N-1)}}, \quad \alpha_\infty = \frac{1}{\sqrt{3}} = 0.57735 \tag{A2-4}$$

Anderson [A2.2] showed that the RMS image radii computed by ray tracing depends not only on the number of rays traced but also on the way rays are distributed over the entrance pupil. He demonstrated that a polar distribution can gain more accuracy with less rays than a

square distribution. However, the square grid was adopted in this work because it does not involve double integral formula, or computation time, as the polar grid does.

A3 Reflected Power Efficiency

A study of the geometrical factors that affect the relation between transmitted power and received power was carried out by Laser Electro-Optics Technology (LEOT) [A3.1]. Here, a summary of power budget of an optical link using retroreflector technology is presented.

Assuming the transmitted beam completely covers the entire area of the target that retroreflects the beam back to the source, Figure A3.1 illustrates the radiation pattern of the transmitter-to-target geometry.

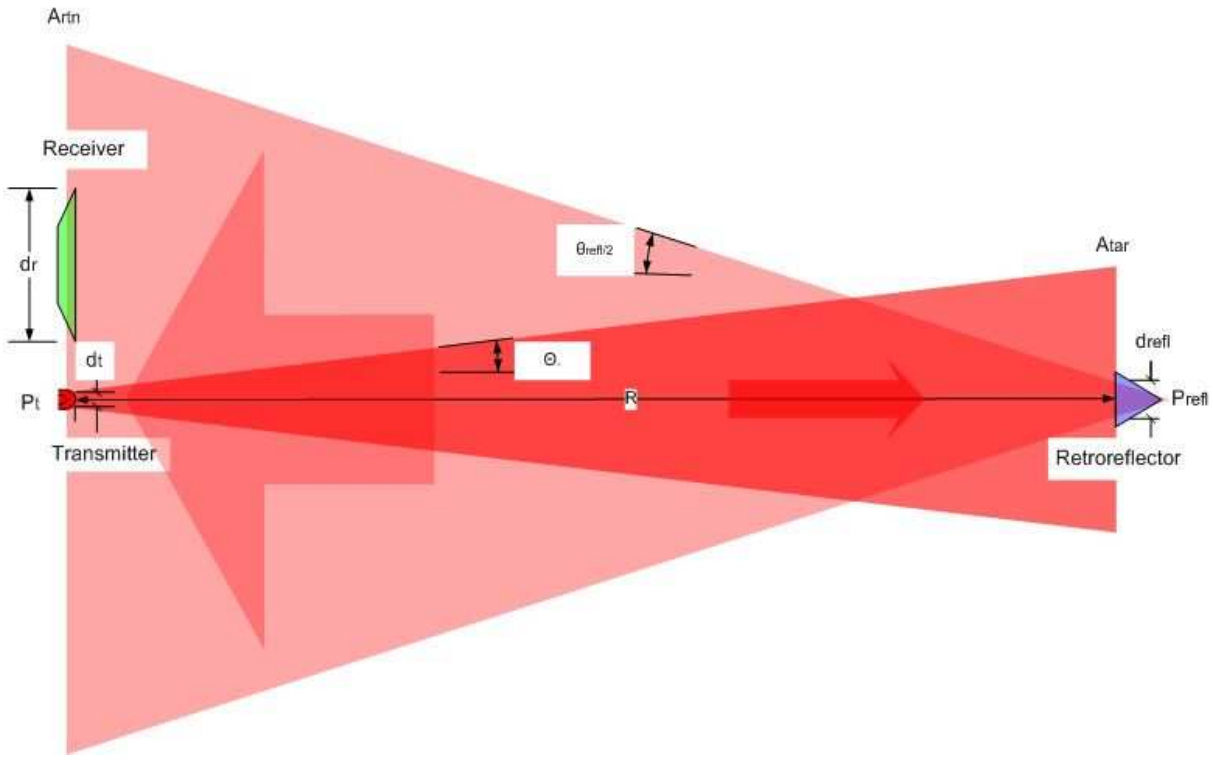

Figure A3.1 Radiation pattern of the transmitter-to-target geometry for efficiency computation

A beam with an aperture diameter d_t and divergence angle θ_t (radians) radiates at a distance R from the target illuminates an area at the target plane:

$$A_{tar} = \frac{\pi}{4}(\theta_t R + d_t)^2 \qquad \textbf{(A3-1)}$$

Then the power density Φ_{tar} within this area is equal to the transmitted power divided by this illuminated area, and reduced by the atmosphere transmission T:

$$\phi_{tar} = \frac{4P_t T}{\pi(\theta_t R + d_t)^2} \qquad \textbf{(A3-2)}$$

The value of T varies from 0 to 1, depending of the amount of absorption and scattering of the light by the atmospheric conditions. T will have a value of 1 for a beam propagating in space.

Assuming 100% surface reflectivity for the reflector, the returned power will be:

$$P_{refl} = \phi_{tar} A_{refl} = \phi_{tar}\left(\frac{\pi}{4} d_{refl}^2\right) \qquad \textbf{(A3-3)}$$

where d_{refl} is the effective diameter of the reflector.

The emerging beam from the reflector will have a divergence angle equal to the divergence of the transmitted beam plus diffraction effects due to the limited size of the reflector. Thus divergence angle θ_{refl} of the return beam is given by:

$$\theta_{refl} = \frac{d_{refl}}{R} + \frac{2.44\lambda}{d_{refl}} \qquad \textbf{(A3-4)}$$

From the divergence angle, the area of the return beam at the receiver can be calculated as follows:

$$A_{rtn} = \frac{\pi}{4} d_{rtn}^2 = \frac{\pi}{4}\left(\theta_{refl} R + d_{refl}\right)^2 = \frac{\pi}{4}\left(2d_{refl} + \frac{2.44\lambda R}{d_{refl}}\right)^2 \qquad \textbf{(A3-5)}$$

Then, the power density of the return beam at the receiver is:

$$\phi_r = \frac{P_{refl}\, T}{A_{rtn}} \qquad \textbf{(A3-6)}$$

and, the power received by the receiver optical system is:

$$P_r = \phi_r A_r \qquad \textbf{(A3-7)}$$

Combining all the above equations gives the received power:

$$P_r = P_t \left(\frac{d_{refl}\, d_r T}{(\theta_t R + d_t)\left(2d_{refl} + \frac{2.44\lambda R}{d_{refl}} \right)} \right)^2 \qquad \textbf{(A3-8)}$$

For very long-range measurements, such that $\theta_t R >> d_t$ and $\frac{2.44\lambda R}{d_{refl}} >> 2d_{refl}$, equation A3-8 reduces to

$$P_r = P_t \left(\frac{d_{refl}^2\, d_r T}{2.44\lambda\theta_t R^2} \right)^2 \qquad \textbf{(A3-9)}$$

For short-range measurements, such that $2d_{refl} >> \frac{2.44\lambda R}{d_{refl}}$, equation A3-8 reduces to

$$P_r = P_t \left(\frac{d_r T}{2(\theta_t R + d_t)} \right)^2 \qquad \textbf{(A3-10)}$$

It is clear that the range has significant effect on the received power. At close range, the received power is dependent on the inverse square value of the range and independent of the reflector area. In contrast, at long range, the received power is dependent on the inverse fourth power of the range and on the fourth power of the reflector diameter. And it is quite possible, at this range, for the atmospheric transmission to be the dominant factor.

A4 MQW Optical Modulator and Eye Safety

The Naval Research Laboratory (NRL) developed a modulating retroreflector system for two-way optical communication was developed [A4.1] (Figure A4.1). Their modulating retroreflector uses an electro-optical shutter and a semiconductor-based Multiple Quantum Well (MQW). Based on this arrangement the system is capable of modulating at rates greater than 10 Mbps at eye safe intensity level.

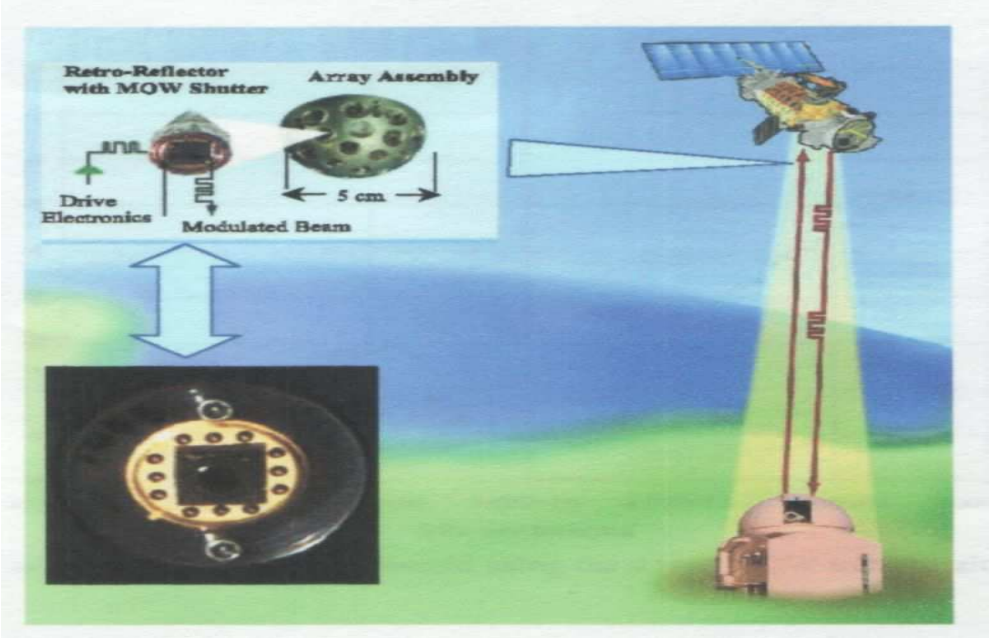

Figure A4.1 Modulating retroreflector system for two-way optical communication

Multiple quantum well modulators have a number of advantages over their alternatives, because the system uses ferro-electric liquid crystals, or MEMS devices. They are inherently fast and draw milliwatts of power to support megabits per second transmission rates. They are also lightweight, robust, and compact. When a moderate voltage (in the range of 12V to 20V) is placed across the device in reverse bias, the absorption feature changes, both shifting in wavelength and dropping in magnitude. So, the transmission of the device near this absorption feature changes dramatically and can serve as an on-off shutter.

The selection of the optical wavelength is one of the most important issues in optical wireless communication. Visible and near-infrared light spectrum (400nm to 1400nm wavelength) is of particular hazard to the retina since this is the range of light at which the eye is sensitive to light and is highly absorptive to it. For example, when a leaser beam of 800nm enters the eye and strikes the retina it is concentrated by a factor of 100,000 times. Because the retina has no pain sensors and the invisible light does not induce a blink reflex, the retina could be permanently damaged in such a case.

In contrast, a laser beam at 1550nm wavelength is absorbed by the cornea and lens, and does not focus onto the retina. Eye-safety regulations permit ~50 times more transmitted power at 1550nm than 800nm, which directly improve the signal to noise ratio of the optical system [A4.2]. The NRL large aperture MQW devices operate between 850nm and 1.06μm to date. Currently, NRL are designing and fabricating MQW devices that operate at 1550nm wavelength [A4.3, A4.4].

A5 *References*

[A1.1] Wikimedia Foundation, Inc., http://en.wikipedia.org/wiki/Aberration_in_optical_systems

[A1.2] Olympus America, Inc., http://www.olympusmicro.com/primer/anatomy/aberrations.html

[A2.1] J. W. Foreman, Jr., "Computation of RMS Spot Radii by Ray Tracing", *Applied Optics*, Vol. 13, No. 11, November 1974.

[A2.2] T. B. Anderson, "Evaluating RMS Spot Radii by Ray Tracing", *Applied Optics*, Vol. 21, No. 7, April 1982.

[A3.1] Laser Electro-Optics Technology (LEOT) curriculum materials from the Center for Occupational Research and Development (CORD) in Waco, Texas.

[A4.1] US Naval Research Laboratory, “Large-Aperture Multiple Quantum Well Modulating Retroreflector for Free-Space Optical Data Transfer on Unmanned Aerial Vehicles”, *Society of Photo-Optical Instrumentation Engineers* (2001).

[A4.2] *fSONA Communications Corporation*, “Free Space Optical Networking Architecture”, www.fsona.com.

[A4.3] W. S. Rabinovich, R. Mahon, H. R. Burris, G. C. Gilbreath, P. G. Goetz, C. I. Moore, M. F. Stell, M. J. Vilcheck, J. L. Witkowsky, L. Swingen, M. R. Suite, E. Oh, and J. Koplow, “Free-space optical communications link at 1550 nm using multiple-quantum-well modulating retroreflectors in a marine environment”, *Optical Engineering* - Volume 44, Issue 5, 056001 (12 pages) May 2005.

[A4.4] Gilbreath, G. Charmaine; Rabinovich, William S.; Meehan, Timothy J.; Vilcheck, Michael J.; Stell, Mena F.; Mahon, Rita; Goetz, Peter G.; Oh, Eun; Vasquez, John A.; Cochrell, Kerry; Lucke, Robert; Mozersky, Sharon, “Real Time Video Transfer using Multiple Quantum Well Retromodulators”, *Proceedings of the SPIE - Free-Space Laser Communication and Laser Imaging II*, Vol. 4821, p. 155-162, Dec 2002.

Appendix B

B1 ATmega128 Layout

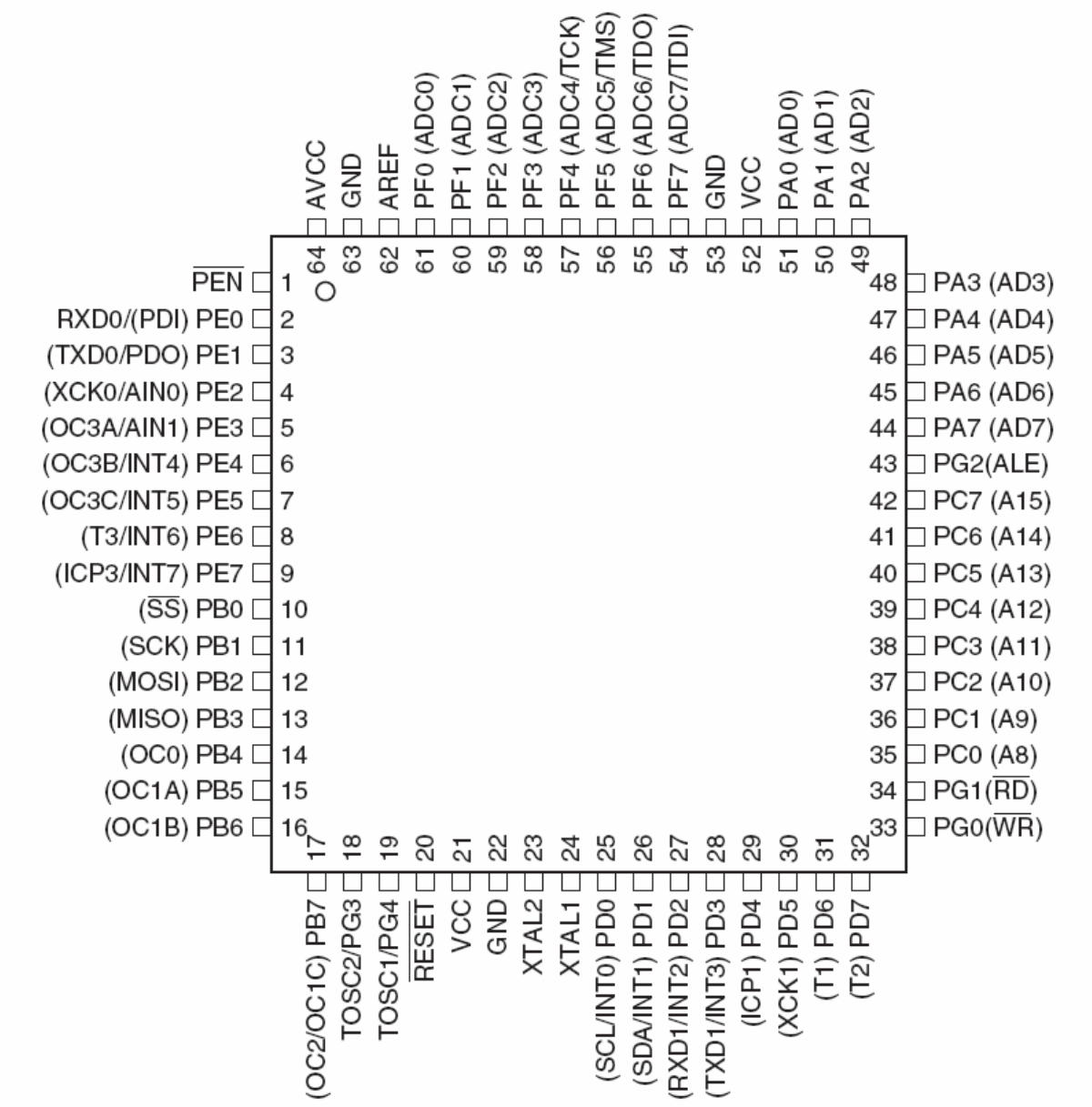

Figure B1.1 Pinout ATmega128

B2 Transceivers Schematic Drawings

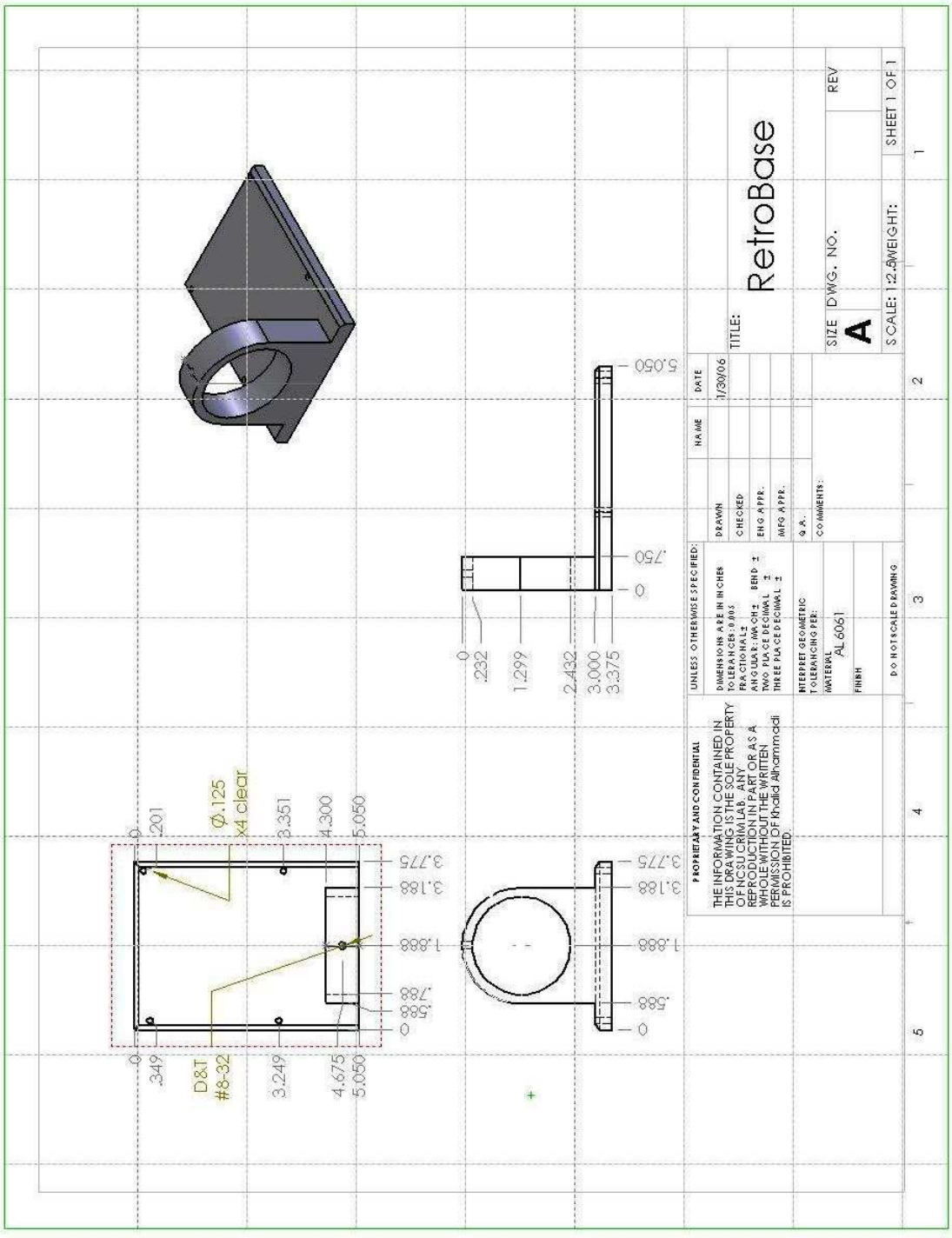

Figure B2.1 Retroreflector modulator base

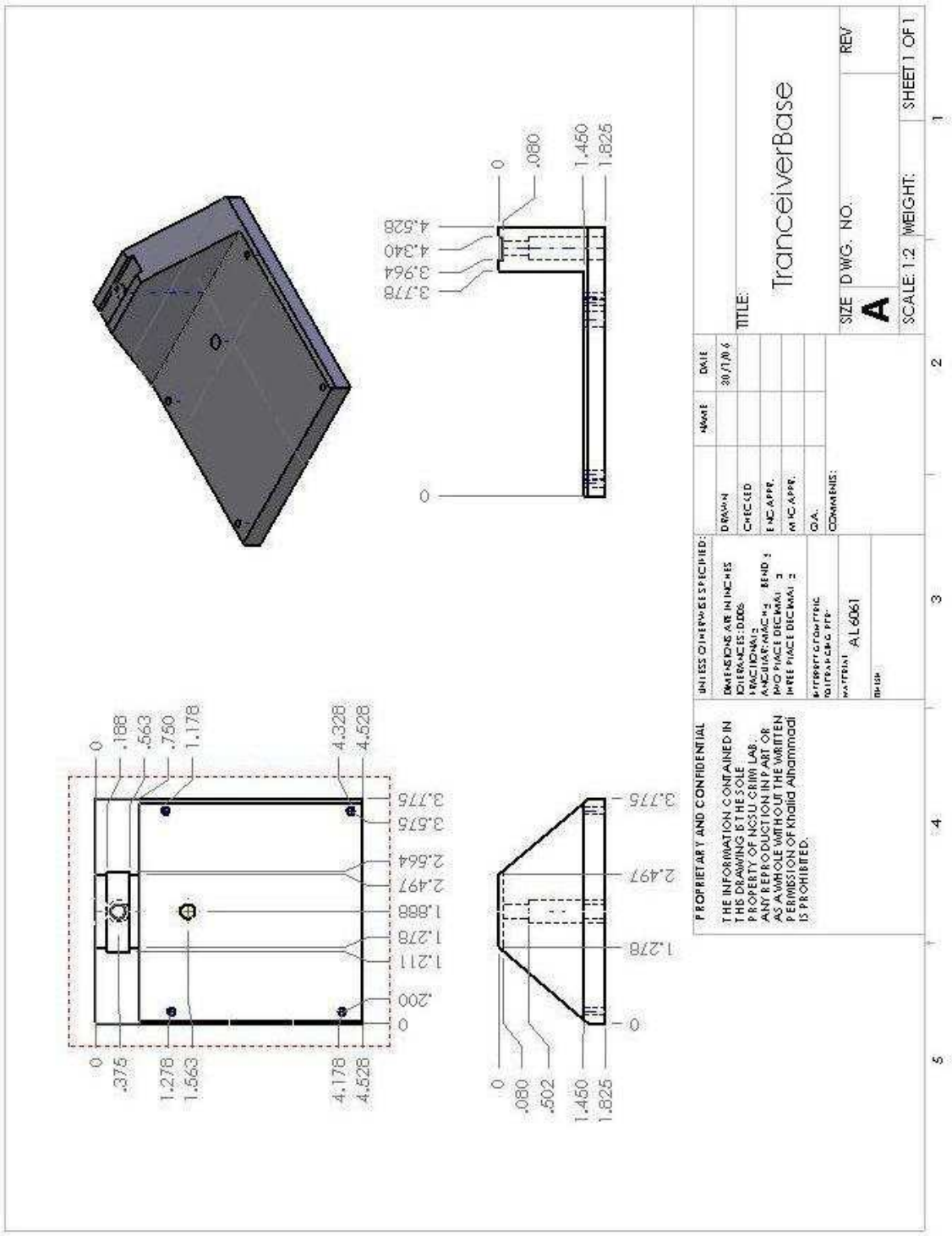

Figure B2.2 Laser transceiver base

B3 Laser Diode Datasheet

THORLABS INC
435 Route 206 • P.O. Box 366
Newton, NJ 07860-0366
SALES 973-579-7227
FAX 973-300-3600

DL7147-201
RED LASER DIODE

Features

- wavelength : 658 nm (Typ.)
- High output power : 100 mW at 75°C (pulse)
- Low threshold current : Ith = 40 mA (Typ.)
- Small package : ø5.6 mm
- TE mode

Applications

- DVD-R/±RW/RAM

Package

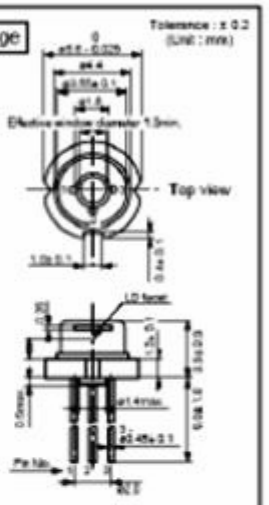

Pin Connection

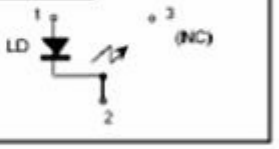

Absolute Maximum Ratings

(Tc=25°C)

Parameter		Symbol	Ratings	Unit
Light Output	CW	Po (CW)	60	mW
	Pulse [1]	Po(pulse)	100	
Reverse Voltage	Laser	VR	2	V
Operating Temperature		Topr	-10 to +75	°C
Storage Temperature		Tstg	-40 to +85	°C

1) Pulse Width 0.1μs, Duty 50%

Electrical and Optical Characteristics [2] [3]

(Tc=25°C)

Parameter		Symbol	Condition	Min.	Typ.	Max.	Unit
Threshold Current		Ith	CW	-	40	50	mA
Operating Current		Iop	Po=50mW	-	90	120	mA
Operating Voltage		Vop	Po=50mW	-	2.5	3.0	V
Lasing Wavelength		Lp	Po=50mW	-	658	662	nm
Beam Divergence [4]	Perpendicular	Qv	Po=50mW	15	16	20	°
	Parallel	Qh	Po=50mW	7.5	9	11	°
Off Axis Angle	Perpendicular	dQv	-	-	-	± 2	°
	Parallel	dQh	-	-	-	± 2	°
Differential Efficiency		dPo/dIop	-	-	1.1	-	mW/mA
Astigmatism		As	Po=50mW	-	1	-	μm

2) Initial values 3) All the above values are evaluated with Tottori Sanyo's measuring apparatus
4) Full angle at half maximum

Note : The above product specification are subject to change without

Appendix C

C1 Matlab Skew Raytrace Toolbox

A light ray in an optical system can be axial, meridional, or skewed. Paraxial rays can be traced simply by successive applications of matrix multiplication. In contrast, a skew ray is the most general ray path and much more difficult to trace. Without skew ray tracing, it is impossible to model nonsymmetrical optical systems or evaluate their performance.

In the paraxial region, optical systems have perfect image formation, however, most finite aperture optical systems have a field of view that is far beyond the limits of the paraxial region. As a result, the position and size of practical images are not ideal (i.e., optical aberrations). These aberrations are complex nonlinear functions of the constructional parameters of an optical system that are difficult to be calculated.

Virtually all the current commercial optical software extracts performance quantities, such as aberration and spot size, using finite-difference method. Lin et al developed a technique in which skew rays can be traced more accurately in optical systems. They use a homogeneous transformation matrix to define the position and orientation of a local coordinate frame for each boundary surface. Thus, the boundary surfaces not perpendicular to the optical axis (nonsymmetrical optical systems and elements) are easily subjected to ray tracing.

MATLAB® is a high-performance language for technical computing. It features a family of add-on application-specific solutions called *toolboxes*. Areas in which toolboxes are available include signal processing, control systems, neural networks, fuzzy logic, wavelets, simulation, and many others. Unfortunately, MATLAB does not have a toolbox for ray-tracing. Since the formulated ray tracing technique is matrix based, it can be easily

implemented using MATLAB. Therefore, we wrote the first Skew ray-trace program for optical systems in MATLAB environment.

The skew ray-trace toolbox is still under development. Currently, it consists of two main programs. The first program traces a ray(s) of light in an optical system and computes its points of intersection on each encountered surface. Then, the second program plots the results. User should write his/her input file to call these two programs. Figures C1.1-C1.5 show the Cat's eye lens subjected to different patterns of light source.

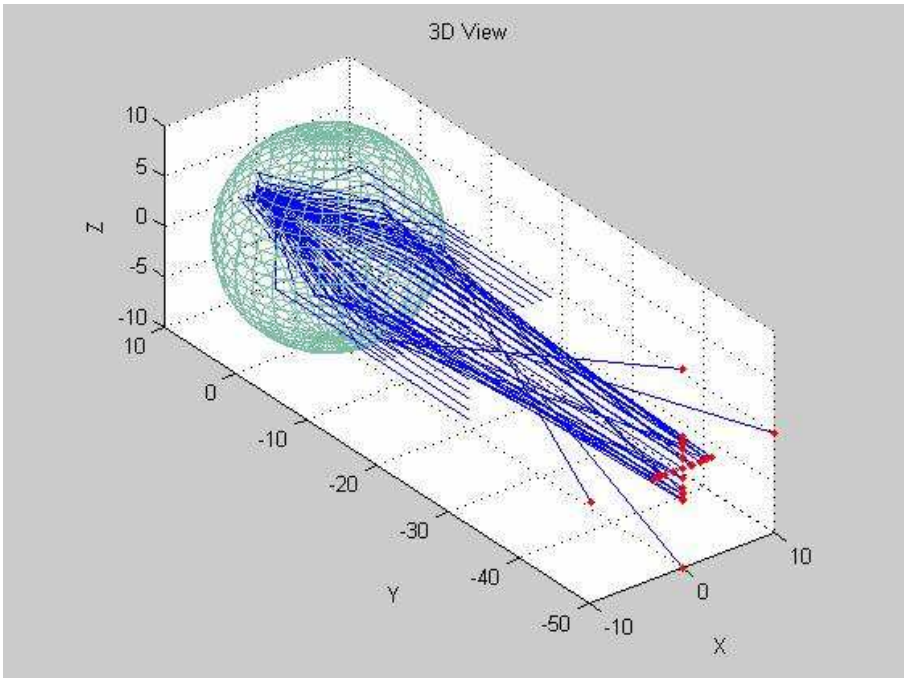

Figure C1.1 Cross light source for image quality and orientation problems

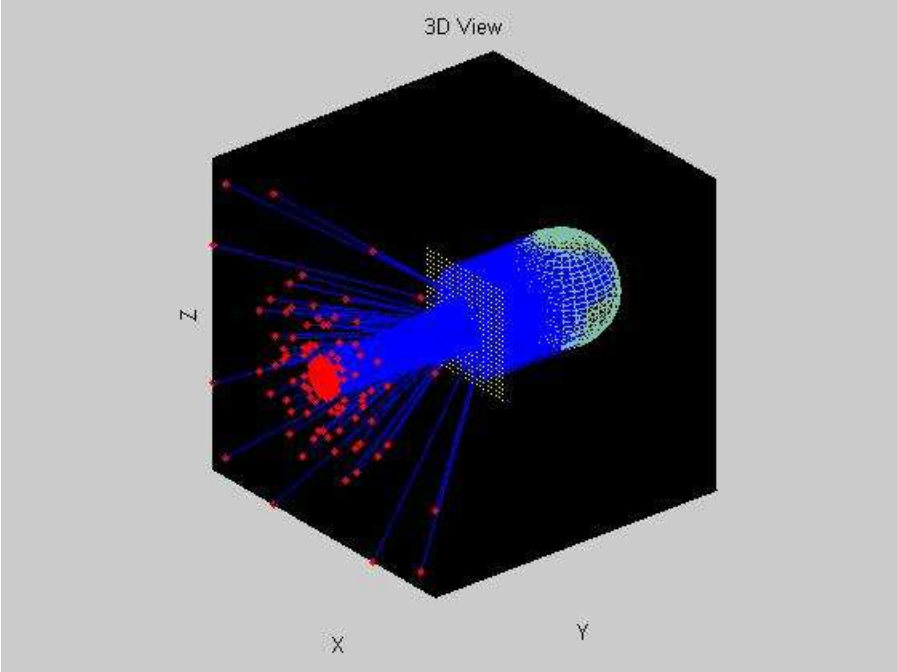

Figure C1.2 Square matrix pattern for general light source and aberration test

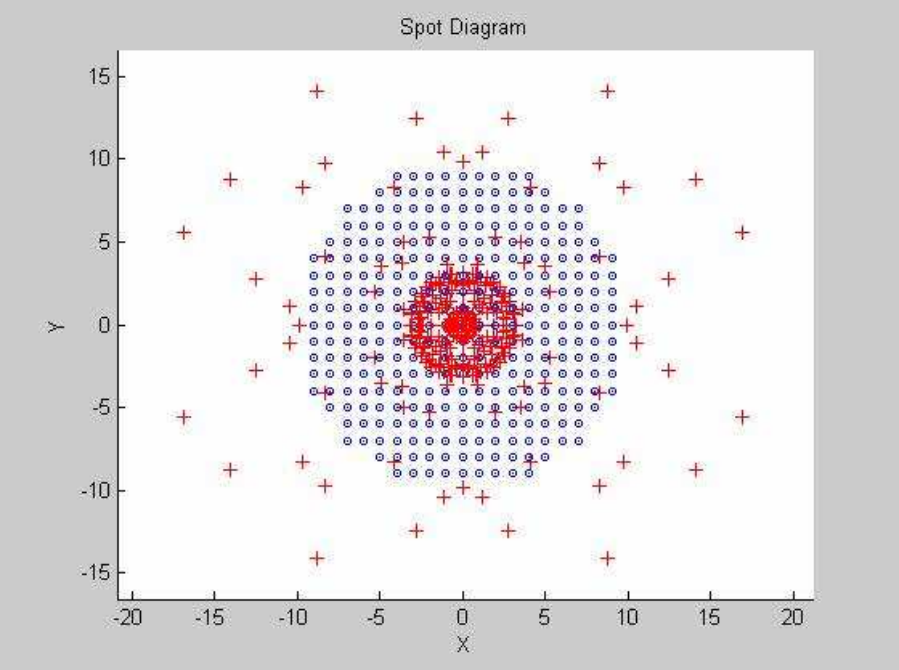

Figure C1.3 Spot diagram of the square matrix pattern

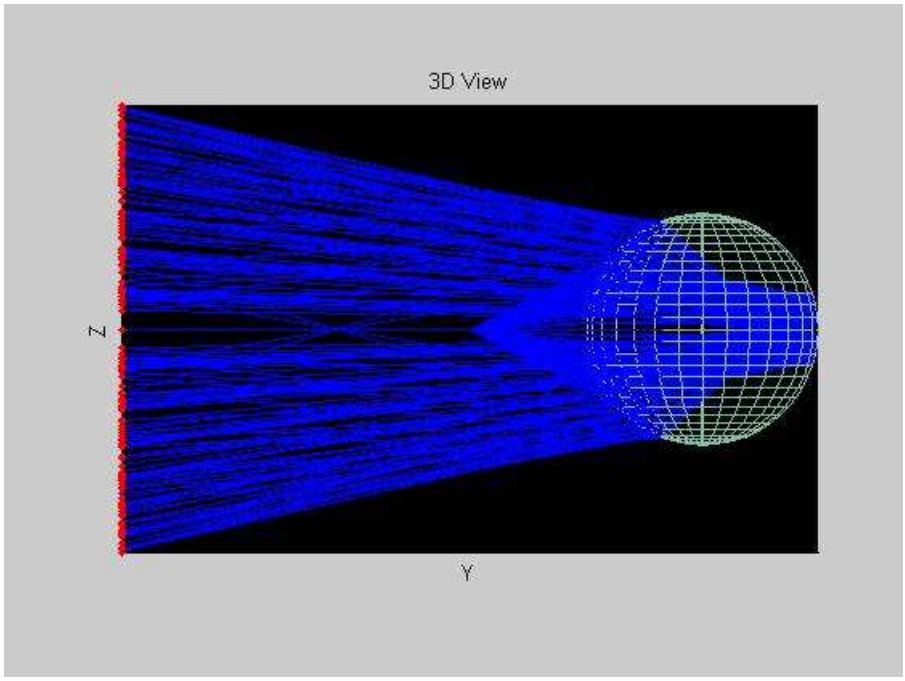

Figure C1.4 Point source light for very short range and fiber optics coupling

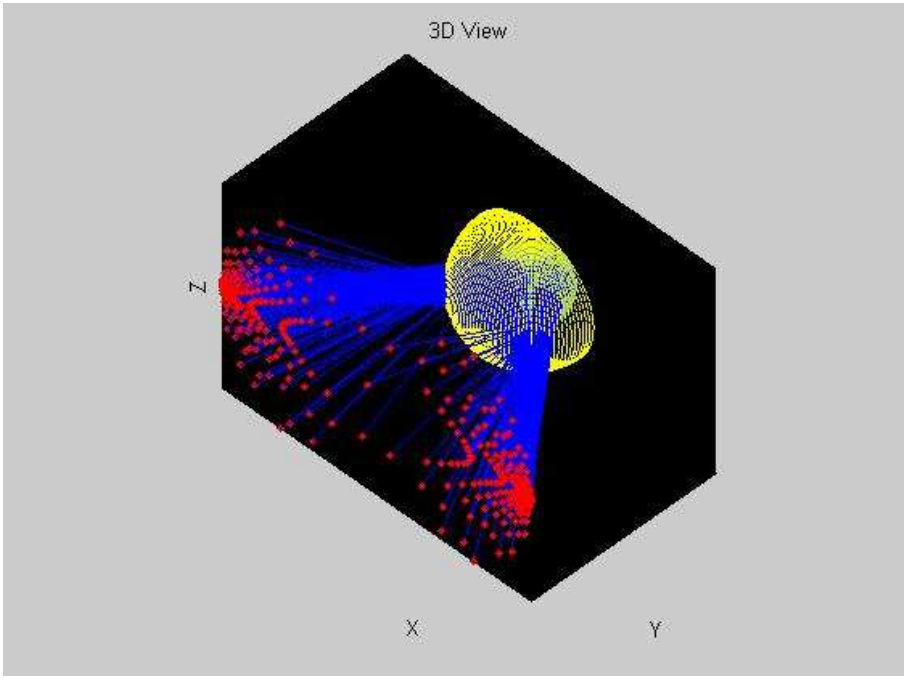

Figure C1.5 Dome light source for wide angle raytrace problems

Skewraytrace.m

```
function [allTrace, patternP0, rayHitCount] = skewraytrace(varargin)
% Rayrace.m is a sequential raytrace function that traces n skewray(s)
% through m surface(s) of an optical system

% Auther: Khalid Alhammadi

% A: 4x4m matrix defines the position and orientation of m frames
%    with respect to origin frame, as A=[A0 A1 A2...]
% P: 4xn initial position vector(s), P0=[Px Py Pz 1]'
% l: 4xn initial unit directional vector l0=[lx ly lz 0]'
% R: mx1 radius of the surface curvetur R=[R1 R2 ...]', -R if concave surface
% N: mx1 relative refractive index of medium i-1 w.r.t. medium i, N=[N1 N2...]'

A = varargin{1};
R = varargin{2};
N = varargin{3};
Rap = varargin{4};
alfa = varargin{5};
beta = varargin{6};

switch nargin
    case 8  % User defined ray(s)
        P0 = varargin{7};
        l0 = varargin{8};
        patternP0=P0;

    case 9  % User selected pattern
        step = varargin{7};
        pattern = varargin{8};
        Ys = varargin{9};
        % Two patterns to be selected for position vector P: 'plussign' and 'square'
        [P0, l0]= rayPattern(step, Rap, pattern, alfa, beta, Ys);
        patternP0= P0(1:3,:);
```

```
end

allTrace=[]; rayHitCount=0;

for k=1:size(P0,2)
    singleTrace = singleRaytrace(A, P0(:,k), l0(:,k), R, N, Rap);
    if (~isempty(singleTrace))
        allTrace=[allTrace; singleTrace];
        if(~isnan(singleTrace)), rayHitCount=rayHitCount+1; end % rayHitCount for last surface
    end
end

% disp(sprintf('\n %d Rays hit the last surface\n %d missed it\n %d Total\n',...
%     rayHitCount,size(P0,2)-rayHitCount,size(P0,2)))


%-------------------------------------------------------------------------
function singleTrace=singleRaytrace(A, P, l, R, N, Rap)
% Skew Raytracing for a single ray from surface one to the last surface

[k,m]=size(A);
surface=m/4;
singleTrace=P(1:3);

for k=1:surface
    [P, l]=skewray(A(:,4*k-3:4*k), P, l, R(k), N(k), Rap(k));
    if(~isreal(P)||isempty(P))
%         P=[]; l=[]; singleTrace=[]; return
        P=[nan nan nan nan]'; l=[nan nan nan nan]';
    end

%     % accept only rays hit first surface first and last surface (befor image)
%     % works with cat's eye problem, may cause problem with other systems
%     if(k==1&&P(2)>0)||(k==surface-1&&P(2)>0)
%         P=[]; l=[]; singleTrace=[]; return
%     end
```

```
    %if(k==surface), P=inv(A(:,4*k-3:4*k))*P; end       % image plane

    singleTrace=[singleTrace P(1:3)];
    %disp(sprintf('Surface#%d\nPi=[%5.3f %5.3f %5.3f %5.3f]\nli=[%5.3f %5.3f %5.3f %5.3f]\n----------------
-----------------------------------',k,P,l))
end


%-------------------------------------------------------------------------
function [Pi, li]=skewray(A, P, l, R, N, Rap)
% Skew Raytracing for a single ray from one surface to another
% Ref. "Analysis and Dsign of Optical system by use of sensitivity analysis
% of kew ray tracing" by P. Lin and C. Lu

if (nargin~=6)
    error('Incorrect number of input arguments.');
end

% lamda: magnitude of vector PQ (physical distance of optical
% path distance between Pi-1 to Pi)
if (R==0)                                           % flat surface
    ni=[0 0 -1 0]';
    lamda= -A(3,:)*P/(A(3,:)*l);
    Pi=P+(l*lamda);                                 % next position vector

else                                                % spherical surface
    D=A(:,4)'*(A*l)+P'*l;
    E=P(1:3)'*P(1:3)+A(1:3,4)'*A(1:3,4)-R*R+2*A(1:3,4)'*(A(1:3,1:3)*P(1:3));

    if(D*D-E==0), Pi=[]; li=[]; return, end % ray by-passes boundry

    % this trick will resolve the ambiguous sign of lamda for the two points
    % of intersection of the ray with a complete sphere of radius R as long
    % P(ray) in the other half of the sphere or outside it. Not passing through
    % the center which the half that contains the surface.
```

```
    if (R<0)
        lamda=-D+sqrt(D*D-E);                          % Concave surface
    else
        lamda=-D-sqrt(D*D-E);                          % Convex surface
    end

    Pi=P+(l*lamda);                                    % next position vector
    APi=A*Pi;
    segma=APi(1);
    roh = APi(2);
    tau=APi(3);
    alfa=atan2(roh,segma);
    beta=asin(tau/abs(R));
    ni=[cos(beta)*cos(alfa) cos(beta)*sin(alfa) sin(beta) 0]';
end

n=inv(A)*ni;                                           % unit normal vector
Ctheta=-l'*n;
if Ctheta==0, Pi=[]; li=[]; return                     % normal incedint
elseif Ctheta<0; si=-1;
else si=1;
end
Ctheta=si*Ctheta; n=si*n;

% next unit directional vector
if N==-1
    li=l+2*Ctheta*n;                                   % mirror (reflection)
else
    k=1-N*N+(N*Ctheta)^2;
    if k<0, Pi=[]; li=[]; return, end                  % Total Internal Reflection
    li=-sqrt(k)*n+N*(l+n*Ctheta);                      % lens (refraction)
end

% % aperture check
if(R==0)
    if(Pi(1)*Pi(1)+Pi(3)*Pi(3)>Rap*Rap), Pi=[]; li=[]; return, end % flat surface
```

```
    %elseif(abs(Pi(2))-A(3,4)>Rap), Pi=[]; li=[]; return   % spherical surface
end
%[Pi li [Ctheta*180/pi R N 1]']
if(0)                    % ******** Debugging ********
    theta=acos(Ctheta);
    disp(sprintf('D=%5.3f E=%5.3f lamda=%5.3f theta=%5.3f\na=%5.3f b=%5.3f |li|=%5.3f Snell`s law
THref=%5.3f\n',...
        D,E,lamda,[theta alfa beta]*180/pi,norm(li),asin(sin(theta)*N)*180/pi))
end


%-------------------------------------------------------------------------
function [PVM,LVM]=rayPattern(step, Rap, shape, alfa, beta, Ys)

% PV: 4x(m*n) position vectors, n=length(alfa)
% LV: 4x(m*n) unit directional vectors

for k=1:length(alfa)
    if (alfa(k)<0||alfa(k)>180||beta(k)<-90||beta(k)>90)
        error('unit directional vector angle violation.. alpha[0,180] and beta[-90,90]')
    end
end

rad=pi/180; PV=[]; LV=[]; PVM=[]; LVM=[];
alfa=alfa*rad;      % ranges [0,180] similar to Azimuth (horizontal) looking to XZ plane
beta=beta*rad;      % ranges [-90,90] similar to Elevation (vertical) looking to XZ plane
% Xrange=abs(Ys(2)) + abs(abs(Ys(1))+abs(Ys(2)))/tan(min(abs(alfa)));
% Xgrid=[0:step:Xrange+step/2]; Xgrid=[-Xgrid(end:-1:2) Xgrid];
% Zrange=abs(Ys(2)) + abs(abs(Ys(1))+abs(Ys(2)))*tan(max(abs(beta)));
% Zgrid=[0:step:Zrange+step/2]; Zgrid=[-Zgrid(end:-1:2) Zgrid];


switch lower(shape)

    case 'cross'                          % plus sign pattern
```

```
        if alfa==0, error('extreme angles are not allowed with cross or matrix paterns. 0<alpha<180 , (-
90<beta<90)'); end                              % avoide zero division
        % select the extreme angles
i=find(abs(pi/2-alfa)==max(abs(pi/2-alfa))); Xth=alfa(i(1));
i=find(abs(beta)==max(abs(beta))); Zth=beta(i(1));

D=abs(2*Ys(2)/sin(Xth)); d=Ys(1)/tan(Xth); Xgrid=0:step:d+D/2+step/2; Xgrid=[-Xgrid(end:-1:2) Xgrid];
D=2*Ys(2)/cos(Zth); d=Ys(1)*tan(Zth); Zgrid=0:step:d+D/2+step/2; Zgrid=[-Zgrid(end:-1:2) Zgrid];

xlen=length(Xgrid); zlen=length(Zgrid);

        PV=[Xgrid zeros(1,zlen); Ys(1)*ones(1,xlen+zlen); zeros(1,xlen) Zgrid; ones(1,xlen+zlen)];

        %         r=abs(Ys(1));
        %         th=2*max(Rap)/r/rad;
        %         % db=rad*[beta-th/2:step:beta+th/2];da=-90*rad*ones(1,length(db));
        %         db=rad*[-90:step:90];da=-90*rad*ones(1,length(db));
        %         Pv=[r*cos(db).*cos(da); r*cos(db).*sin(da); r*sin(db); ones(1,length(da))];
        %         % da=rad*[alfa-180-th/2:step:alfa-180+th/2];db=zeros(1,length(da));
        %         da=rad*[-180:step:0];db=zeros(1,length(da));
        %         Ph=[r*cos(db).*cos(da); r*cos(db).*sin(da); r*sin(db); ones(1,length(da))];
        %         PV=[Pv Ph];
        %
    case 'matrix'
        % select the extreme angles
i=find(abs(pi/2-alfa)==max(abs(pi/2-alfa))); Xth=alfa(i(1));
i=find(abs(beta)==max(abs(beta))); Zth=beta(i(1));

D=abs(2*Ys(2)/sin(Xth)); d=Ys(1)/tan(Xth); Xgrid=0:step:d+D/2+step/2; Xgrid=[-Xgrid(end:-1:2) Xgrid];
D=2*Ys(2)/cos(Zth); d=Ys(1)*tan(Zth); Zgrid=0:step:d+D/2+step/2; Zgrid=[-Zgrid(end:-1:2) Zgrid];

xlen=length(Xgrid); zlen=length(Zgrid);

        matrix=[];
        for z=1:zlen
            for x=1:xlen, matrix=[matrix [Xgrid(x) Ys(1) Zgrid(z) 1]']; end
```

```
        end
        PV= matrix;

    case 'dome'                                          % good for extreme angles for incedent
        k=60/step; [x,y,z]=sphere(k); r=max(abs(Rap));
        for i=1:floor(k/2+1)
            PV=[PV [r*x(:,i)'; r*y(:,i)'; r*z(:,i)'; ones(1,size(x,1))]];
        end
        %x(:,1:k/2)=[];y(:,1:k/2)=[];z(:,1:k/2)=[];   % extract half of the sphere

    case 'concentric'
        th=0:0.1*step:2*pi; r=abs(Ys(2))*logspace(-1,0,5);
        for k=1:length(r)
            x=r(k)*cos(th);
            z=r(k)*sin(th);
            PV=[PV [x; Ys(1)*ones(1,length(x)); z; ones(1,length(x))]];
        end

    case 'point'
        r=-abs(Ys(2)):step:abs(Ys(2));
        beta=atan(r/abs(Ys(1))); alfa=beta'+90*rad;
        PV=zeros(4,length(alfa)); PV(2,:)=Ys(1)+PV(2,:); PV(4,:)=1+PV(4,:);
        for k=1:length(beta)
            b=beta(k)*ones(length(alfa),1);
            LV=[cos(b).*cos(alfa) cos(b).*sin(alfa) sin(b) zeros(length(alfa),1)]';
            LVM=[LVM LV];
            PVM=[PVM PV];
        end
        return
end

m=size(PV,2);
for k=1:length(alfa)
    a=alfa(k)*ones(m,1);
    b=beta(k)*ones(m,1);
    LV=[cos(b).*cos(a) cos(b).*sin(a) sin(b) zeros(m,1)]';
```

```
    LVM=[LVM LV];
    PVM=[PVM PV];
end
```

Skewraygraph.m

```
function skewraygraph(R,N,Rap,thickness,Ys,alfa,beta,image,R_image,Rap_image,options)

% options to control ray ploting:
%       options(1)=1 ->plot only rays reach last surface
%       options(2)=1 ->plot incedent ray for spot diagram
%       options(3)=1 ->proceed with plot even if rayhit=0
%       options(4)=1 ->plot only spot diagram of last surface
%       options(5)=1 ->trace position of all rays hit image surface
%       options(6)=1 ->plot all input rays initial position
%       options(7)=1 ->trace ray pattern; not user defined ray(s)
%       options(8)=1-5 ->pattern selection
%       options(9)=0.5-5 ->ray density factor

% patterns:'Cross'1,'Concentric'1,'Matrix'5,'Dome'2,'Point'5
pattern=[{'Cross'},{'Concentric'},{'Matrix'},{'Dome'},{'Point'}];
shape=char(pattern(options(8)));
step=options(9);                                % ray density factor

Nsurface=length(R);                             % number of physical surfaces
RayDir=ones(size(R));
mirror=find(N==-1);
if(mirror)
    N=[N 1./N(end-1:-1:1) 1];
    R=[R -R(end-1:-1:1) R_image];
    Rap=[Rap Rap(end-1:-1:1) Rap_image];
    thickness=[thickness -thickness(end:-1:2) image];
    RayDir=ones(size(R));
    RayDir(mirror+1:end)=-1;
else
    N=[N 1];
    R=[R R_image];
    Rap=[Rap Rap_image];
    thickness=[thickness image];
```

```
    RayDir=ones(size(R));
end

D=cumsum(thickness);
% origin position of Global coordinate at Local coordinate of surface(i)
SurfaceCoord=D+RayDir.*R;               % Dispalcement for skew raytrace

A=[];
for k=1:length(R)
    if(R(k)~=0)
        Ak=[1 0 0 0;0 1 0 -SurfaceCoord(k);0 0 1 0;0 0 0 1];    % spherical surface
    else
        Ak=[-1 0 0 0;0 0 1 0;0 1 0 -SurfaceCoord(k);0 0 0 1];   % flat surface
    end
    A=[A Ak];
end

% ******************  OPTICAL SYSTEM DRAWING  ***************************
% draw all surfaces till reflector
f1=figure;
h1 = axes('Position',[0 0 1 1],'Visible','off');
n=0;
for k=1:2:Nsurface
    n=n+1;
    lens=['Lens ' int2str(n) ': R= [' num2str(R(k)) ',' num2str(R(k+1)) ']'];
    str(n) = cellstr(lens);
end

if(Nsurface>2)
%str(n+1) = cellstr(['Distance:' 'D= [' num2str(thickness(3)) ',' num2str(thickness(5)) ']']);
end
set(gcf,'CurrentAxes',h1)
text(.8,.8,str,'FontSize',8)

axes('Position',[0.07 0.07 .7 .8])
hold on, grid
```

```
for k=1:Nsurface, h(k) = surfaceMaker(RayDir(k)*R(k), Rap(k), D(k));end
h(k+1) = surfaceMaker(RayDir(k)*R(end), Rap(end), D(end));    % get the image surface
set(h,'FaceColor',[0.25 0.75 1],'edgecolor','none'); alpha(.5)
daspect([1 1 1]), axis tight, grid on, camlight('left'), material shiny
right=[90,0]; view(right), xlabel('X'), ylabel('Y'), zlabel('Z'), drawnow
disp('press any key to continue with ray tracing ...'), pause

% ***************************  RAY TRACING  *******************************
tic
if(~options(7))                    % trace user defined ray(s)
    alfa=[90 70]'; beta=[0 0]';
    m=length(alfa); rad=pi/180; a=alfa*rad; b=beta*rad;
    P0=[[0 Ys(1) 2/sqrt(2) 1]' [0 Ys(1) -2/sqrt(2) 1]'];          % example
    l0=[cos(b).*cos(a) cos(b).*sin(a) sin(b) zeros(m,1)]';
    patternP0=P0; shape='user defined ray(s)';
    [allTrace, patternP0, rayHitCount] = skewraytrace(A, R, N, Rap, alfa, beta, P0, l0);
end

if(options(7))                     % trace a pattern of light
    [allTrace, patternP0, rayHitCount] = skewraytrace(A, R, N, Rap, alfa, beta, step, shape, Ys);
end
toc

disp(sprintf('\n %d Rays hit the last surface\n %d missed \n %d Total rays hit first surface \n OUT/IN
RayRatio= %f\n',...
    rayHitCount,size(allTrace,1)/3-rayHitCount,size(allTrace,1)/3,rayHitCount/(size(allTrace,1)/3)))

if(rayHitCount==0 && ~options(3)), close(f1), return, end
showme(allTrace, patternP0, alfa, beta, R, Rap, shape, options)


%-------------------------------------------------------------------------------------
function showme(allTrace, patternP0, alfa, beta, R, Rap, shape, options)
if(~isempty(allTrace))
    % ************************  RAY TRACE DRAWING  ************************
```

```
    Xmax=0; Zmax=0;
    [m,n]=size(allTrace); n=ceil(n/2);  % coloring incedent (blue) and reflected (red) rays
    for k=1:3:size(allTrace,1)
        singleTrace=[allTrace(k,:)', allTrace(k+1,:)', allTrace(k+2,:)'];
        %         plot3(singleTrace(1,1), singleTrace(1,2), singleTrace(1,3),'color','b',...
        %             'Marker','.','MarkerSize',1.4)
        %        plot3(singleTrace(end,1), singleTrace(end,2), singleTrace(end,3),'.r');
        if(sum(sum(isnan(singleTrace)))&&options(1)), continue, end
        line(singleTrace(1:n,1), singleTrace(1:n,2), singleTrace(1:n,3),'Color',...
            'b','Marker','.','LineWidth',1);
        line(singleTrace(n:end,1), singleTrace(n:end,2), singleTrace(n:end,3),...
            'Color','r','Marker','.','LineWidth',1)
        if(Xmax<abs(singleTrace(1,1))), Xmax=abs(singleTrace(1,1)); end
        if(Zmax<abs(singleTrace(1,3))), Zmax=abs(singleTrace(1,3)); end
        if(options(5)),disp('------------------------------------------------');singleTrace, end
    end

    if(options(6))
        for k=1:size(patternP0,2)
            if(Xmax<0.85*abs(patternP0(1,k)) || Zmax<0.85*abs(patternP0(3,k))), continue, end
            plot3(patternP0(1,k), patternP0(2,k), patternP0(3,k),...
                'LineStyle','none','Color','y','Marker','*','MarkerSize',1.4)
        end
    end

    axis equal, axis tight, view(3), title(['3D View, "', shape,'-shape" light source'])
    xlabel('X'), ylabel('Y'), zlabel('Z')
    disp('hit any key to see different views of the figure'), pause
    front=[0,0]; view(front),title('Front View'), pause
    top=[0,90]; view(top),title(['Top View,  \it\alpha= ',int2str(alfa'),']^o']),pause
    right=[90,0]; view(right),title(['Right View,  \it\beta= ',int2str(beta'),']^o']),pause
    title('3D View'), set(gcf,'color','black'), set(gca,'color','black')
    set(gca,'XGrid','off','YGrid','off','ZGrid','off'),set(gca,'XTick',[],'YTick',[],'ZTick',[])
    %    for az=90:2:400, view(az,30), pause(.1), end
    hold off, pause, close(gcf)
```

```
    % ****************************  SPOT DIAGRAM PLOT  ***************************
    f2=figure; xlabel('X'), ylabel('Y')

    for Nsurface=2:size(allTrace,2)
        if(options(4)&&Nsurface~=size(allTrace,2)), continue, end    % plot only image surface
        hold on,
        for k=1:3:size(allTrace,1)
            singleTrace=[allTrace(k,:)', allTrace(k+1,:)', allTrace(k+2,:)'];
            plot(singleTrace(Nsurface,1), singleTrace(Nsurface,3), '+r')
            if(options(2)), plot(singleTrace(1,1), singleTrace(1,3),...
                    'Color','b','Marker','o','MarkerSize',1.5), end
        end

        if (Nsurface==size(allTrace,2)), last=' image plane'; else last=[]; end
        title(['Spot Diagram, "', shape,'-shape" light source, surface# ',int2str(Nsurface-1), last])
        r=Rap(Nsurface-1); x=linspace(-r,r,100); y=sqrt(r^2-x.^2);        % show aperture
        plot(x,y,'--b',x,-y,'--b'), axis equal, axis tight, drawnow, hold off, pause,
    end
    close(f2)
end


%-------------------------------------------------------------------------
function h = surfaceMaker(R, Rap, D)
% generate a surface (flat or spherical) about y-axis with vertix at origin

if R==0, R=Rap; flat=0; else flat=1; end    % R=0 -> flat surface
th= asin(Rap/abs(R));
step= 0.025*Rap/abs(R);
b=-th:step:th;
a=-th-pi/2:step:th-pi/2;
[a,b]= meshgrid(a,b);

x= R*cos(b).*cos(a);
y= R*cos(b).*sin(a);
z= R*sin(b);
```

```
% disregard all points beyond surface aperture
[i,j]= find(abs(y)<sqrt(R^2-Rap^2));
for k=1:length(i), x(i(k),j(k))=nan; y(i(k),j(k))=nan; z(i(k),j(k))=nan; end
y=flat*(y+R)+D;    % shift surface vertix by D distance on y-axis direction

h = surf(x,y,z);
```

Optics.m

An example MATLAB M-file uses the skewraytrace program.

```
function optics(sys)

% options to control ray ploting:
%       options(1)=1 ->plot only rays reach last surface
%       options(2)=1 ->plot incedent ray for spot diagram
%       options(3)=1 ->proceed with plot even if rayhit=0
%       options(4)=1 ->plot only spot diagram of last surface
%       options(5)=1 ->trace position of all rays hit image surface
%       options(6)=1 ->plot all input rays initial position
%       options(7)=1 ->trace ray pattern; not user defined ray(s)
%       options(8)=1-5 ->pattern selection
%       options(9)=0.5-5 ->ray density factor
% patterns:'Cross','Concentric','Matrix','Dome','Point'
options=[0 1 1 1 0 1 1 1 1];
% limits: alfa[0,180],max=90-asin(Rap/R), beta[-90,90],max=asin(Rap/R)
alfa=[90]'; beta=[0*ones(size(alfa'))]';        % make sure same dimensions

%**********************  OPTICAL SURFACES  ************************
switch sys
    case 1        % RETROREFLECTOR: meniscus+achromatic lens
        % relative refractive index. set N=-1 for reflective surface
        ach=1.62004;
        N=[1/1.5 1.5 1/1.52288 1.52288/1 1/ach ach 1/2 -1];  % N=-1 for reflective surface
        R=[200 40 35 -35 -35 -78.625 2.5 -2.5]; % -R if ray facing concave surface, 0 for flat surface
        Rap=[50.8 25 12.5 12.5 12.5 12.5 2.5 2.5]; % aperture radius
        thickness=[0 5 20 6.6 0 1.7 75 5];      % distance between surface's vertices
        Ys=[-20 15];                            % light source distance from origin on Y0-axis
        image=-30;                              % image distance from the last surface
        R_image=0;                              % image radius
        Rap_image=20;                           % image aperture
```

```
case 2        % Cat's eye retroreflector lens
    N=[1/2 -1];                      % N=-1 for reflective surface
    R=[2.5 -2.5];                    % -R if ray facing concave surface, 0 for flat surface
    Rap=[2.5 2.5];                   % radius of aperture of every surface
    thickness=[0 5];                 % distance between surface's vertices
    Ys=[-10 5];                      % object distance from origin on Y-axis
    image=-20;                       % from the last surface
    R_image=0;                       % image radius
    Rap_image=10;                    % image aperture

 case 3        % cateye  with BX/Achromatic retroreflector lens
    ac=1.62004; nac=1;
    N=[1/1.52288 1.52288/ac ac 1/2 -1]; % N=-1 for reflective surface
    R=[35 -35 -78.625 2.5 -2.5];     % -R if ray facing concave surface, 0 for flat surface
    Rap=[12.5 12.5 12.5 2.5 2.5];    % aperture radius
    thickness=[0 6.6 1.7 42 5];      % distance between surface's vertices
    Ys=[-20 10];                     % light source distance from origin on Y0-axis
    image=-30;                       % image distance from the last surface
    R_image=0;                       % image radius
    Rap_image=25;                    % image aperture

case 4        % biconvex lens of refractive index=1.5
    N=[2/3 3/2];                     % N=-1 for reflective surface
    R=[10 -10];                      % -R if ray facing concave surface, 0 for flat surface
    Rap=[7 7];                       % radius of aperture of every surface
    thickness=[0 10];                % distance between surface's vertices
    Ys=-10;                          % object distance from origin on Y-axis
    image=10;                        % from the last surface
    R_image=0;                       % image radius
    Rap_image=20;                    % image aperture

case 5        % biconcave lens of refractive index=1.5
    N=[2/3 3/2];                     % N=-1 for reflective surface
    R=[-10 10];                      % -R if ray facing concave surface, 0 for flat surface
    Rap=[7 7];                       % radius of aperture of every surface
```

```
        thickness=[0 2];                % distance between surface's vertices
        Ys=-10;                         % object distance from origin on Y-axis
        image=18;                       % from the last surface
        R_image=0;                      % image radius
        Rap_image=20;                   % image aperture

    case 6        % Meniscus lens of refractive index=1.5. Rays enter from convex side
        N=[2/3 3/2];                    % N=-1 for reflective surface
        R=[200 40];                     % -R if ray facing concave surface, 0 for flat surface
        Rap=[100 35 100];               % radius of aperture of every surface
        thickness=[0 5];                % distance between surface's vertices
        Ys=-50;                         % object distance from origin on Y-axis
        image=60;                       % from the last surface
        R_image=0;                      % image radius
        Rap_image=100;                  % image aperture

    case 7        % Meniscus lens of refractive index=1.5. Rays enter from concave side
        N=[2/3 3/2];                    % N=-1 for reflective surface
        R=[-40 -200];                   % -R if ray facing concave surface, 0 for flat surface
        Rap=[39.5 120];                 % radius of aperture of every surface
        thickness=[0 5];                % distance between surface's vertices
        Ys=-60;                         % object distance from origin on Y-axis
        image=25;                       % from the last surface
        R_image=0;                      % image radius
        Rap_image=150;                  % image aperture

    case 8        % reflective hemi-sphere
        N=[-1];                         % N=-1 for reflective surface
        R=[10];                         % -R if ray facing concave surface, 0 for flat surface
        Rap=[10];                       % radius of aperture of every surface
        thickness=[20];                 % distance between surface's vertices
        Ys=-10;                         % object distance from origin on Y-axis
        image=-40;                      % from the last surface
        R_image=0;                      % image radius
        Rap_image=50;                   % image aperture
```

```
    case 9        % Refractive plane
        N=[1/2];                          % N=-1 for reflective surface
        R=[0];                            % -R if ray facing concave surface, 0 for flat surface
        Rap=[30];                         % radius of aperture of every surface
        thickness=[0];                    % distance between surface's vertices
        Ys=-20;                           % object distance from origin on Y-axis
        image=50;                         % from the last surface
        R_image=0;                        % image radius
        Rap_image=50;                     % image aperture

    case 10        % mirror plane
        N=[-1];                           % N=-1 for reflective surface
        R=[0];                            % -R if ray facing concave surface, 0 for flat surface
        Rap=[10 ];                        % radius of aperture of every surface
        thickness=[0];                    % distance between surface's vertices
        Ys=-10;                           % object distance from origin on Y-axis
        image=-40;                        % from the last surface
        R_image=0;                        % image radius
        Rap_image=50;                     % image aperture

    case 11        % Achromatic lens (MELLES GRIOT PART# 01 LAO 014)
        ac=1.62004; nac=1;
        N=[1/1.52288 1.52288/ac ac];      % N=-1 for reflective surface
        R=[35 -35 -78.625];               % -R if ray facing concave surface, 0 for flat surface
        Rap=[12.5 12.5 12.5];             % radius of aperture of every surface
        thickness=[0 6.6 1.7];            % distance between surface's vertices
        Ys=-20;                           % object distance from origin on Y-axis
        image=60;                         % from the last surface
        R_image=0;                        % image radius
        Rap_image=20;                     % image aperture

    case 12         % RETROREFLECTOR: meniscus+cat's eye lens; Optimized distance
        N=[1/1.5 1.5 1/3 3 1/2 -1];       % N=-1 for reflective surface
        R=[200 40 0 0 2.5 -2.5];          % -R if ray facing concave surface, 0 for flat surface
        Rap=[50.8 25 2 2 2.5 2.5];        % aperture radius
        thickness=[0 5 20 1 1 5];         % distance between surface's vertices
```

```
        Ys=[-20 50];                        % light source distance from origin on Y0-axis
        image=-20;                          % image distance from the last surface
        R_image=0;                          % image radius
        Rap_image=100;                      % image aperture

    otherwise
        disp('type optics(n), where n is a number from 1 to 11 for different examples.')

end

skewraygraph(R,N,Rap,thickness,Ys,alfa,beta,image,R_image,Rap_image,options)
```

C2 C++ Transceiver Program Code

Laser Communication main file

```
/*****************************************************************************************
File Name       : main.c
Title           : Mobile Robot Optical Communication
Author          : Khalid ALhammadi
Date            : 3-July-2006
Target MCU      : Atmega128
Editor Tabs     : 4

UART0 communicates with MicroController (BasicX) to drive wheels motors
UART1 Tx pulses to laser driver circuit and Rx pulses from PD circuit

EvBot Mobile Robot Commands (UART0) for BasicX microcontroller:
1)      Go a specified number of centimeters ['G' MotorDirection HighByte LowByte]
        MotorDirection:
                0= both motors backwards
                1= right forward and left backward
                2= left forward and right backward
                3= both motors forwards
```

Example: cmnd='G'; Mdir=3; HB=2; LB=1 (i.e., move forward for 513cm)

2) Turn a specified angle ['T' 'R/L' Angle]
'R': turn right; 'L': turn left; angle<=180 degree
Example: cmnd='TR'; angle=50 (i.e., turn right 50 degrees)

3) Any extra character followed these commands will stop the motor.
Command letter 'G' or 'T' will be received at the beginig of the execution and
When mission accomplished 'D'-Done letter will be received.

Only when comm. optically (UART1), use dummy char (eg, U) for every data packet
so that Rx receives start bit for synchronization.
reason: AC-coupled circuit elliminate start bit of the first byte

EXAMPLE

```
//move forward 100cm
Message[0]='G'; Message[1]=3; Message[2]=0; Message[3]=100;
uartSendBuffer(0, Message, 4);
while(!(uartReceiveByte(0, &RxByte) && (RxByte=='D')));                    // waite to finish excu.

// turn left 90deg
Message[0]='T'; Message[1]='L'; Message[2]=90;
uartSendBuffer(0, Message, 3);
while(!(uartReceiveByte(0, &RxByte) && (RxByte=='D')));                    // waite to finish excu.
```

```
*****************************************************************************************/

//----- Include Files ---------------------------------------------------
#include <avr/interrupt.h>              // include interrupt support
#include <math.h>
#include <stdio.h>                                                      // sprintf
#include <stdlib.h>                                                     // itoa
#include <string.h>
#include "uart2.h"                                                      // include uart function library
#include "delay.h"

void Initialization(void);
void uartRx_Enable(unsigned char nUart, unsigned char enable);
char Task(char Tasknum);
u16 man_encode(u08 unenc);
u08 man_decode(u16 enc);
void Send_ME_Data(char nUart, unsigned char *Message, unsigned int numByte);
char Synchronize(char nUart, unsigned char XByte);
unsigned int GetData(char nUart, unsigned char *Message);
char packet_received_check(unsigned char nUart);

extern cBuffer uartRxBuffer[2];
extern cBuffer uartTxBuffer[2];
unsigned int BuffSize = 100;
```

```
u08 RxByte='U', odd_byte, even_byte;
char receive_error=0;                                   // Flag: ME error in the received byte
unsigned int distCorr=0, angleCorr=0;                   // correct any discrepancies in robot movement
unsigned char debug=0;                                  // debug in heyperterminal connected to UART0
char RX_state=1;                                        // change Rx enable/disable status (0: no change)

//------------------------------ Begin Code ------------------------------------
int main(void)
{
        volatile unsigned char Message[BuffSize];       // buffer for Tx/Rx message
        u16 numByte, i;

        Initialization();

        while (TRUE) {
                Task(1);

                if(packet_received_check(1)) Task(4);

                delay_ms(5000);
        }

        return 0;
}
```

```
char packet_received_check(unsigned char nUart)
{// check for acknoledgment of the transmitted packet from other receiver
	unsigned char i;

	uartFlushReceiveBuffer(nUart);

	for (i=1; i<5; i++){
		delay_ms(30);
		uartReceiveByte(nUart, &RxByte);
		if (debug) uartSendByte(0, RxByte);			// debug
		if (RxByte=='U') return 1;
	}

	return 0;
}

char Task(char Tasknum)
{
//	command Robot to Tx/move according to task number
	unsigned char Message[BuffSize];			// buffer for Tx/Rx message
	unsigned int numByte, i=1;				// Byte counter

	Message[i]='U';						// to elliminate unwanted AC-coupling effect on start bit
```

```
Message[++i]='(';                       // data packet start character

switch (Tasknum) {
        case 1:                                 // command other robot to move backward 30cm (1 foot)
                Message[++i]='G'; Message[++i]=0; Message[++i]=0; Message[++i]=30;
                break;

        case 2:                                 // command other robot to move forward 30cm
                Message[++i]='G'; Message[++i]=3; Message[++i]=0; Message[++i]=30;
                break;

        case 3:                                 // command other robot to move in U-shape
                // move backward 100cm
                Message[++i]='G'; Message[++i]=0; Message[++i]=0; Message[++i]=100;
                // turn right 90
                Message[++i]='T'; Message[++i]='R'; Message[++i]=90;
                // move forward 100cm
                Message[++i]='G'; Message[++i]=3; Message[++i]=0; Message[++i]=100;
                // turn left 90
                Message[++i]='T'; Message[++i]='L'; Message[++i]=90;
                // move forward 100cm
                Message[++i]='G'; Message[++i]=3; Message[++i]=0; Message[++i]=100;
                break;
```

```
        case 4:                                                 // move robot to meeting location
                // turn left 90deg
                Message[1]='T'; Message[2]='L'; Message[3]=90;
                for (i=1; i<=3; i++) {uartSendByte(0, Message[i]);}
                while(!(uartReceiveByte(0, &RxByte) && (RxByte=='D')));   // waite to finish excu.

                // move forward 100cm
                Message[1]='G'; Message[2]=3; Message[3]=0; Message[4]=100;
                for (i=1; i<=4; i++) {uartSendByte(0, Message[i]);}
                while(!(uartReceiveByte(0, &RxByte) && (RxByte=='D')));   // waite to finish excu.

                // turn right 90deg
                Message[1]='T'; Message[2]='R'; Message[3]=90;
                for (i=1; i<=3; i++) {uartSendByte(0, Message[i]);}
                while(!(uartReceiveByte(0, &RxByte) && (RxByte=='D')));   // waite to finish excu.

                return 1;
}

// End of command line
Message[++i]=')';                                               // data packet end character

numByte=i;
```

```
        Send_ME_Data(1, Message, numByte);

        return 1;
}


unsigned int GetData(char nUart, unsigned char *Message)
{// grab transmitted data after synchronizing with the start packet character
        unsigned int numByte, i;

        while(!Synchronize(1, ('));                                     // wait for synchronization character

        for (i=1; i<=BuffSize; i++) {

                while(!(uartReceiveByte(nUart, &even_byte)));
                while(!(uartReceiveByte(nUart, &odd_byte)));
                RxByte = man_decode(((u16)odd_byte<<8)|even_byte);

                if (receive_error) {                                    // Error in data packet.... quit.
                        if (debug) {                                    // debug line in hyperterminal connected to UART0
                                numByte = sprintf(Message," Manchester Decoding Error ...");
                                uartSendBuffer(0, Message, numByte);
                                uartSendByte(0, '\r'); uartSendByte(0, '\n');           // debug: newline
                        }
```

```
            uartFlushReceiveBuffer(nUart);
            return 0;
}

if(i>BuffSize) {                                        // invalid data packet
            if (debug) {                                // debug line in hyperterminal connected to UART0
                        numByte = sprintf(Message," Out of range error ...");
                        uartSendBuffer(0, Message, numByte);
                        uartSendByte(0, '\r'); uartSendByte(0, '\n');       // debug: newline
            }

            uartFlushReceiveBuffer(nUart);
            return 0;
}
else if (RxByte==')') {                                 // A complete valid data packet is received
            if (RX_state) {
                        uartRx_Enable(nUart, 0);                            // disable receiver
                        uartSendByte(nUart, 'U'); uartSendByte(nUart, 'U'); // inform transmitter
                        uartSendByte(nUart, 'U'); uartSendByte(nUart, 'U');
                        uartRx_Enable(nUart, 1);                            // enable receiver
            }
            return (i-1);                                   // valid data packet
}
```

```
                Message[i]= RxByte;
                if (debug) uartSendByte(0, Message[i]);                    // debug
        }
}

char Synchronize(char nUart, unsigned char XByte)
{
// Burst communication synchronization
// Example: waite for data packet starting character '('. Should receive even_byte first.
        u16 u16Byte, temp;
        unsigned char Xodd_byte, Xeven_byte;

        u16Byte = man_encode(XByte); temp = u16Byte;
        Xodd_byte = temp>>8; Xeven_byte = (u08)u16Byte;

        while(!(uartReceiveByte(nUart, &even_byte) && (even_byte == Xeven_byte)));
        while(!(uartReceiveByte(nUart, &odd_byte)));

        if (odd_byte == Xodd_byte) return(1);
        else return(0);
}
```

```
void Send_ME_Data(char nUart, unsigned char *Message, unsigned int numByte)
{       // send Manchester encoded data (even_byte first).
        u16 u16Byte, i, temp;

        // disable receiver so no pickup echoes from the reflected Tx data
        if (RX_state) uartRx_Enable(nUart, 0);                          // disable receiver

        for (i=1; i<=numByte; i++) {
                u16Byte = man_encode(Message[i]);
                temp = u16Byte;
                odd_byte = temp>>8;
                even_byte = (u08)u16Byte;
                uartSendByte(nUart, even_byte);
                uartSendByte(nUart, odd_byte);

                if (debug) uartSendByte(0, Message[i]);                  // debug
        }

        if (RX_state) {
                uartFlushReceiveBuffer(nUart);
                uartRx_Enable(nUart, 1);                                // enable receiver
        }
}
```

```
u16 man_encode(u08 unenc)
{/*     ------------------------------------------------------------------------------
        u16 man_encode(int enc)
        written by Aaron Ramsey, Jan. 25th, 2000
        This function encodes a 8 bit value into a 16 bit manchester encoded variable which it
        then returns.

        This function encodes the bits in a unique way. The odd bits (7,5,3,1) are encoded into
        the msb 8 bits of data to return and the even bits (6,4,2,0) are encoded into the lsb 8
        bits of data to return. Encoding this way saves alot of bit testing and flipping.

        0x0E (00001110) encodes into 0x5AA6 (0101101010100110)
        instead of the more natural 0x55A9 (0101010110101001)
        ------------------------------------------------------------------------------
*/
        u08 odd_byte,even_byte,temp;

        odd_byte=unenc&0xAA;
        temp=(~unenc&0xAA)>>1;
        odd_byte=odd_byte|temp;

        even_byte=unenc&0x55;
        temp=(~unenc&0x55)<<1;
```

```
	even_byte=even_byte|temp;

	return((u16)odd_byte<<8)|even_byte;
}


u08 man_decode(u16 enc)
{/*	-------------------------------------------------------------------------------
	u08 man_decode(u16 enc)
	written by Aaron Ramsey, Jan. 25th, 2000
	This function decodes a 16 bit manchester encoded variable and returns the actual 8 bit
	unencoded value. See man_encode for a description of the encoding technique.
	-------------------------------------------------------------------------------
*/
	u08 odd_byte,even_byte;

	odd_byte=(u08)(enc>>8);
	if((odd_byte&0xAA)^((~odd_byte&0x55)<<1)) {
		receive_error=1;
		return(0);
	}
	else odd_byte&=0xAA;
	even_byte=(u08)enc;
	if((even_byte&0x55)^((~even_byte&0xAA)>>1)) {
```

```
                receive_error=1;
                return(0);
        }
        else even_byte&=0x55;
        receive_error=0;

        return(odd_byte|even_byte);
}


void Initialization(void)
{

        uartInit();                                                     // initialize UART0 and UART1 (serial ports)
        uartSetBaudRate(1,1000);                                        // set the baud rate of the UART1 to Optical Modulator
        uartSetBaudRate(0,19200);                                       // set the baud rate of the UART0 to Robot MCU
        sei();                                                          // enable global interrupts
}


void uartRx_Enable(unsigned char nUart, unsigned char enable)
{       // disable/enable Uart# receiver
        if(nUart) {         // Uart1
                if(enable) UCSR1B = (1<<RXEN1)|(1<<TXEN1)|(1<<RXCIE1)|(1<<TXCIE1);// enable receiver
```

```
                else UCSR1B = (0<<RXEN1)|(1<<TXEN1)|(0<<RXCIE1)|(1<<TXCIE1);                // disable receiver
        }
        else {          // Uart0
                if(enable) UCSR0B = (1<<RXEN0)|(1<<TXEN0)|(1<<RXCIE0)|(1<<TXCIE0);          // enable receiver
                else UCSR0B = (0<<RXEN0)|(1<<TXEN0)|(0<<RXCIE1)|(1<<TXCIE1);                // disable receiver
        }
}
```

Retroreflector Communication main file.

```
/*****************************************************************************************
 File Name         : main.c
 Title             : Mobile Robot Optical Communication
 Author  : Khalid ALhammadi
 Date              : 3-July-2006
 Target MCU        : Atmega128
 Editor Tabs: 4

 UART0 communicates with MicroController (BasicX) to drive the motor
 UART1 Tx pulses to driver LCPG modulator circuit and Rx pulses from PD circuit

EvBot Mobile Robot Commands (UART0) for BasicX microcontroller:
1)      Go a specified number of centimeters ['G' MotorDirection HighByte LowByte]
        MotorDirection:
                0= both motors backwards
                1= right forward and left backward
                2= left forward and right backward
                3= both motors forwards
        Example: cmnd='G'; Mdir=3; HB=2; LB=1  (i.e., move forward for 513cm)

2)      Turn a specified angle ['T' 'R/L' Angle]
```

'R': turn right; 'L': turn left; angle<=180 degree
Example: cmnd='TR'; angle=50 (i.e., turn right 50 degrees)

3) Any extra character followed these commands will stop the motor.
Command letter 'G' or 'T' will be received at the beginig of the execution and
When mission accomplished 'D'-Done letter will be received.

Only when comm optically (UART1), use dummy char (eg, space) for every data packet so that Rx receives start bit for synchronization.
reason: AC-coupled circuit elliminate start bit of the first byte

EXAMPLE

```
//move forward 100cm
Message[0]='G'; Message[1]=3; Message[2]=0; Message[3]=100;
uartSendBuffer(0, Message, 4);
while(!(uartReceiveByte(0, &RxByte) && (RxByte=='D')));                    // waite to finish excu.

// turn left 90deg
Message[0]='T'; Message[1]='L'; Message[2]=90;
uartSendBuffer(0, Message, 3);
while(!(uartReceiveByte(0, &RxByte) && (RxByte=='D')));                    // waite to finish excu.

*****************************************************************************************/
```

```
//----- Include Files -------------------------------------------------------
#include <avr/interrupt.h>                                  // include interrupt support
#include <math.h>
#include <stdio.h>                                          // sprintf
#include <stdlib.h>                                         // itoa
#include <string.h>
#include "uart2.h"                                          // include uart function library
#include "delay.h"

void Initialization(void);
void uartRx_Enable(unsigned char nUart, unsigned char enable);
char Process_received_Data(unsigned char *Message, unsigned int i);
u16 man_encode(u08 unenc);
u08 man_decode(u16 enc);
void Send_ME_Data(char nUart, unsigned char *Message, unsigned int numByte);
char Synchronize(char nUart, unsigned char XByte);
unsigned int GetData(char nUart, unsigned char *Message);

extern cBuffer uartRxBuffer[2];
extern cBuffer uartTxBuffer[2];
unsigned int BuffSize = 100, TxDelay=0;
u08 RxByte, odd_byte, even_byte;
char receive_error=0;                                       // There is a problem with the byte received
char RX_state=1;                                            // change Rx enable/disable status (0: no change)
```

```
char debug=0;

//------------------------------- Begin Code --------------------------------------
int main(void)
{
	unsigned char Message[BuffSize];		// buffer for incoming message
	u16 numByte, i;

	Initialization();

	while (TRUE) {
		numByte = GetData(1, Message);

		if(numByte!=0) Process_received_Data(Message, numByte);		// execute command

		if (debug) {
			for(i=1;i<=numByte;i++) uartSendByte(0, Message[i]);
			uartSendByte(0, '\r'); uartSendByte(0, '\n');		//debug
		}
	}

	return 0;
}
```

```
unsigned int GetData(char nUart, unsigned char *Message)
{// grab transmitted data after synchronizing with the start packet character
        unsigned int numByte, i;

        while(!Synchronize(1, '('));                                    // wait for synchronization character

        for (i=1; i<=BuffSize; i++) {

                while(!(uartReceiveByte(nUart, &even_byte)));
                while(!(uartReceiveByte(nUart, &odd_byte)));
                RxByte = man_decode(((u16)odd_byte<<8)|even_byte);

                if (receive_error) {                                    // Error in data packet.... quit.
                        if (debug) {                                    // debug line in hyperterminal connected to UART0
                                numByte = sprintf(Message," Manchester Decoding Error ...");
                                uartSendBuffer(0, Message, numByte);
                                uartSendByte(0, '\r'); uartSendByte(0, '\n');           // debug: newline
                        }

                        uartFlushReceiveBuffer(nUart);
                        return 0;
                }
```

```
                if(i>BuffSize) {   // invalid data packet
                        if (debug) {                                            // debug line in hyperterminal connected to UART0
                                numByte = sprintf(Message," Out of range error ...");
                                uartSendBuffer(0, Message, numByte);
                                uartSendByte(0, '\r'); uartSendByte(0, '\n');   // debug: newline
                        }

                        uartFlushReceiveBuffer(nUart);
                        return 0;
                }
                else if (RxByte==')') {                                         // A complete valid data packet is received
                        if (RX_state) {
                                uartRx_Enable(nUart, 0);                        // disable receiver
                                uartSendByte(nUart, 'U'); uartSendByte(nUart, 'U');   // inform transmitter
                                uartSendByte(nUart, 'U'); uartSendByte(nUart, 'U');
                                uartRx_Enable(nUart, 1);                        // enable receiver
                        }
                        return (i-1);                                           // valid data packet
                }

                Message[i]= RxByte;
                if (debug) uartSendByte(0, Message[i]);                         // debug
        }
}
```

```
char Synchronize(char nUart, unsigned char XByte)
{
// Burst communication synchronization
// Example: waite for data packet starting character '('. Should receive even_byte first.
        u16 u16Byte, temp;
        unsigned char Xodd_byte, Xeven_byte;

        u16Byte = man_encode(XByte); temp = u16Byte;
        Xodd_byte = temp>>8; Xeven_byte = (u08)u16Byte;

        while(!(uartReceiveByte(nUart, &even_byte) && (even_byte == Xeven_byte)));
        while(!(uartReceiveByte(nUart, &odd_byte)));

        if (odd_byte == Xodd_byte) return(1);
        else return(0);
}



void Send_ME_Data(char nUart, unsigned char *Message, unsigned int numByte)
{       // send Manchester encoded data (even_byte first).
        u16 u16Byte, i, temp;
```

```
	// disable receiver so no pickup echoes from the reflected Tx data
	if (RX_state) {
		uartRx_Enable(nUart, 0);					// disable receiver
		uartFlushReceiveBuffer(nUart);
	}

	for (i=1; i<=numByte; i++) {
		u16Byte = man_encode(Message[i]);
		temp = u16Byte;
		odd_byte = temp>>8;
		even_byte = (u08)u16Byte;
		uartSendByte(nUart, even_byte);
		uartSendByte(nUart, odd_byte);

		if (debug) uartSendByte(0, Message[i]); // debug
	}

	if (RX_state) uartRx_Enable(nUart, 1);				// enable receiver
}


char Process_received_Data(unsigned char *Message, unsigned int i)
{// execute received commands through UART0 and stop at first invalid command
```

```
unsigned int numByte, j=1, k;                                   // byte counters

if (RX_state) {
        uartRx_Enable(1, 0);                                    // disable UART1 receiver
        uartFlushReceiveBuffer(1);
}

// extract each command for execution on the mobile robot (EvBot)
while (j<i)
{
        if(Message[j]=='G')                                     // Go command
        {
                for (k=j;k<j+4;k++) {uartSendByte(0, Message[k]);}
                while(!(uartReceiveByte(0, &RxByte) && (RxByte=='D')));   // waite to finish excu.
                j=j+4;
        }
        else if(Message[j]=='T')                                // Turn command
        {
                for (k=j;k<j+3;k++) {uartSendByte(0, Message[k]);}
                while(!(uartReceiveByte(0, &RxByte) && (RxByte=='D')));   // waite to finish excu.
                j=j+3;
        }
        else                                                    // Invalid command. Cancel the process
        {
```

```
                        if (debug) {
                                numByte = sprintf(Message," Invalid Command ... no G or T.");
                                uartSendBuffer(0, Message, numByte);            // debug at hyper terminal
                        }
                        if (RX_state) uartRx_Enable(1, 1);                      // enable UART1 receiver
                        return 0;
                }
        }

        if (RX_state) uartRx_Enable(1, 1);                                      // enable UART1 receiver
}


u16 man_encode(u08 unenc)
{/*     ------------------------------------------------------------------------------------
        u16 man_encode(int enc)
        written by Aaron Ramsey, Jan. 25th, 2000
        This function encodes a 8 bit value into a 16 bit manchester encoded variable which it
        then returns.

        This function encodes the bits in a unique way. The odd bits (7,5,3,1) are encoded into
        the msb 8 bits of data to return and the even bits (6,4,2,0) are encoded into the lsb 8
        bits of data to return. Encoding this way saves alot of bit testing and flipping.
```

```
        0x0E (00001110) encodes into 0x5AA6 (0101101010100110)
        instead of the more natural 0x55A9 (0101010110101001)
        ----------------------------------------------------------------------------------
*/
        u08 odd_byte,even_byte,temp;

        odd_byte=unenc&0xAA;
        temp=(~unenc&0xAA)>>1;
        odd_byte=odd_byte|temp;

        even_byte=unenc&0x55;
        temp=(~unenc&0x55)<<1;
        even_byte=even_byte|temp;

        return((u16)odd_byte<<8)|even_byte;
}


u08 man_decode(u16 enc)
{/*     ----------------------------------------------------------------------------------
        u08 man_decode(u16 enc)
        written by Aaron Ramsey, Jan. 25th, 2000
        This function decodes a 16 bit manchester encoded variable and returns the actual 8 bit
        unencoded value. See man_encode for a description of the encoding technique.
```

```
        ----------------------------------------------------------------------------
*/
        u08 odd_byte,even_byte;

        odd_byte=(u08)(enc>>8);
        if((odd_byte&0xAA)^((~odd_byte&0x55)<<1)) {
                receive_error=1;
                return(0);
        }
        else odd_byte&=0xAA;
        even_byte=(u08)enc;
        if((even_byte&0x55)^((~even_byte&0xAA)>>1)) {
                receive_error=1;
                return(0);
        }
        else even_byte&=0x55;
        receive_error=0;

        return(odd_byte|even_byte);
}


void Initialization(void)
{
```

```
	uartInit();				// initialize UART0 and UART1 (serial ports)
	uartSetBaudRate(1,1000);		// set the baud rate of the UART1 to Optical Modulator
	uartSetBaudRate(0,19200);		// set the baud rate of the UART0 to Robot MCU
	sei();					// enable global interrupts
}


void uartRx_Enable(unsigned char nUart, unsigned char enable)
{	// disable/enable Uart# receiver
	if(nUart) {		// Uart1
		if(enable) UCSR1B = (1<<RXEN1)|(1<<TXEN1)|(1<<RXCIE1)|(1<<TXCIE1);// enable receiver
		else UCSR1B = (0<<RXEN1)|(1<<TXEN1)|(0<<RXCIE1)|(1<<TXCIE1);		// disable receiver
	}
	else {		// Uart0
		if(enable) UCSR0B = (1<<RXEN0)|(1<<TXEN0)|(1<<RXCIE0)|(1<<TXCIE0);// enable receiver
		else UCSR0B = (0<<RXEN0)|(1<<TXEN0)|(0<<RXCIE1)|(1<<TXCIE1);		// disable receiver
	}
}
```